UTS UNIVERSITY OF TECHNOLOGY SYDNEY

# Data-driven Structure health monitoring (SHM) using Wireless Sensor Network

**by Mingzhe Gao**

Thesis submitted in fulfilment of the requirements for the degree of

**Doctor of Philosophy**

under the supervision of Prof. Xinqun Zhu and Prof.Jianchun Li

University of Technology Sydney
Faculty of Engineering and Information Technology

July 2025

## CERTIFICATE OF ORIGINAL AUTHORSHIP

I, Mingzhe Gao declared that this thesis is submitted in fulfilment of the requirements for the award of Doctor of Philosophy, in the School of Civil and Environmental Engineering, Faculty of Engineering and Information Technology at the University of Technology Sydney.

This thesis is wholly my own work unless otherwise referenced or acknowledged. In addition, I certify that all information sources and literature used are indicated in the thesis.

This document has not been submitted for qualifications at any other academic institution.

This research is supported by the Australian Government Research Training Program.

Date: 15/07/2025

Production Note:
Signature removed prior to publication.

Mingzhe Gao

**ACKNOWLEDGEMENT**

It is with great gratitude and appreciation that I reflect on the journey of completing this thesis. Without the help, advice, and inspiration of many people who have believed in me and my scientific pursuits, I never would have reached this milestone.

Firstly, I owe my deepest thanks to Professor Xinqun Zhu, my supervisor, for his outstanding mentorship. His profound knowledge, critical insights, and continuous support greatly influenced the course of my studies. He has always been patient and generous with his time, guiding me through the complexities of my work with wisdom and understanding. His high standards and passion for research have inspired me to pursue academic excellence.

It is with deep gratitude that I write to Professor Jianchun Li for his invaluable advice, constructive feedback, and constant encouragement. His expertise has helped refine many aspects of my research, and his thoughtful comments have contributed significantly to the improvement of this thesis. His collaboration and support have been essential to the success of my work.

In additional, I am incredibly grateful to my research group. The many discussions, brainstorming sessions, and collaborative efforts have enriched my research experience. I deeply appreciate the technical advice, camaraderie, and teamwork that made even the most challenging days rewarding and enjoyable. It has been a privilege to learn and grow alongside such talented individuals.

I wish to convey my sincere thank to my parents for their love and steadfast belief in me. Their sacrifices, patience, and support have been my paramount source of strength during this trip. They have always stood by me in both moments of triumph and hardship, encouraging me to persevere and pursue my dreams. For this, I am forever grateful.

Lastly, I would like to acknowledge all those whose names may not appear here but who have supported me in various ways during my PhD journey. Whether through acts of kindness, encouragement, or advice, your contributions have made a difference in helping me reach this goal.

Thank you all for being a part of this incredible journey.

**List of publications**

1) Mingzhe Gao, Xinqun Zhu and Jianchun Li (2023) “Time-frequency analysis of vehicle-bridge interaction system for bridge health monitoring using synchrosqueezing transform”. *Proceedings of the 12th International Conference on Structural Health Monitoring of Intelligent Infrastructure*, pp.346-351, 19-22 October 2023, Hangzhou, China.

2) Mingzhe Gao, Xinqun Zhu and Jianchun Li (2024) “Time-frequency analysis of vehicle-bridge interaction system using multi-synchrosqueezing transform” *Proceedings of the 1st International Conference on Engineering Structures*, pp.167-176, 7-11 November 2024, Guangzhou, China.

3) Mingzhe Gao, Xinqun Zhu and Jianchun Li (2025) “Time-Frequency Characteristics of Vehicle-bridge Interaction System for structural damage detection using Multi-Synchrosqueezing Transform.” *Sensors*, 25(14), 4398.

4) Mingzhe Gao, Xinqun Zhu and Jianchun Li (2025) “Dual-Source Vehicle-Bridge Interaction Analysis Using Dual-Stream CNN and Synchrosqueezing Transform for Structural Health Monitoring” (manuscript in preparation)

5) Mingzhe Gao, Xinqun Zhu and Jianchun Li (2025) “Time-Frequency Characteristics of Vehicle-bridge Interaction System for structural damage detection using Second order-Synchrosqueezing Transform” (manuscript in preparation)

**TABLE OF CONTENTS**

**ABSTRACT**

Due to ageing, and operating and environmental loads, civil infrastructure is deteriorating, especially for transportation infrastructure under traffic loadings. Structural Health Monitoring (SHM) is an efficient method for determining the state of a structure so that condition-based maintenance is conducted for cost-effective asset management. Quite a few bridges with large spans have been equipped with long-term monitoring systems. The vast volume of monitoring data has been collected and extracting the valuable information from observed data presents a significant difficulty. In this study, a new data-driven technique is developed to assess the structural condition of bridges under moving vehicles. The wireless sensor network is employed to collect vehicle-bridge interaction (VBI) data for real-time evaluation of bridge conditions. To execute structural condition evaluation, the machine learning-based algorithm can be implemented in the wireless sensor node for decentralized structural monitoring.

This project is to develop a VBI-based SHM approach. The moving vehicle passing over the bridge constitutes a time-dependent dynamic process. The wireless sensor network is utilized to monitor dynamic responses of the VBI system. The advanced signal processing-based techniques are developed to extract the time-varying features of the VBI system. The time-varying characteristics serve as the input of machine learning models for predicting bridge conditions. Firstly, a second-order synchrosqueezing transform (SST2) based method is developed to extract time-varying features from dynamic responses of the passing vehicle for bridge condition assessment; Secondly, a multi-

synchrosqueezing transform (MSST) based method is proposed to extract the time-varying features from dynamic responses of the bridge subjected to moving vehicles for bridge condition monitoring; Finally, the time-varying features from dynamic responses of the vehicle and bridge are fused through a dual-stream convolutional neural network (CNN) model for robust damage classification of bridge structures. Numerical and experimental results have been conducted to verify the performance of the proposed approach. The outcome of the project will provide a reliable, accurate, rapid structural condition assessment for a large population of short and medium span bridges in road networks.

# CHAPTER 1 Introduction

## 1.1 Research background and motivation

Bridges are critical transport infrastructure to link communities. Ageing, environmental and operating loading will inevitably lead to the deterioration of bridge structures, thereby impacting on the performance of bridges and the safety of their occupants ( ASCE 2017). In recent decades, catastrophic bridge failures, such as the collapse of the I-35W Mississippi River Bridge in Minnesota (2007), the Skagit River Bridge break down in Washington State (2013), and the Morandi Bridge collapse in Genoa, Italy (2018), have highlighted the necessity for more advanced and reliable structural health monitoring (SHM) systems.

The traditional evaluation of bridge conditions has predominantly relied on visual inspections. Visual scientific techniques may assist in identifying critical defects such as cracking and corrosion. They are often labor-intensive, subjective, and exhibit inadequate spatial resolution (OBrien et al. 2017). Furthermore, visual inspections may require lane closures or the utilization of costly equipment, such as scaffolding or rope access, thereby increasing operational expenses and disrupting traffic flow. This essential limitation has motivated the development of automated and data-driven SHM technologies, mostly reliant on vibration monitoring using sensor networks (Sazonov et al. 2004).

Direct bridge vibration monitoring primarily entails the placement of sensors (accelerometers, strain gauges, fiber optics) directly on the bridge to evaluate its dynamic response to external and internal loads (Her and Chung 2019). Although this system provides highly accurate global data, the installation of wired sensors incurs significant cabling costs, both initially and for ongoing maintenance. Moreover, the spatial resolution

attained via a dense sensor infrastructure complicates data processing, data management, and sensor protection considerably (Noel et al. 2017). Consequently, there is a growing demand for affordable, high-resolution, and durable SHM solutions to monitor large population of short and medium span bridges with a lower quantity of sensors and minimal overhead.

Recently, there has been considerable interest in indirect monitoring tactics, using an instrumented vehicle, particularly as a mobile sensor network. The dynamic response from a vehicle crossing the bridge is utilized to derive the intrinsic features of the bridge based VBI system (Li et al. 2024). The principal benefit of this indirect method is that a single instrumented vehicle may collect data of many spatial points throughout the bridge span in a short period with a few sensors on the vehicle. This not only reduces the number of sensors needed but also lowers the cost related to the installation and maintenance of monitoring systems (Malekjafarian et al. 2015).

Nonetheless, numerous challenges are linked to indirect bridge monitoring. The primary issue is road surface roughness, which might potentially make the bridge information undetectable from dynamic responses of the vehicle (Yang and Wang 2022). Nonstationary nature and measurement noise additionally obscure to extract the bridge's dynamic information. Consequently, the elimination of noise effect, the extraction of bridge frequency components, and the mitigation of road roughness effects from dynamic responses of the vehicle are complex tasks that necessitate advanced signal processing techniques (Jian et al. 2022). Moreover, the bridge subjected to moving vehicles constitutes a time-varying process, and extracting time-varying features from dynamic responses of VBI systems necessitates advanced time-frequency analysis techniques.

In this context, data-driven methods have emerged as effective tools for SHM, and the

time-history vibration data has been transformed to the frequency and time-frequency domains. Traditional signal processing methods (Fourier transform, wavelet analysis) either assume stationarity or employ manually crafted features that do not capture the underlying properties of structural responses (Nguyen et al. 2024). Data-driven methods, including methods based on machine learning can autonomously identify representative features without extensive feature engineering from raw or minimally processed data. With adequate training data, these models can identify damage anomalies effectively with noisy or missing data (Lu et al. 2024; Plevris and Papazafeiropoulos 2024).

For data-driven SHM, deep learning based methods including convolutional neural network (CNN), and autoencoders have demonstrated remarkable potentials (Pathirage et al. 2018). CNN is proficient in extracting spatial features from images or time-frequency data, making them particularly suitable for analyzing spectrograms generated by vibration signals (Ni et al. 2024). By transforming raw vibration data from either the bridge or vehicle into spectrograms or other two-dimensional representations, CNN can autonomously identify damage signatures that conventional signal analysis methods may overlook.

However, the majority of existing studies utilizing data-driven methods for bridge monitoring focus either on vehicle or bridge responses only. Few have considered how to leverage the complementary characteristics of both vehicle and bridge responses to capitalize on the supplementary data from the VBI system. Bridge signals directly reflect the global conditions of the structure, while vehicle signals indicate the local structural status through the local response when the vehicle is passing the local damage. Connecting these two datasets provides a clearer understanding of the structure's health and it may facilitate the identification and localization of structural deterioration.

The double-stream CNN architecture proposed for action recognition in computer vision is a viable contender for this integration (Qiao et al. 2021). In the framework of SHM, dual-stream CNNs can be trained to process bridge-derived spectrograms in one stream and vehicle-derived spectrograms in the other. This architecture may independently learn representations from each domain and subsequently integrate them at various stages to illustrate the connectivity between the two data sets. This addition is beneficial in scenarios where bridge and vehicle data may be incomplete, unreliable, or excessively affected by external factors (e.g., uneven roads, heavy traffic, noise) (Yang et al. 2021).

Wireless Sensor Networks (WSNs) are fundamental facilitators of data-driven solutions. Wireless sensors eliminate the logistical challenges associated with lengthy cables and offer economical, cost-efficient, and scalable monitoring solutions. Capturing synchronous vibration data is facilitated by positioning WSN nodes on both the bridge deck and the equipped vehicle. The integration of WSNs and data-driven algorithms might significantly streamline the SHM workflow, including data collection, real-time processing, and extensive deployment across several bridge locations. High-end networking protocols and edge computing solutions provide on-site early data processing, hence minimizing bandwidth usage and enhancing overall resistance to communication failures (Armijo and Zamora-Sánchez 2024).

### 1.2 Research objectives

This research aims to develop a rapid, accurate and cost-effective bridge SHM approach for dynamic parameter identification and damage detection. To overcome the shortcomings of direct bridge monitoring systems involving fixed sensor networks and the limitations of current direct approaches, an indirect approach that uses responses of passing vehicles is developed in this thesis. Wireless sensors are deployed on the vehicle

to create a wireless sensory system, which integrates with wireless networks surveillance system on the bridge. Compared to conventional approaches, the proposed system requires fewer sensors and provides richer spatial data vital to bridge condition assessment.

The following objectives will be pursued in this research:

1) Develop an approach to extract time-varying features from dynamic responses of bridges under moving vehicles using multi-synchrosqueezing transform (MSST).

2) Implement a wireless sensing strategy for VBI monitoring and develop an approach to extract time-varying features from dynamic responses of a passing instrumented vehicle using second-order synchrosqueezing transform (SST2).

3) Integrate bridge and vehicle time–frequency features into a dual-stream CNN architecture for robust damage classification of the bridge structure.

### 1.3 Significance of the study

It offers an approach for monitoring bridge structural health with data collected from a moving vehicle equipped with sensors and the bridge, enabling precise, prompt, and cost-effective assessments of bridges. This research advances the state of the art in SHM through the integration of WSNs for an autonomous platform, high-throughput time-frequency analysis, and a dual-stream CNN for damage classification. This approach would enhance the cost-effectiveness of fixed sensor network installation and maintenance while simultaneously augmenting spatial resolution and diagnostic capabilities, hence further improving infrastructure safety management. The expectations from this research are as follows:

An innovative and indirect method for time-dependent structural data pertaining to bridges, derived by vehicles, enables more comprehensive and flexible monitoring strategies without the need for important bridge instrumentation.

With high-resolution time-frequency analysis techniques, nonstationary vehicle-bridge interaction signals are constantly evaluated and analyzed to provide a deep understanding of both their global and local structural features.

A dual stream CNN classification algorithm integrating bridge time-frequency data with vehicle time-frequency data enhances damage detection accuracy and efficacy. It improves proactive maintenance, extends bridge durability, and reduces risks to human life.

### 1.4 Structure of the thesis

This thesis consists of six chapters, each focusing on a specific aspect of the research:

Chapter 1 presents the research context, rationale, aims, and importance. It highlights the importance of SHM and outlines the innovative methodologies proposed in this research.

Chapter 2 provides an extensive analysis of prior research efforts on vibration-based bridge SHM methods. The review is conducted from different perspectives, including VBI systems, advanced signal processing techniques, and data-driven approaches, identifying research gaps and setting the stage for the proposed methodologies.

Chapter 3 focuses on the time-varying features of VBI systems, utilizing advanced techniques such as SST2 to extract dynamic features. To demonstrate how effective these methods are, numerical simulations and experimental validations are provided.

Chapter 4 introduces MSST based approach as an enhancement to time-frequency analysis of VBI systems. This chapter investigates the influence of parameters including road surface roughness, vehicle velocity, and bridge deterioration on the dynamic interaction between the vehicle and bridge.

Chapter 5 details the development of a dual-stream CNN designed to integrate and classify time-frequency features from both bridge and vehicle responses. The model's architecture, parameter tuning, and performance are evaluated through extensive case studies and experimental data.

Chapter 6 culminates the thesis by synthesizing important findings, highlighting contributions to the domain of SHM, and offering suggestions for subsequent research to address limitations and expand the applicability of the proposed methods.

# CHAPTER 2 Literature review

## 2.1 Overview

This chapter provides an overview of vibration-based SHM for bridges, focusing primarily on developments that utilize VBI. VBI has demonstrated its appeal in SHM because of its capability to conduct bridge assessments in operational environments with minimal instrumentation. Using dynamic features like modal frequencies and mode shapes as a lens, this chapter will initially trace the evolution of vibration-based bridge damage detection as structural changes are recognized.

Subsequently, VBI techniques for SHM are provided, encompassing both direct and indirect methodologies. The direct approach involves monitoring bridge behavior using sensors installed on the bridge, while the indirect method utilizes the instrumented vehicle to assess the bridge performance without requiring an extensive bridge monitoring system. Innovations in time-frequency analysis, such as Synchrosqueezing transform (SST) and wavelets, are assessed to identify time-varying characteristics of VBI systems.

The chapter additionally addresses machine learning models for SHM, particularly dual-stream CNN. These models have demonstrated the ability to incorporate time-frequency domain data for damage assessment. The challenges associated with the implementation of VBI-based SHM are examined, including noise sensitivity, data disparity, and generalization across diverse situations.

The final part summarizes existing research limitations and potential avenues for advancement in VBI-based SHM. These comprise superior feature fusion algorithms, enhanced preprocessing techniques, and the incorporation of real-time monitoring

platforms. This chapter's results and comments provide a commendable introduction to the current state and future directions of VBI-based bridge SHM.

## 2.2 Vehicle-bridge interaction-based bridge monitoring

The advancement of sensors and information technology has rendered SHM a data-driven approach for the security of civil infrastructure. In the last twenty years, the domain of SHM has evolved significantly due to the advent of intelligent and portable sensor technologies. Advanced signal processing and machine learning technologies are employed in civil engineering, especially SHM. Advanced signal processing includes Continuous Wavelet transform (CWT), Short time Fourier transform (STFT) and Hilbert-Huang transform (HHT). MSST, SST, Synchroextracting transform (SET). Machine learning includes decision tree (DT), deep learning (DL). In this section, the methods for analyzing signals and machine learning models for SHM of VBI system are introduced.

### 2.2.1 Vehicle bridge interaction system

The intricacy of the bridge construction makes finite element analysis a common tool for modeling it. To construct the VBI system, the vehicle and bridge subsystems communicate with one another through theoretically or numerically determined wheel-road contact. A model of the VBI system has been used to simulate the way bridges and automobiles react in real time (Li et al. 2017). In many cases, probabilistic assessments necessitating extensive simulations or online evaluations requiring rapid predictions may render VBI analysis, which integrates the entire vehicle model and spatial dynamic interactions, computationally expensive (Zhai et al. 2009; Li et al. 2021).

Various techniques have been developed to utilize the VBI analysis for structural damage detection of bridges last decade. These methods can be categorized as: using data from

the bridge alone, responses from the vehicles alone, or responses from both the vehicles and the bridge. The direct approach relates to techniques based on bridge data, when methods are discussed in terms of the indirect approach based on data obtained from the instrumented vehicle crossing the bridge deck. The methods seek changes of structural responses as the fingerprint of the bridge, which referred to as "data-driven" techniques. Anomaly is identified without any background in the physical procedure or the reference model of the structure (Zhu and Law 2015).

### 2.2.2. Structure identification from bridge responses

Evaluating the bridge's dynamic response to vehicular passage produces critical data necessary for structural identification, focusing on dynamic features including natural frequencies, mode shapes, and damp ratios. Dynamic loads generated by vehicles influence bridge response, as they vary with vehicle speed, mass, and axle configuration. The bridge's natural frequency is crucial as it reflects the structure's stiffness and mass distribution. Monitoring temporal variations in a bridge's response indicates structural damage or degradation, rendering such surveillance essential for structural health assessments. Engineers employ fast Fourier transform (FFT) and time-frequency analysis (TFA) techniques, including SST, to discern critical vibration modes in bridges and assess their stability and deviations from standard conditions.

The transit of cars over a bridge induces dynamic interactions between the structures, leading to bridge vibrations recorded as acceleration reactions. Structural alterations, including modifications in stiffness, mass, or boundary conditions, will affect signal qualities such as amplitude, frequency content, and damping properties, as these responses exhibit significant sensitivity to such changes. Structure identification utilizes this sensitivity by analyzing bridge reactions to identify abnormalities and determine

damage patterns while updating dynamic parameters. Utilizing modern data processing techniques, such as wavelet transformations and modal decomposition, enhances our capacity to distinguish between environmental noise and structural degradation indicators. The examination of bridge reaction data is an essential instrument for evaluating bridge conditions and predicting long-term structural performance under traffic loads.

### 2.2.3 Bridge damage detection from vehicle responses

In recent decades, numerous indirect bridge monitoring techniques utilizing responses recorded from automobiles traversing bridges have been established. These methods have the benefit of using sensors installed on the vehicle, which eliminates the requirement for sensors or a data collecting system on the bridge. The inherent frequency of a bridge can be indirectly determined from the vehicle acceleration response during its crossing (Siringoringo and Fujino 2012). Most of existing methods are focused on identifying dynamic bridge properties from vehicle responses, including natural frequency, mode forms, and damping (Chen et al. 2014; Malekjafarian et al. 2015).

When a vehicle crosses a bridge, causing both to vibrate and interact dynamically. As a result, the bridge response has an impact on the vehicle response. According to the SHM principle, if a bridge is damaged, such as bridge pounding or concrete cracking, will alter the stiffness, damping, and/or mass of the bridge, and its vibration characteristics will change as well (Yang and Wang 2022).

## 2.3 Advanced signal processing techniques for VBI analysis

To extract the frequency changes caused by the VBI impact, a highly efficient time-varying feature analysis method is required for bridge health monitoring in operational environments. Advanced signal processing techniques, like STFT, HHT, SET and CWT

could be used for the VBI analysis (Li et al. 2020).

### 2.3.1 Short time Fourier transform

Fourier transform (FT) has a significant drawback in that it cannot do combined time-frequency analysis. FT must be calculated from negative infinity to positive infinity, which is in direct opposition to immediate analysis in practice (Braeewell 1965). To compensate for the FT's flaw, a window function is utilized on the signal, and FT of the windowed function is calculated after the signal has been windowed (Li et al. 2024). It may be moved across the whole-time axis in response to a change in time location, and the time period spectrum near any point can be acquired using the window function, allowing for time localization. The FT of a windowed signal is referred to as the STFT. When a signal's frequency components change over time, the STFT can pinpoint those changes, while the standard FT delivers frequency information averaged across the entire duration of the signal (Luo et al. 2016). The STFT is used in later time-frequency analysis.

Use the window function to cut the signal in the time domain and then perform the FT on the cut local signal, that is, get the FT of the signal at time t and keep moving t, that is, keep moving the window function's center position, to get the FT of the signal at time t. The TFA is achieved by acquiring the FT at various times (Durak and Arikan 2003).

STFT and Wigner distribution (WD) versions have been used to characterize signals in the time-frequency domain. The STFT's widespread use in practice is due to the lack of undesirable cross terms and its computational efficiency (Stanković et al. 2014). Yang and Lin (2005) use STFT for analyzing vehicle-bridge interaction dynamics. The efficiency of STFT has become less relevant as faster processors have become available. The capacity of STFT to express the absence of cross terms in the time-frequency content

of signals is the principal advantage of STFT approaches compared to WD-related quadratic time-frequency distributions.

### 2.3.2 Wavelet transform

CWT is an exceptional TFA tool that has garnered significant attention during the past thirty years. For a comprehensive mathematical elucidation of CWT. The signal is analyzed into a series of coefficients across two dimensions: translation and scaling, with scales being roughly inversely correlated with frequency. The signal is compared to a basis function that has been translated (shift) and stretched (scale). Elevated coefficients indicate a strong correspondence between the signal and the wavelet at a specific time and frequency (Sadowsky 1996). CWT provides changeable resolution and a map of the signal's energy content in this way. Complex wavelets are utilized in CWT for time-frequency analysis and they separate the phase and amplitude constituents of the signal. The Morlet wavelet is the most often utilized complex wavelet, comprising a complex sinusoid enveloped by a Gaussian function (Addison 2018).

Time-domain signals can exhibit exceptionally high temporal resolution yet possess zero frequency resolution. The signal in the frequency domain derived from the Fourier transform attains high frequency resolution yet possesses zero temporal resolution. STFT possesses a fixed resolution in both time and frequency domains, with uniform time-frequency resolution throughout. However, owing to the constraints imposed by Heisenberg's uncertainty principle in quantum physics, the dimensions of each time-frequency window remain constant (Wang et al. 2024). The temporal and spectral resolutions are inversely proportional, and these two resolutions cannot be high at the same time.

WT has time-frequency windows of varying dimensions at distinct times and frequencies, enabling enhanced frequency resolution in the low-frequency domain (Dey et al. 2024). Nevertheless, it remains constrained by Heisenberg's uncertainty principle, preventing optimal resolution in both time and frequency domains. At the same time, the time-frequency window of WT is not entirely self-adaptive and requires the manual selection of the basis function. CWT is effective in identifying damage-induced irregularities in bridge responses. For example, Zhu and Law (2006) applied wavelet analysis to locate cracks in bridge structures under moving loads. The wavelet coefficients revealed crack locations and severity by isolating local signal irregularities in the time-frequency domain. Kim et al (2011) employed CWT to analyze dynamic responses of a bridge under vehicular loading and successfully identify modal frequencies and damping ratios. The wavelet-based approach enhanced the resolution of transient responses compared to traditional Fourier methods.

The above methods are all limited by Heisenberg's uncertainty principle and are not fully adaptive methods. Next, introduced a time-frequency analysis method that is not limited by Heisenberg's uncertainty principle and has better adaptability - HHT.

### 2.3.3 Hilbert-Huang transform (HHT)

Hilbert transform (HT) is often used for modulation and demodulation in communication systems, and it can also be used for time-frequency analysis of signals. In the field of time-frequency analysis, HT is mainly used for instantaneous frequency estimation. It can be seen from the above analysis that the analytical signal of the original signal can be obtained by using HT.

HT cannot be performed directly on the multi-frequency component signal. Further

process is needed to decompose the original signal into a superposition of single-frequency signals. HHT (Huang 2007) is used for empirical modal decomposition (EMD) of signals. Zhu and Law (2016) reviewed the application of HHT in addressing inverse problems in VBI systems. The study highlighted HHT's effectiveness in bridge damage detection and analyzing non-stationary dynamic responses of a bridge subjected to traversing vehicles.

### 2.3.4 Synchrosqueezing transform (SST)

SST is a type of time-frequency reassignment method that concentrates the energy of the spectrogram and produces a sparser time-frequency graphic. Three steps are involved in SST. The first step is to obtain $W_f(a,b)$ of $f(t)$ using CWT. In the second step, using $W_f$ as a support, an initial estimation of the frequency demodulated by the frequency modulation, $\omega_f(a,b)$ is determined. Finally, by compressing $W_f$ via reassignment, this estimate is utilised to determine SST (Herrera et al. 2014).

The energy of the harmonic signal will be allocated across the time-scale plane in wavelet representation. Taking derivatives is used in a sort of frequency demodulation to eliminate the wavelet's impact on this frequency. Mostafa et al (2020) proposed a wavelet synchrosqueezed transform (WSST)-based method to extract IF from railway bridge vibration responses. This method effectively analyzes the dynamic interactions of VBI systems for SHM. Gao et al (2023) utilized SST for TFA of VBI systems. The research focused on identifying time-varying characteristics in VBI systems for effective bridge health monitoring.

### 2.3.5 Multisynchrosqueezing transform (MSST)

The SST is good at dealing with substantially time-varying signals. It must be noted that

by employing a single SST procedure, we may get a crisper TFR than that of the STFT result. Another SST technique is warranted based on the previously obtained SST results. in this scenario. As a result, the TF result is substantially sharper than the SST result (Yu et al. 2018). The energy of the TF outcome should be focused progressively by performing several SST processes.

MSST is to obtain time-frequency (TF) through multiple SST operations. Its mathematical theory demonstrates its concentration efficacy of TF. Given that the MSST is an iterative process, the major emphasis of the technique to handle the TFR is through a comparison of the MSST with the SST original (Yu et al. 2018). Xin et al. (2021) proposed a hybrid method combining MSST and analytical mode decomposition. This approach enables high-resolution extraction of instantaneous frequencies from structural dynamic responses, allowing precise monitoring of time-varying characteristics.

### 2.3.6 Synchroextracting transform (SET)

A unique TFA method has been created to research the trend and IF of nonlinear and non-stationary data. SET (Li et al. 2020), is a STFT based approach for time-frequency analysis. When compared to conventional TFA approaches, the suggested technique can offer a more energy-focused TFR and enable signal reconstruction. Li et al. (2020) demonstrated the use of SET to analyze time-varying features of bridges under moving vehicles. The study focused on extracting instantaneous frequencies from bridge vibration signals, enhancing the accuracy of bridge health monitoring.

### 2.3.7 Second-order synchrosqueezing transform (SST2)

Recent innovations have introduced SST2, which improves upon traditional SST by concentrating energy in time-frequency representations (Behera et al. 2018). SST2

enhances the clarity of transient dynamics and allows precise reconstruction of local frequency components, making it particularly effective for analyzing non-stationary signals in VBI systems. Tan et al. (2023) utilized SST2 to extract bridge frequencies during the vehicle passage. The study demonstrated SST2's capability for high-resolution time-frequency analysis, enhancing its application in bridge health monitoring. Zhang et al. (2024) proposed a novel method combining SST2 and wave-packet transform for real-time detection of cable stress in cable-stayed bridges. The research focused on analyzing time-varying dynamic characteristics of bridge cables, demonstrating the method's effectiveness in capturing precise tension variations under changing structural conditions.

### 2.3.8 Comparison

The inherent frequency elements of non-stationary responses and time-varying properties, as well as random and transient occurrences, have all been successfully revealed via TFA. For bridge responses, some TFA methods have been applied. Non-stationary and transient signal analysis can benefit from TFA methods (Sandsten 2016). FFT techniques (spectrogram, Wigner–Ville, etc.) might be used to do TFA. However, these time–frequency analysis methods have intrinsic flaws that restrict their ability to extract time-varying characteristics for accurate bridge condition assessment. Although the HHT provides excellent TFR, it is devoid of cross-term interferences with EMD using spline interpolation (Xiao et al. 2017).

TFA can be utilized for output-only modal identification. The suggested output exclusively validates modal identification approaches utilizing STFT, EMD, HT, and wavelet methods utilizing a three-degree-of-freedom system. Test structure at a 1:10 scale (Fan and Qiao 2011). The responses to free and forceful vibrations are considered. The free-vibration response is derived from recorded ambient vibration data via techniques

such as the random decrement method, which can subsequently be analyzed using TF-based modal identification (Nagarajaiah and Basu 2009).

### 2.4 Data-driven approaches for SHM

Various methods for SHM have developed in the previous few decades. Conversely, data-driven methodologies have grown in prominence in recent years as computing resources and big data sciences have improved. Deep learning, which is a rebranding of neural networks, is one of them. A portion of deep learning is supervised or semi-supervised learning, whereas another portion is unsupervised learning (LeCun et al. 2015). Machine learning based VBI models can be classed as supervised, unsupervised, and reinforcement learning. With supervised learning, a machine learning model can be taught utilizing a collection of labeled training data. A regression model is normally used (e.g., ANN, linear and nonlinear regression). When outputs are discreet or categorical variables, the model functions as a classifier. (e.g., SVM, KNN, Bayesian algorithm) (Goodfellow 2016).

#### 2.4.1 Convolutional neural network (ConvNet/CNN)

A CNN is a DL model that analyzes an input image, attributing importance (learnable weights and biases) to various components within the image and differentiating among them. The pre-processing demands of a ConvNet are significantly lower than those of alternative classification methods. CNN can autonomously learn filters and features after sufficient training, whereas rudimentary methods require manual engineering of filters (Aloysius, N and Geetha, M. 2017).

CNN is available in a number of sizes and configurations, but it typically has three layers: Convolutional, pooling, and completely linked layers. In the convolutional layer, several convolutional kernels acquire feature representations of the inputs and generate feature

maps. The input is first convolved using a learned kernel, and then the convolved outputs are applied to an element-wise non-linear activation function (Shyam, 2021).

Neurons in convolution neural networks, like those in other neural networks, learn weights and biases. The CNN architecture encodes some features since it believes the inputs are images. This improves the effectiveness of the forwards function while minimizing the quantity of parameters within the network. CNN neurons are structured in three dimensions: width, height, and depth, in contrast to neurons in other neural networks. Unlike ANN, neurons in each layer are coupled solely to a limited subset of neurons from the preceding layer (Polat, and Danaei Mehr, 2019).

### 2.4.2 Damage detection using CNN

The damage in the VBI system is detected using vibration-based CNN in this part. The temporal frequency spectrum was used to train the CNNs. SST was used to extract the time-frequency characteristics, which were then fed into the CNN. CNNs dislike excessive computational costs and lack of robustness and offer recommendations accordingly. Convolutional layers, activation layers, pooling layers, fully linked layers, and output layers make up CNN.

Among the different machine learning algorithms, the DL approach, a sub-branch of machine learning, has garnered the greatest interest. It has been extensively utilized for natural language processing. medical diagnosis, internet advertising. and computer vision. Autopilot and translation are two things that come to mind. A deep neural network (DNN) is a specific category of neural network. Multi-layers are used to learn data characteristics with multiple intrinsic patterns. Corbally et al. (2024) explores the potential of machine learning, specifically CNN, in bridge health monitoring. The authors propose an indirect

monitoring technique that utilizes vibration data collected from vehicles driving over the bridge to analyze the bridge's dynamic characteristics. This method eliminates the need for traditional expensive and complex fixed sensor installations on bridges, relying solely on vibration responses of a passing instrumented vehicle to assess the structural health of bridges.

### 2.4.3 Bridge structural damage detection using CNN

Structural degradation can influence the modal parameters of a structure. To capture these variations, convolution operations were applied to extract essential features related to these parameters, and a classification method was used to assess the damage state. The CNN training data were generated by simulating the free vibration of a steel frame and calculating the first-order modal strain energy across various damage cases using finite element analysis. Modal parameters were subsequently determined through the analysis of vibration signals. Experimental data were then input into the CNN to evaluate its performance in identifying structural damage (Teng et al. 2019). Since then, CNN has paid more attention to structural damage detection, and more study has been undertaken in this area.

An effective way for detecting data anomalies is to build physical models and make probabilistic predictions. To identify abnormalities and provide sensor failure warning, and deal with problems such sensor drift, Goebel and Yan (2008) used sensor validation with fuzzy principles and parameter optimization methodologies. To quickly detect the malfunctioning sensor, Li et al (2019) used a hypothesis test based on the generalized likelihood ratio. Sensor failures and structural damage are distinguished by the fact that sensor problems are local while structural damage is widespread.

### 2.4.4 Bridge structural damage detection using CNN

Zhou et al. (2021) proposed a fully automated method for vehicle weight identification via Extraction of structural response patterns and DL, wherein acceleration signals are employed for the classification of vehicles. Cost-effective and readily deployable accelerometers are employed to collect vehicle-induced bridge acceleration responses, while time-frequency analysis converts the one-dimensional signals into two-dimensional representations. The collected structural patterns are partitioned into training and testing datasets, subsequently employed to train the DCNN.

For vision-based weld line evaluation, an automated and robust approach is established for the localization and classification of the region of interest (ROI) (Sajedi and Liang 2019; Yeum et al. 2019). To automatically locate fractures, a semantic segmentation neural network is constructed based on SegNet. The accuracy rate and recall rate of several training methods, such as stochastic gradient descent (SGD), RMSprop, Adagrad, Adadelta, Adam, and Adamax, were compared. To identify cracks in concrete bridges, a Unmanned Aerial Vehicle (UAV) and Region-Based CNN(R-CNN)-based technique is proposed by Kim and Cho (2018). Crack pictures were employed to refine a pre-trained R-CNN for crack identification, and Image Processing Techniques (IPTs) were utilized to quantify the identified cracks. For the examination of post-disaster bridges, a three-level deep learning-based solution is proposed by Liang et al (2019). Faster R-CNN and SegNet were used to identify component-level and local-level damage, respectively, and VGG-16 was used to detect system-level failure.

### 2.4.5 Image classification using CNN

A very effective neural network architecture for image classification utilizing CNN.

Numerous CNN architectures have demonstrated exceptional performance in object recognition (Krizhevsky et al. 2012; Simonyan 2014). The output of the penultimate layer, referred to as asfc7, serves as a generic image descriptor for various recognition tasks, such as attribute classification and scene recognition. Developing analogous networks for videos has continued to pose difficulty. It necessitates a substantial quantity of annotated video data and considerable computer resources. Efforts have been made to design CNNs for videos (Wang et al. 2013).

Object recognition in remote sensing techniques is crucial for various applications including urban planning and environmental assessment. Recent advancements in deep learning, particularly the feature extraction using CNNs, have significantly improved object recognition capabilities (Goodfellow 2016). R-CNN, one of the earliest CNN-based algorithms, has had a profound impact on object detection by integrating selective search algorithms to generate regions of interest (ROIs) and then using CNNs for target localization (Girshick et al. 2015). Since the advent of R-CNN, numerous related models have been developed, including 2R-CNN, which refines the ROI generation process using selective search (Uijlings et al. 2013).

### 2.4.6 Dual stream CNN

In recent years, DL-based SHM methods have gained significant attention, especially in SHM. CNN is widely used in SHM. Handcrafted features derived from traditional methods inadequately describe the acquired signals, leading to suboptimal classification performance. CNNs can autonomously derive ideal damage-sensitive characteristics from raw acceleration signals, enhancing their efficacy for damage detection (Avci et al. 2017; de Rezende et al. 2020). The majority of CNN methods have acceleration signals as the main input. Other features are ignored by only one type of input signals. In order to

increase the accuracy of damage detection for bridges, dual-stream CNN was developed as a novel technique for simultaneously integrating vibration response from bridge and vehicle (Ye et al. 2015). Dual-stream CNN reads the date from these two sources in parallel and it is used for the condition evaluation with feature fusion (Yang et al. 2021), which facilitates a more thorough evaluation of the bridge's structural integrity. Xu et al (2024) introduced a method that integrates the one-dimensional FFT spectrum with the two-dimensional time-frequency representation of bearing vibration. These inputs are fed into the model's 1D-CNN and 2D-CNN channels for separate feature extraction, after which the extracted features are fused. Ni et al (2024) proposed using CWT and STFT spectra of bearing vibration signals as input channels for 2D-CNNs to effectively detect bearing faults.

### 2.5 Summary and research gaps

Recently, many data-driven methods advanced signal processing techniques have been developed for structure health monitoring. This project is to develop a novel approach for VBI based SHM. A little research has been conducted on this topic. There are two types of vehicle assisted SHM methods: direct and indirect. The direct approach is to install a group of sensors on bridges for SHM. The indirect approach is to instrument the vehicle, and the dynamic properties of the bridge structure are collected using the passing instrumented vehicle as "drive-by" approach (Tan et al. 2019). Damage detection with traditional direct approach has a large cost for sensor installation and maintenance, whereas the indirect approach only needs the installation of one or a few vibration sensors on the test vehicle. As a result, the indirect approach provides considerable mobility, low-cost, and high efficiency. Several studies have been carried out to investigate the use of instrumented vehicles for bridge damage detection. Numerical simulations have shown

that it is an efficient technique (Shokravi et al. 2020). The challenges and limitations in this topic are summarized as follows:

1) The traditional deep learning-based approach required a large number of high-quality training data (Abdeljaber et al. 2017). For structure health monitoring, acquiring the training data is challenging or unfeasible. for all damage scenarios in practice. Numerical simulations are normally used to generate synthetic data.

2) The variations in operational environments significantly impact the outcomes of bridge condition assessments, particularly for bridges subjected to traffic-induced excitations. The conventional evaluation of bridge conditions assumes that traffic excitation behaves as white noise. The temporal and spatial information about the traffic excitation is not considered. This will significantly affect the structural damage identification accuracy.

3) For traditional bridge health monitoring systems, the sensory systems are installed on the bridge with cables. The expenses associated with the installation and upkeep of the monitoring system are considerable.

4) Despite the vast volume of work described in SHM, it is limited to modest and academic issues. The reliable and accurate bridge damage detection is still a major challenge as there is high noisy in the large volume of measurement data.

This project aims to address these research gaps. A SHM method based on VBI will be developed. The car traversing the bridge constitutes a time-varying process. The wireless sensor network is utilized to observe the dynamic responses of VBI systems. Advanced signal processing methodologies will be devised to elucidate the time-varying properties of the VBI system. Then the machine learning models will be used to predict the condition of the bridge.

# CHAPTER 3 Time-frequency characteristics of dynamic responses from a passing vehicle using second order-synchrosqueezing transform

## 3.1 Overview:

In modern transportation infrastructure, bridges serve as critical connectors between different regions, playing an essential role in the smooth flow of economic and social activities. The health and integrity of bridges directly affect the safety and efficiency of transportation networks. Thus, their stability and safety are of paramount importance. With increasing awareness of bridge health monitoring, VBI analysis has become a core research direction in this field.

The vehicle traveling over the bridge constitutes a dynamic, time-varying process. This chapter aims to develop an SST2-based approach to extract time-varying characteristics from an instrumented vehicle for indirect bridge condition assessment. By comparing the conventional SST, the SST2-based method offers a more refined and accurate TFR. The study initially evaluated the influence of various factors on the time-varying features of VBI systems, including vehicle mass, speed, damping, road surface conditions, measurement noise, and different damage scenarios. The time-dependent features relevant to indirect bridge condition evaluation are explored.

The results demonstrate the accuracy of SST2 in capturing time-varying characteristics for effective bridge condition assessment. The proposed method's performance has been validated through numerical simulations and experimental testing. The method offers a fresh perspective and advanced tool for VBI system analysis, improving the overall accuracy and efficiency of bridge health monitoring in real-world applications.

## 3.2 Theory

### 3.2.1 Vehicle-bridge interaction systems

#### 3.2.1.1 The VBI modeling

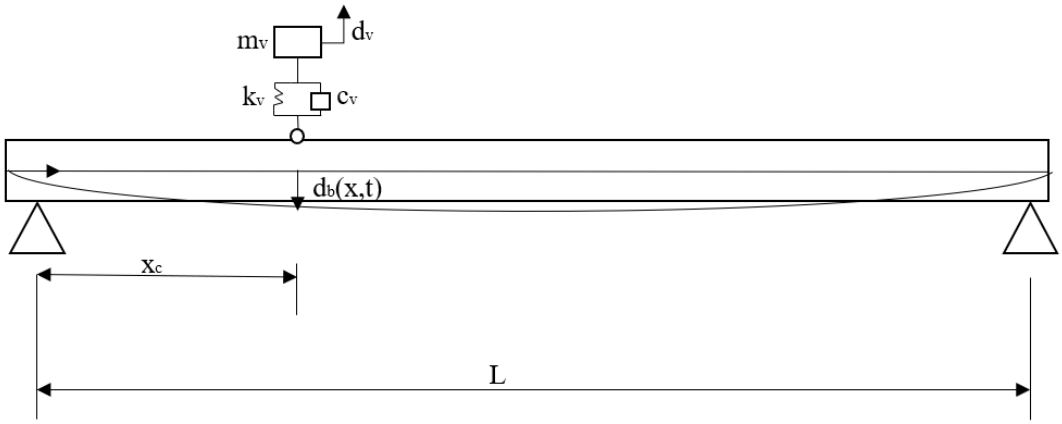


Figure 3-1 Vehicle-bridge interaction model

Figure 3-1 illustrates The VBI system is represented as a continuous uniform beam affected by a moving vehicle. The vehicle is assumed to travel in the longitudinal direction of the bridge at a constant speed $v$. The simply supported bridge is analyzed utilizing a finite element method. The equations that dictate the dynamics of the bridge and vehicle subsystems are articulated as follows (Li et al. 2020),

$$m_v\ddot{d}_v(t) + c_v\dot{d}_v(t) + k_v d_v(t) = P_{vint}(t) \tag{3-1}$$

$$\mathbf{M}_b\ddot{\mathbf{d}}_b(t) + \mathbf{C}_b\dot{\mathbf{d}}_b(t) + \mathbf{K}_b\mathbf{d}_b(t) = \mathbf{H}_c(t)P_{\text{bint}}(t) \tag{3-2}$$

where $\ddot{d}_v, \dot{d}_v, d_v$ are represent the vehicle's vertical acceleration, speed, and displacement responses, respectively. Similarly, $\ddot{\mathbf{d}}_b, \dot{\boldsymbol{d}}_b, \boldsymbol{d}_b$ denotes the vertical acceleration, velocity and displacement responses of the bridge, respectively. $\mathbf{M}_b$, $\mathbf{C}_b$, $\mathbf{K}_b$ correspond to the mass, damping, and stiffness properties of the bridge, respectively. $P_{vint}(t) =$

$k_v d_{cp}(t) + c_v \dot{d}_{cp}(t)$ represents the force exerted on the vehicle system at the interface between the vehicle and the bridge. $d_{cp}(t) = d_b(x(t), t) + r(x(t))$ represents the contact displacement between the vehicle and the bridge at the position $x(t)$. $r(x)$ denotes the roughness of the road surface. $P_{\text{bint}}(t) = m_v g - P_{vint}$. $P_{\text{bint}}(t)$ represents the force exerted by the vehicle on the bridge. $\mathbf{H}_c(t) = \{\mathbf{0},\ \mathbf{0},\ \dots,\ \boldsymbol{H_i}(t), \dots,\ \mathbf{0}\}^T$ is a Hermitian cubic interpolation function of time. $\boldsymbol{H}_i(t)$ denotes the vector of the shape function in the *ith* element where the moving vehicle is situated at time *t,*

$$\boldsymbol{H}_i(t) = \{1 - 3\xi(t)^2 + 2\xi(t), (\xi(t) - 2\xi(t)^2 + \xi(t)^3)l_e, 3\xi(t)^2 - 2\xi(t)^3, (-\xi(t)^2 + \xi(t)^3)l_e\}^T \tag{3-3}$$

where $\xi(t) = (x(t) - (\mathrm{i} - 1)l_e)/l_e$. (i-1) $l_e \le x(t) \le i l_e$. $l_e$ is the length of the element.

### 3.2.1.2 The non-stationary dynamic characteristics of VBI system

The equation of motion for the VBI system can be obtained as

$$\begin{bmatrix} \mathbf{M}_b & m_v \mathbf{H}_c \\ 0 & m_v \end{bmatrix} \begin{Bmatrix} \ddot{\mathbf{d}}_b \\ \ddot{d}_v \end{Bmatrix} + \begin{bmatrix} \mathbf{C}_b & 0 \\ -c_v \mathbf{H}_c^T & c_v \end{bmatrix} \begin{Bmatrix} \dot{\mathbf{d}}_b \\ \dot{d}_v \end{Bmatrix} + \begin{bmatrix} \mathbf{K}_b & 0 \\ -k_v \mathbf{H}_c^T - c_v \dot{\mathbf{H}}_c^T & k_v \end{bmatrix} \begin{Bmatrix} \mathbf{d}_b \\ d_v \end{Bmatrix} = \begin{Bmatrix} \mathbf{H}_c m_v g \\ k_v r(x) + c_v v r'(x) \end{Bmatrix} \tag{3-4}$$

where *r(x)* denotes the surface roughness profile of the bridge deck. In Eq. (3-4), the system matrices of the interaction system exhibit temporal dependence. contingent upon the vehicle's location, and the system's frequencies fluctuate with time.

The derivation involves simplifying the VBI system's equations of motion into two uncoupled second-order differential equations (Yang et al. 2013). By solving the

associated eigenvalue problem, the instantaneous frequencies of the system are obtained. The analytical solutions for these frequencies are given as follows:

When $\omega_{v0} > \omega_{b0}$, the IF of the vehicle is:

$$\omega_v^2(t) = \frac{1}{2}\left( \omega_{v0}^2 + \omega_{b0}^2 + \frac{m_v \omega_{v0}^2}{m_b L} \sin^2\left(\frac{\pi x_c(t)}{L}\right) + \sqrt{\left(\omega_{v0}^2 + \omega_{b0}^2 + \frac{m_v \omega_{v0}^2}{m_b L} \sin^2\left(\frac{\pi x_c(t)}{L}\right)\right)^2 - 4\omega_{v0}^2 \omega_{b0}^2} \right) \tag{3-5}$$

The instantaneous frequency of the bridge is:

$$\omega_b^2(t) = \frac{1}{2}\left( \omega_{v0}^2 + \omega_{b0}^2 + \frac{m_v \omega_{v0}^2}{m_b L} \sin^2\left(\frac{\pi x_c(t)}{L}\right) - \sqrt{\left(\omega_{v0}^2 + \omega_{b0}^2 + \frac{m_v \omega_{v0}^2}{m_b L} \sin^2\left(\frac{\pi x_c(t)}{L}\right)\right)^2 - 4\omega_{v0}^2 \omega_{b0}^2} \right) \tag{3-6}$$

When $\omega_{v0} < \omega_{b0}$, the instantaneous frequency of the vehicle is:

$$\omega_v^2(t) = \frac{1}{2}\left( \omega_{v0}^2 + \omega_{b0}^2 + \frac{m_v \omega_{v0}^2}{m_b L} \sin^2\left(\frac{\pi x_c(t)}{L}\right) - \sqrt{\left(\omega_{v0}^2 + \omega_{b0}^2 + \frac{m_v \omega_{v0}^2}{m_b L} \sin^2\left(\frac{\pi x_c(t)}{L}\right)\right)^2 - 4\omega_{v0}^2 \omega_{b0}^2} \right) \tag{3-7}$$

The IF of the bridge is:

$$\omega_b^2(t) = \frac{1}{2}\left( \omega_{v0}^2 + \omega_{b0}^2 + \frac{m_v \omega_{v0}^2}{m_b L} \sin^2\left(\frac{\pi x_c(t)}{L}\right) +$$

$$\sqrt{\sqrt{\left(\omega_{v0}^2+\omega_{b0}^2+\frac{m_v\omega_{v0}^2}{m_bL}\sin^2\left(\frac{\pi x_c(t)}{L}\right)\right)^2-4\omega_{v0}^2\omega_{b0}^2}} \quad (3\text{-}8)$$

where $\omega_{v0}$ denotes the vehicle's inherent frequency. $\omega_{b0}$ denotes the bridge's inherent frequency. $m_v$ is the mass of the vehicle. $m_b$ is the mass of the bridge. $L$ represents bridge's length. $x_c(t)$ denotes the vehicle's position on the bridge as a function of time.

#### 3.2.1.3 Damage simulation for reinforced concrete beams

According to Abdel Wahab et al (1999), the damage zone in reinforced concrete beams can be defined as a reduction in rigidity.

$$EI(x)=E_0I\left(1-\alpha\cos^2\left(\frac{\pi}{2}\left(\frac{|x-l_c|}{\beta L/2}\right)^m\right)\right),\quad \text{for } l_c-\beta L/2<x<l_c+\beta L/2 \quad (3\text{-}9)$$

In Eq. (3-9), the damage extent is quantified using three parameters: $\alpha, \beta$, and $m$. The variable $l_c$ indicates the midpoint of the damage area along the beam, commencing at the left support. The parameter $\beta$ indicates the relative length of the damage zone along the beam, with possible values between 0.0 and 1.0. The parameter $\alpha$ gauges the damage's intensity, where 0.0 means no damage and 1.0 signifies complete loss of bending stiffness in the middle of the damaged area. The $m$ parameter is related to the variation in Young's modulus from the center of the damage zone towards its edges. $E_0$ represents the initial modulus of elasticity of the undamaged beam.

### 3.2.2 Sychrosqueezing transform (SST)

SST is a TFA method. There are two types of SST approaches, such as based on STFT or CWT. In this study, the STFT based approach is adopted. The measurement signal represented as $s(t)$ and it may refer to the reaction of a vehicle traversing a bridge, or

the reaction of the bridge to the moving vehicle. The car traversing the bridge constitutes a time-varying process, $s(t)$ is a non-stationary multicomponent signal. The signal can be expressed as the superposition of the intrinsic mode functions (IMFs) as,

$$s(t) = \sum_{k=1}^{N} A_k(t) e^{i\varphi_k(t)} \tag{3-10}$$

The STFT of the signal $s(t)$ with a window function $g(t) \in L^2(\mathbb{R})$ is defined as,

$$G(t,\omega) = \sum_{k=1}^{N} \int_{-\infty}^{\infty} A_k(\tau) e^{i\phi_k(\tau)} g(\tau - t) e^{-i\omega\tau} d\tau \tag{3-11}$$

where $G(t,\omega)$ is a time-frequency spectrum at a specific time $t$ and frequency $\omega$. It incorporates contributions from each component of the signal, specified as IMF. The $k$-th IMF is defined as its amplitude $A_k(\tau)$ and phase $\phi_k(\tau)$ at any given time $\tau$. To effectively localize the signal in time, a window function $g(\tau - t)$ is centered around the time $t$. The frequency variable $\omega$ in the Fourier transform helps convert the time-domain signal into its frequency components, providing a time-frequency spectrum of the signal.

$$G(t,\omega) = \sum_{k=1}^{N} A_k(t) e^{i\phi_k(t)} \int_{-\infty}^{\infty} g(\tau - t) e^{-i(\omega - \phi_k'(t))\tau} d\tau \tag{3-12}$$

where $\phi_k'(t)$ is first derivative of the phase of the $k$-th IMF, representing the IF of the $k$-th component at time $t$.

Then, IF estimation is determined as,

$$\omega'(t,\omega) = \frac{\partial}{\partial t} \arg\left(G(t,\omega)\right) \tag{3-13}$$

where $\omega'(t,\omega)$ is the IF at time $t$ and frequency $\omega$, derived from the phase derivative

of the STFT.

SST operates through a frequency reassignment operator, concentrating the dispersed time-frequency coefficients in the STFT results to a compact region near the IF trajectories of each mode. The formula is:

$$sst(t,\omega') = \int_{-\infty}^{\infty} G(t,\omega)\delta(\omega' - \omega'(t,\omega))d\omega \tag{3-14}$$

### 3.2.3 Second-order synchrosqueezing transform (SST2)

SST2 is an enhancement of the basic SST (Behera et al. 2018), specifically designed to better handle signals with rapidly changing frequencies. In SST2, new complex reassignment operators, $\Phi_f(t,\omega)$ and $\tau_f(t,\omega)$, are introduced. These operators capture the high-order variations in the frequency and time of the signal, respectively.

SST2 employs a second-order local modulation operator $q_{2,f}(t,\omega)$. It is defined as the ratio of the derivative of the original IF estimate $\omega_f(t,\omega)$ to the derivative of $\tau_f(t,\omega)$, provided that the derivative of $\tau_f(t,\omega)$ is non-zero. The new IF estimate, $\omega_f^{[2]}(t,\omega)$, combines the original IF estimate with adjustments from the local modulation operator, reflecting higher-order changes in the frequency and time domains. This estimate is used when $\partial_t\tau_f(t,\omega) \neq 0$; otherwise, the original IF estimate $\omega_f(t,\omega)$ is used.

The final formula for SST2 is given as:

$$T_{2,f}^{g,\gamma}(t,\omega) = \frac{1}{g^*(0)}\int_{\eta,\left|V_f^g(t,\eta)\right|>\gamma} G(t,\eta)\delta\left(\omega - \omega_f^{[2]}(t,\eta)\right)d\eta \tag{3-15}$$

Here, $G(t,\eta)$ is the result of the STFT, and $g^*(0)$ is the conjugation of the window function at zero frequency. The parameter $\gamma$ serves as a threshold for focusing energy

concentration.

SST2 enhances the clarity and precision of the TFR of signals, especially those with rapidly varying frequencies, making it a valuable tool in areas like audio signal processing and seismic analysis. In this study, it is used for VBI analysis.

### 3.2.4 Ridge detection

TFR is an instrument for examining the variations in temporal frequency components of a signal. (Thakur et al. 2013). In numerous applications, including signal processing, speech recognition, and image processing, it is essential to identify and monitor the temporal variations of specific frequency components inside a signal. Nonetheless, the frequency components of a signal frequently fluctuate over time, necessitating a method that can accurately extract these time-varying characteristics.

Brevdo et al (2011) employed ridge detection technology to identify the optimal frequency curve in the TFR $\Omega(t)$. Ridge detection is a stable visual feature extraction technique that can extract the TFR with a high resolution and find the best frequency curve. The method is to find an optimal frequency curve, $\Omega(\mathrm{t})$, in the TFR $S_x$, and the energy under this frequency curve is maximized while also satisfying a smoothness constraint, implemented by a complete variation penalization term. The formula is as follows:

$$\hat{\Omega} = \underset{\Omega}{\operatorname{argmax}} \left( \int_R |S_x(t, \Omega(t))|^2 dt - \lambda \int_R \left| \frac{d\Omega}{dt}(t) \right|^2 dt \right) \tag{3-16}$$

In this formula, $S_x(t, \Omega(t))$ represents the squared magnitude of the TFR at time $t$ and frequency $\Omega(\mathrm{t})$. The first term $\int_R |S_x(t, \Omega(t))|^2 dt$ represents the total energy along the

frequency curve $\Omega(t)$ within the entire signal range $R$, and the second term $-\lambda\int_R \left|\frac{d\Omega}{dt}(t)\right|^2 dt$ is the integral of the square of the rate of change of the frequency curve, with $\lambda$ adjusting the strength of the smoothness constraint. The method lies in its ability to accurately extract time-varying characteristics from complex signals, which is very useful in fields like signal analysis, feature extraction, and pattern recognition. This method provides us with a powerful tool for analyzing and understanding the time-frequency characteristics of signals.

### 3.2.5. Signal verification

To show the performance of SST2 for TFA, the following non-stationary signal is used as an example.

$$x(t) = \cos\big(2\pi \times (0.1t^{2.6} + 3\sin(2t) + 10t)\big) + e^{-0.2t}\cos\,(2\pi \times (40 + t^{1.3})t) \tag{3-17}$$

Figure 3-2 shows the non-stationary signal and its TFRs using SST and SST2. Figure 3-2(a) shows the non-stationary signal $x(t)$. The TFRs using SST and SST2 are shown in Figures 3-2(b) and 3-2(c) respectively. Compared the result using SST, the energy concentration of its TFR is significantly enhanced by the incorporation of the signal's second-order derivative information in SST2. This improvement is attributed to its precise tracking of rapid frequency variations over time, such as the signal component $e^{-0.2t}\cos\,(2\pi(40 + t^{1.3})t)$. It results in a more concentrated energy allocation in the time-frequency domain, reduces the ambiguity, and increases the resolution.

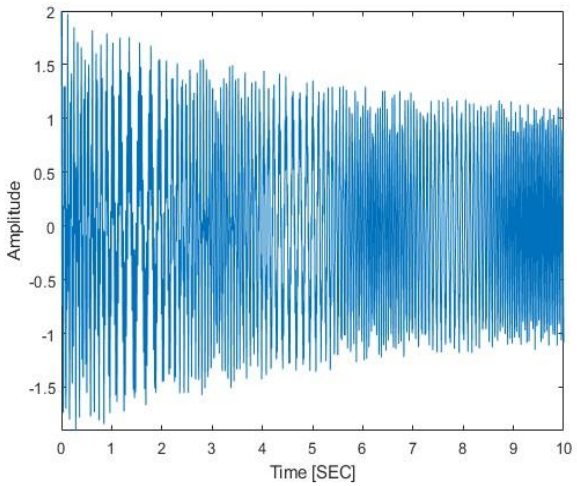


(a) The non-stationary signal

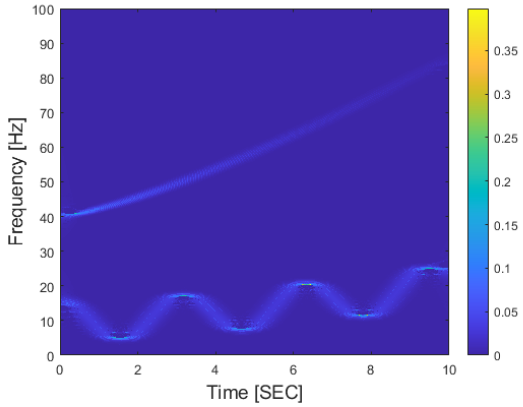


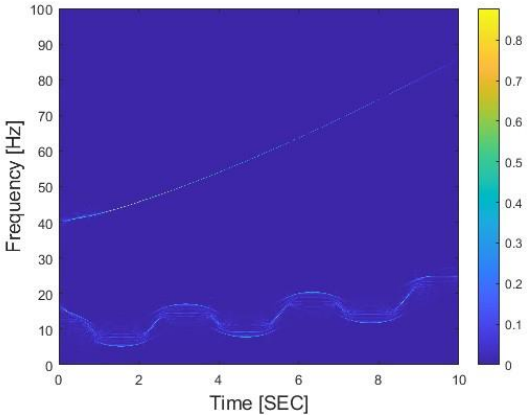


(b) TFR using SST (c) TFR using SST2

Figure 3-2 non-stationary signal under SST and SST2

Furthermore, compared with SST, SST2 has a high proficiency in dissecting complex modalities and frequency evolutions. SST is difficult to process the signal with the compound frequency variations, such as the nonlinear frequency shifts induced by $0.1t^{2.6}$ and $t^{1.3}$. The frequency variations can be accurately captured and represented by

the high-order information of SST2. SST2 enables to reveal the signal's intricate time-frequency characteristics in detail, especially for analyzing signals with rapid frequency shifts and transient features.

As above, the ability of SST2 to capture signal details, especially its sensitivity to transient changes and faint signal components, further confirms its advantages in the analysis of non-stationary signals. Transient components like $3\sin(2t)$ and the exponential decay term $e^{-0.2t}$ are captured with greater precision by SST2, reflecting its powerful capacity to provide detailed insights into the dynamic variations within the signal. Through this advanced time-frequency analysis, SST2 not only improves the clarity of the time-frequency plot but also enhances the understanding of the signal's inherent dynamic changes, showcasing significant improvements and efficient capabilities in handling complex non-stationary signals.

### 3.3. Numerical study

In this section, the acceleration data for a bridge under various loading and damage conditions are simulated. The data are then analyzed using the SST method to identify and quantify time-varying features for damage detection. This methodology's accuracy was tested through a series of numerical simulations.

#### 3.3.1 Vehicle-bridge interaction models

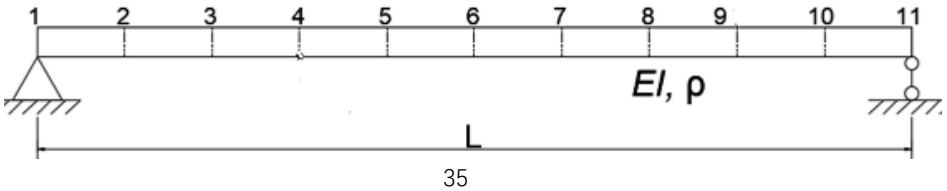

Figure 3-3 Finite element model of the bridge

Figure 3-1 illustrates the vehicle-bridge interaction system, which is simplified to a simply-supported bridge experiencing a moving vehicle at a constant velocity v. The bridge is represented as a finite element model, as illustrated in Figure 3-3. The simply-supported bridge is represented as a finite element model. The vehicle is represented as a quarter-vehicle model with two degrees of freedom. It encompasses fundamental dynamics of vehicle-bridge interaction systems, including critical parameters such as the mass, stiffness, and damping coefficients of the vehicle, as well as the bridge's mass, rigidity, and damping. Tables 3-1 and 2 enumerate the vehicle and bridge parameters utilized in this study. (Li et al. 2020). The natural frequency of the vehicle is 3.20Hz. The Rayleigh damping of the bridge is assumed with $\mathbf{C}_b = \alpha_1 \mathbf{M}_b + \alpha_2 \mathbf{K}_b$ and $\alpha_1 = 0.243, \alpha_1 = 0.0001$, where $\mathbf{M}_b, \mathbf{C}_b$ and $\mathbf{K}_\mathrm{b}$ are the mass, damping and stiffness matrices of the bridge in Eq. (3-2) respectively.

Table 3-1 Vehicle parameters

| Parameters | Description | Values |
|---|---|---|
| $m_v$ | Mass of the vehicle | 7000 kg |
| $k_v$ | Stiffness of the vehicle suspension system | 2.82e+6 N/m |
| $c_v$ | Damping of the vehicle suspension system | 390 Ns/m |

Table 3-2 Bridge parameters

| Parameters | Description | Value |
|---|---|---|
| L | Length of the bridge | 30 m |
| EI | Flexural rigidity of the bridge | 2.5e+10 Nm² |
| pa | Mass per unit length of the bridge | 6.0e+3 kg/m |
| h | Height | 1 m |

### 3.3.2 Responses of VBI systems

Numerical simulations in this study are conducted with a focused approach, considering a limited yet essential set of parameters, thus providing a clear understanding of VBI dynamics. Despite its simplicity, the quarter-vehicle model with two degrees of freedom effectively captures fundamental aspects of VBI, offering insights into how vehicle and bridge masses, along with suspension stiffness and damping, affect the system's overall behavior that is dynamic. This study derives the response of the VBI by solving the coupled VBI Eq. (3-4) using the Newmark-β method. The sampling rate is 500 Hz. The vehicle speed is 2 m/s. To simulate measurement data with a SNR of 26, the 5% white noise is added to the calculated acceleration as below,

$$acc_m = acc_{cal} + E_p \times N_{\text{oise}} \times \sigma(acc_{cal}) \quad (3\text{-}12)$$

where $acc_{cal}$ denotes the computed acceleration response. $E_p$ denotes the intensity of white noise. $N_{\text{oise}}$ is a vector that aligns with a standard normal distribution, characterized by having a zero average and a variance of one. $\sigma(acc_{cal})$ represents the standard deviation of the computed acceleration.

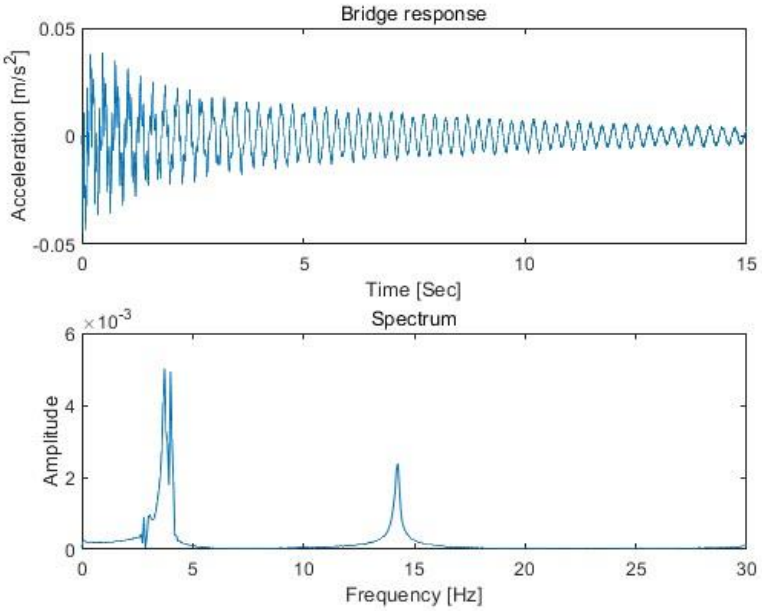


Figure 3-4 Response of the bridge at Node 4 and its spectrum

Figure 3-4 illustrates the bridge's reaction at Node 4 along with its spectrum. Two principal peaks are identified at around 3.55 Hz and 13.40 Hz in the figure, which nearly align with the first two natural frequencies of the bridge. Figure 3-5 depicts the vehicle's response and its spectrum, indicating a peak of about 3.20 Hz, which aligns with the vehicle's natural frequency.

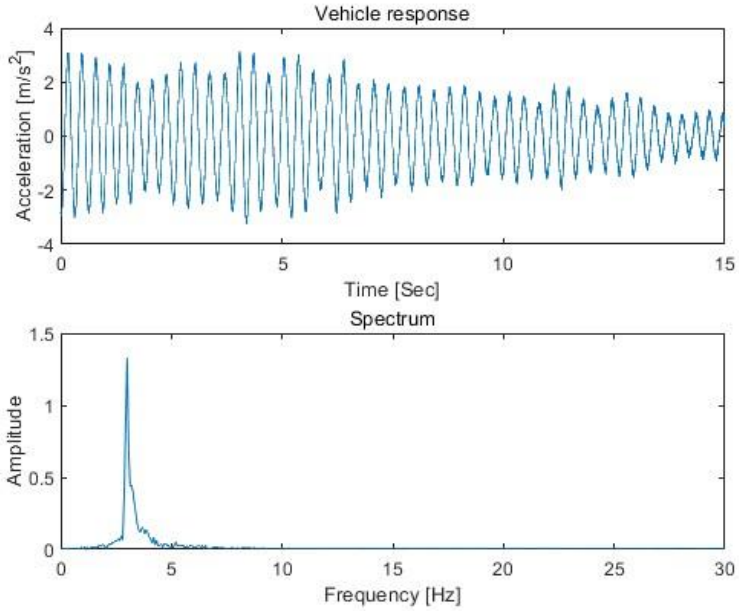


Figure 3-5 Vehicle response and its spectrum

### 3.3.3 Comparison of results using SST2 and SST

In this section, SST and SST2 are used to extract the time-varying features of the VBI systems. the responses of the vehicle passing over the bridge are used in the analysis. The results are compared to demonstrate the performance of these two techniques in this section.

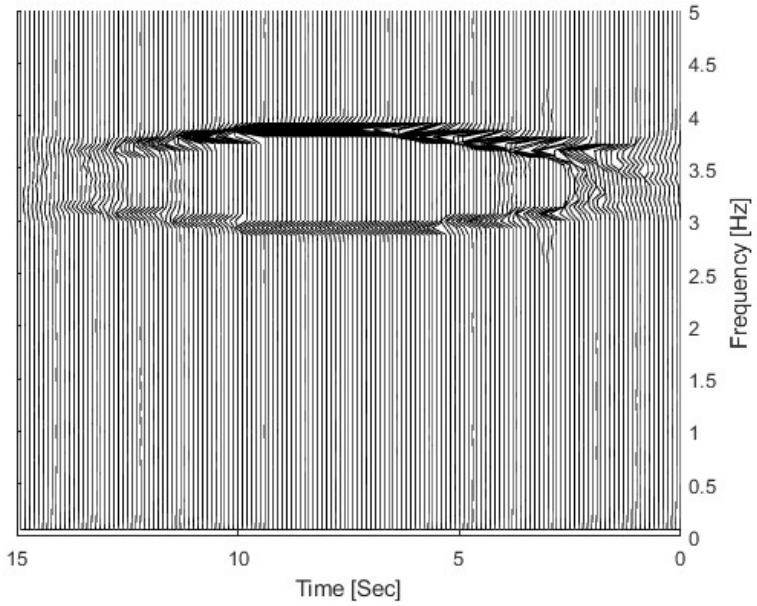


Figure 3-6 TFR of the vehicle response using SST

TFR spectrograms are obtained using SST and SST2 as shown in Figures 3-6 and 3-7. Figure 3-6 shows the TFR of vehicle response using SST. Figure 3-7 shows TFR of the vehicle response using SST2. As shown in figures, there are trajectories around 3.5 Hz. One trajectory is above 3.5 Hz and another one is below it. Compared the result using SST in Figure 3-6, the trajectories by SST2 in Figure 3-7 are thinner. That means the spectral energy is much concentrated by SST2. This improvement in concentration refers to SST2's more effective sharpening of the signal's energy distribution within the time-frequency domain. Specifically, SST2 employs an advanced algorithm that not only considers the first-order instantaneous frequency information of the signal but also incorporates the information from the second-order derivative. This allows SST2 to track the signal's instantaneous frequency changes more precisely. Such an approach is particularly suited for handling signal features that change rapidly over time, as it can reduce blurring and leakage, thus making the signal's local features more pronounced and

clearer in the time-frequency spectrogram.

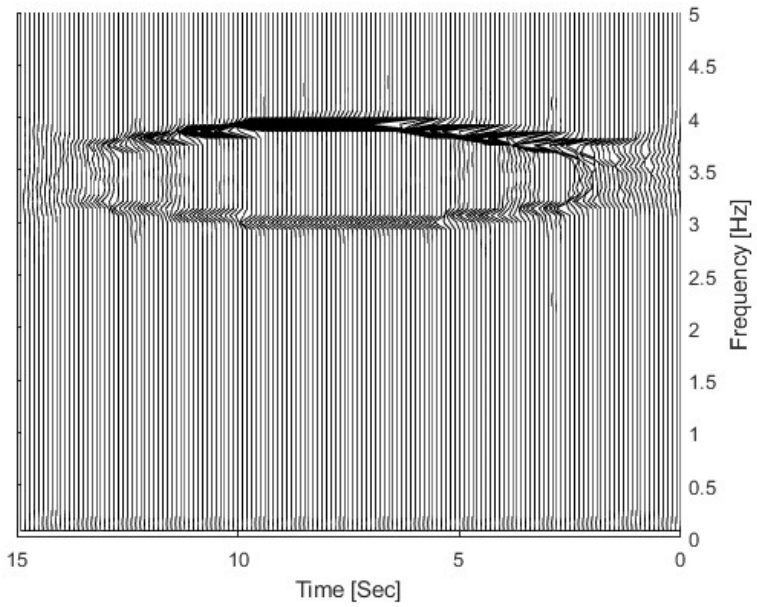


Figure 3-7 TFR of the vehicle response using SST2

Using the ridge detection in Section 3.2.4, the time-varying characteristics of the response can be extracted, that is the IF. Figure 3-8 shows the time-varying characteristics computed using SST and SST2. In the figure, the black line is the theoretical values using Eqs. (3-5) to (3-8). The blue line depicts IF remains using SST2 and the red line is the result using SST.

As the vehicle frequency is 3.2 Hz is lower than that of the first natural frequency of the bridge 3.5 Hz, Eqs. (3-7) and (3-8) are used to calculate the theoretical instantaneous frequencies (IFs). As shown in Figure 3-8, the results using SST and STT2 are close to the theoretical value. The curve above 3.5 Hz is corresponding to the IF of the bridge and another one below it is related to the IF of the vehicle. The result using SST2 is stable over most of the timeline, with abrupt changes at certain moments. This suggests that for the majority of the time, the bridge maintains consistent vibrational characteristics under

the dynamic load of vehicles, but at specific times, these characteristics undergo significant shifts due to external factors or changes within the system itself. Red line represents the IF using SST, which changes smoothly over time without the sharp transitions. Additionally, the frequency values in the same sections of the timeline are lower compared with those using SST2. This might indicate that the SST method captures the dynamic changes of the system more continuously when dealing with such loads, although it seems less sensitive to abrupt changes or might provide more conservative frequency estimates for signals with higher frequency variations.

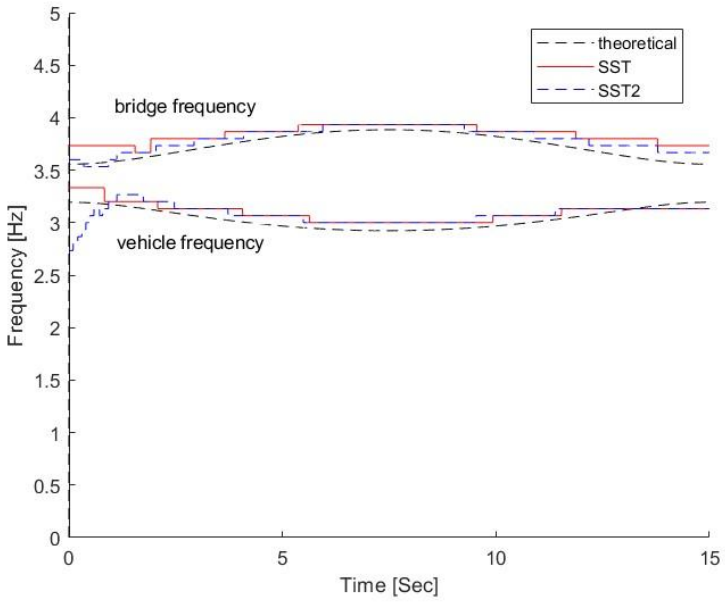


Figure 3-8 IFs of the vehicle response using SST2

To quantitatively evaluate the difference of IFs, the mean squared error (MSE) between the estimated and theoretical frequency curves is used an indicator for the performance of SST and SST2 methods. As shown in Figure 3-8, three distinct curves are compared: the theoretical frequency (black dashed line), SST-estimated frequency (blue dashed line),

and SST2-estimated frequency (red dashed line). The MSE values are computed over the period 0-15 seconds to ensure sufficient temporal resolution for bridge vibration analysis. The results show that SST2 achieves significantly lower MSE value 0.0066 compared to conventional SST 0.0158. The results confirm its superior capability in precisely extracting time-varying frequency components. SST2 effectively captures time-varying characteristics through its iterative compression approach.

### 3.3.4 Effect of VBI system parameters

#### 3.3.4.1 Effect of road surface roughness on VBI system

In this section, the impact of road surface roughness on VBI is explored. By examining how various levels of surface roughness affect vehicle response, the study aimed to deepen the comprehension of how road conditions affect the overall dynamics of the VBI system based SST2.

The study involved selecting road surfaces with varying degrees of roughness, ranging from smooth to more rugged (ISO 8086, 1995). Other parameters are the same as that in Section 3.3.3. The acceleration responses of the vehicle passing over the bridge with different road surface roughness are studied using SST2.

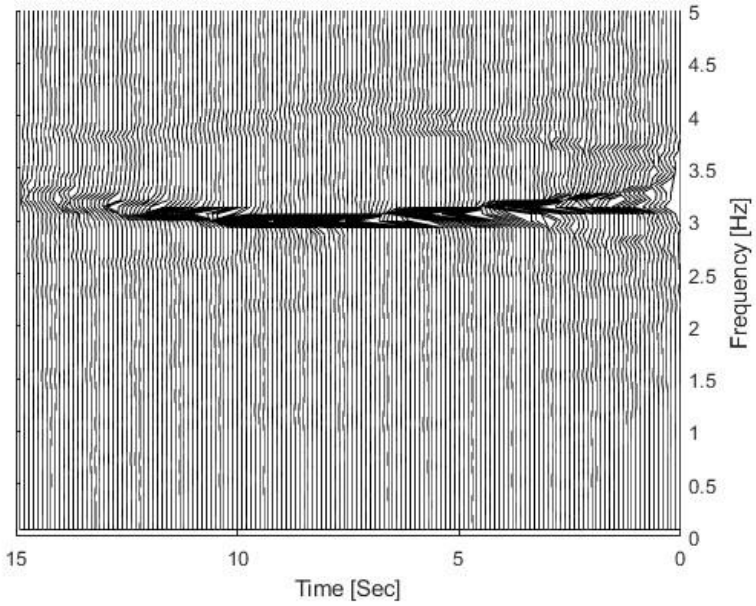


Figure 3-9 TFR of the response with Level B roughness using SST2

Figure 3-9 illustrates the TFR of the vehicle response with Level B roughness using SST2. Compared with Figure 3-7, the curve below 3.5 Hz is highlighted, and it shows the vehicle response component is dominated with a high energy. A high roughness road surface makes the vehicle response component dominated. On irregular roads, the vehicle's response displayed elevated frequency components and greater amplitude fluctuations, presumably resulting from intensified vibrations and shocks from the rugged terrain.

Figure 3-10 shows IFs of the responses from the vehicle passing over the bridges with different road surface roughness. Two road roughness classes A and B are studied. The results show that the IF with high road roughness is more concentrated and intense, exhibiting greater variations and anomalies than that with low road roughness. The uneven road surface establishes a more intricate, dynamic connection between the vehicle and the bridge. When roughness is minimal, the TFR exhibits more uniformity and

linearity, resulting in reduced vehicular shock during operation and a stable dynamic response of the system. The current frequencies of the bridge and vehicle vary considerably during the traversal under high roughness circumstances, with the most substantial frequency discrepancies occurring in the mid and late phases of the crossing.

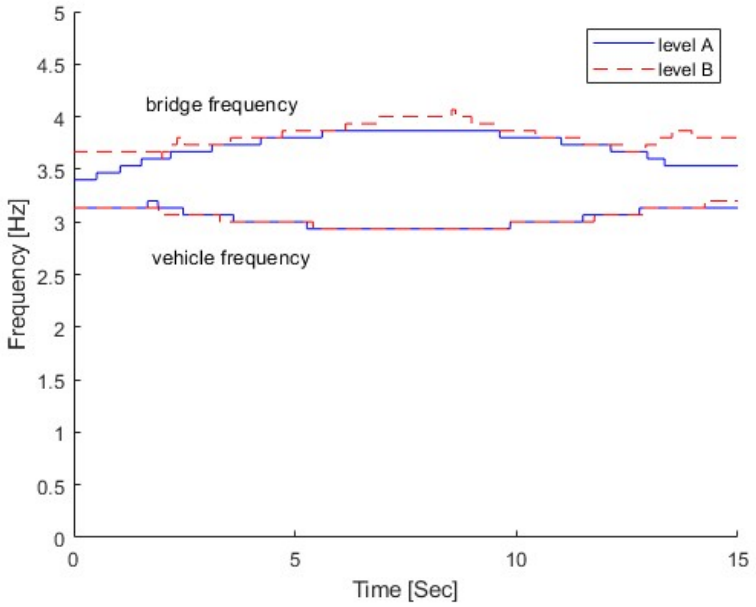


Figure 3-10 IFs of responses with different road surface roughness

### 3.3.4.2 Effect of the vehicle speed

The vehicle's responsiveness is influenced by its speed of motion. This section examines the influence of vehicle speed on the time-varying properties of the vehicle-bridge interaction system using SST2. Two distinct velocities, $\boldsymbol{v}$ =3 m/s and $\boldsymbol{v}$ =4 m/s, are examined. All other parameters are identical to those in Section 3.3.3.

Figures 3-11 and 3-12 show the TFRs of the vehicle responses with *v=3 m/s* and *4 m/s* respectively. From Figures 3-11 and 3-12, the frequency curves for both speeds are clearly identified. The frequency curve includes the bridge frequency above 3.5 Hz and the vehicle frequency below 3.5 Hz. Compared with that with the higher speed (4 m/s), the

result at a lower speed (3 m/s) is very clear and the frequency distribution is much concentrated. Also, the bridge frequency component is highlighted. This indicates the bridge response component with high energy at lower speeds. At a higher speed (4 m/s), the frequency distribution is much broader, particularly in the mid to high frequency spectra, where the frequency lines show noticeable spreading and blurring. This reflects higher dynamic activity. The wide frequency distribution demonstrates that the interaction between the vehicle and the bridge structure becomes increasingly intricate at elevated speeds, exciting more vibrational modes.

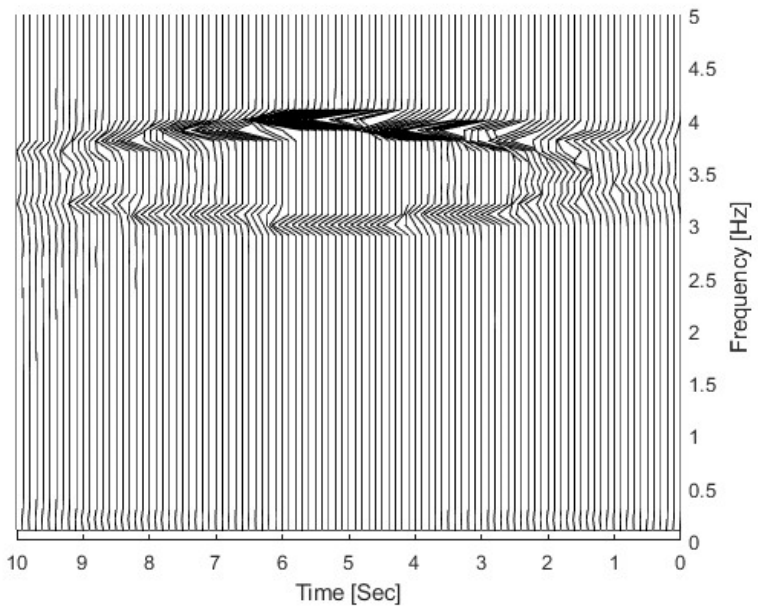


Figure 3-11 TFR of SST2 with the vehicle speed *v=3 m/s*

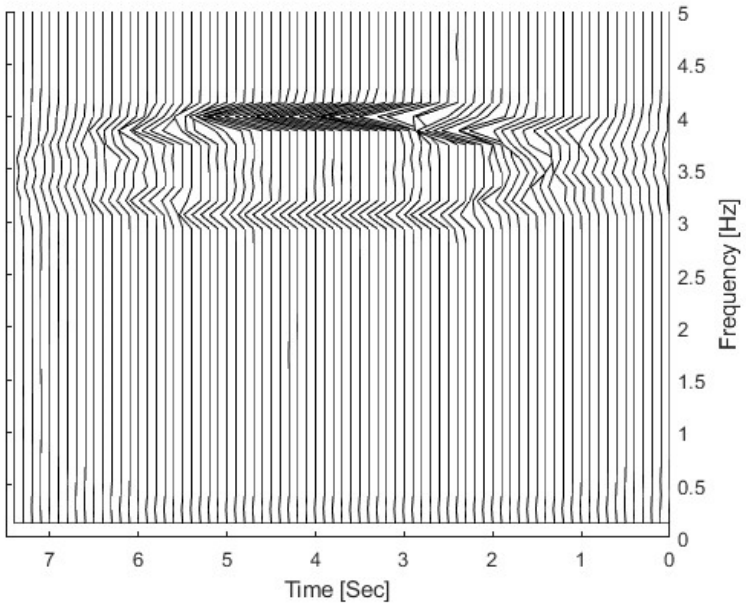


Figure 3-12 TFR of SST2 with the speed *v=4 m/s*

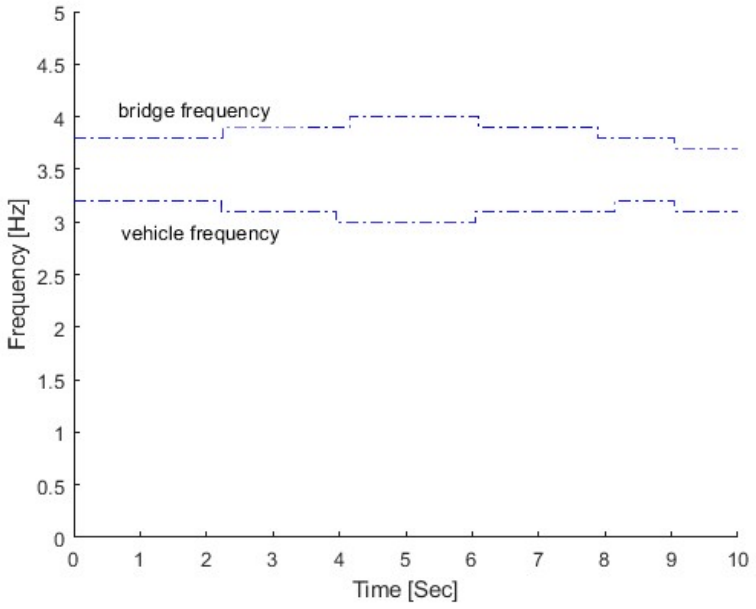


Figure 3-13 IF of SST2 with the speed *v=3 m/s*

Figures 3-13 and 3-14 show their corresponding IFs. Both bridge and vehicle IFs are clearly identified using SST2. Sampling frequency is 500Hz, from the result, the changes in the time-frequency spectrum are more abrupt at a higher speed, with frequency lines rapidly changing and spreading, indicating that the vehicle's rapid movement triggers more structural responses, increasing the dynamic stress and vibrational disturbances the

bridge may encounter.

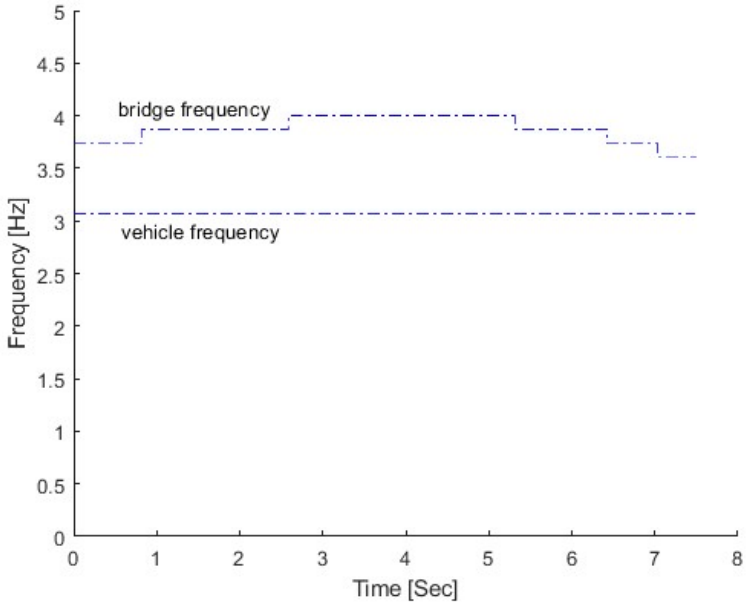


Figure 3-14 IF using SST2 with the speed *v=4 m/s*

### 3.3.5 Time-varying characteristics of VBI systems for bridge damage detection

In this section, time-varying features of VBI systems are analysed using SST2. Two damage scenarios are simulated, e.g. small and large damage scenarios. The damage location is at one-third of the length along the bridge. The small damage is characterized by α=0.3, β=0.1, m=2. This setup indicates a moderate reduction in stiffness localized to a small portion of the beam. The large damage is defined by α=0.6, β=0.1, m=2. This indicates a significant loss of stiffness, still localized but much more intense than that in the small damage scenario. Other parameters are the same as that in Section 3.3.3.

#### 3.3.5.1 Effect of damage parameter α

From Eq. (3-9), the parameter α is related to the damage extent. The effect of the parameter on VBI is studied through the TFA of the dynamic responses. Three different damage cases are discussed, e.g. α=0, 0.3, and 0.6, while maintaining $\beta$ at 0.1 and $m$ at 2.

The damaged location is one-third of the bridge's length. The dynamic responses of bridges with various damage cases are analyzed using SST2 and the TFRs are obtained.

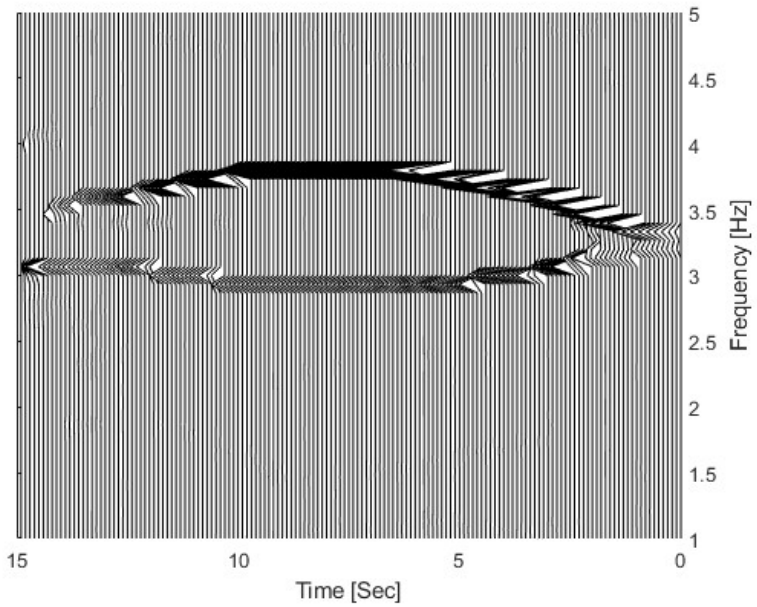


Figure 3-15 TFR of the response with α=0.3

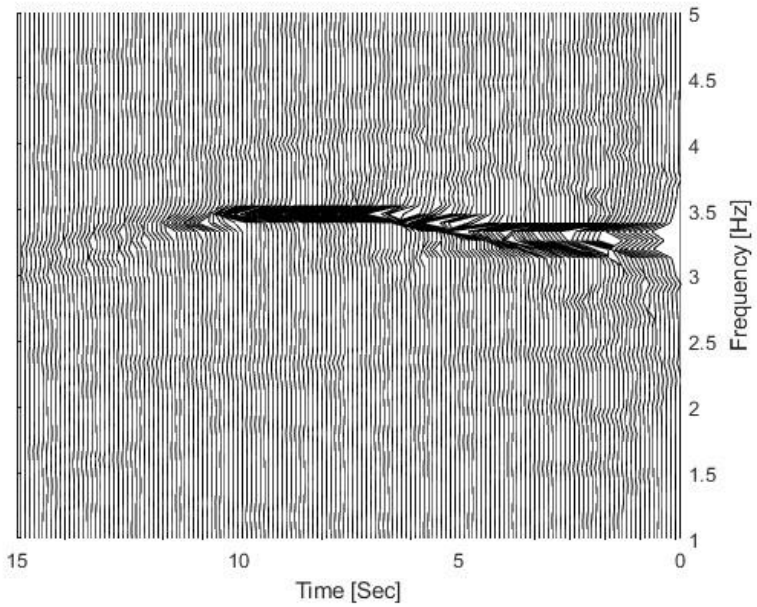


Figure 3-16 TFR of the response with α=0.6

Figures 3-6, 3-15 and 3-16 show the TFRs of the dynamic responses for the bridge with α=0, 0.3, and 0.6 respectively. The frequency of the intact bridge state significantly exceeds that of the damaged state. The frequency diminishes with the damage parameter

α. The impact of bridge damage on the dynamic response of cars crossing the bridge. The change in frequency may indicate the extent of damage to the bridge.

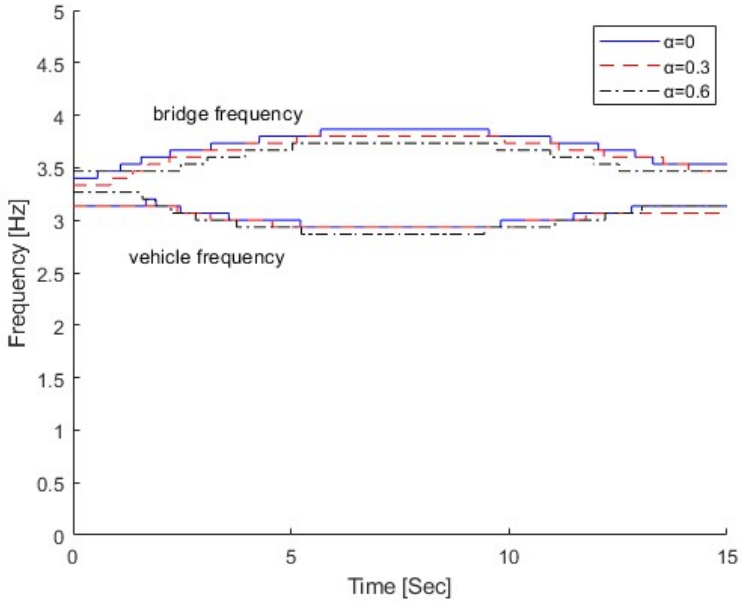


Figure 3-17 IFs for three different cases using SST2

Figure 3-17 displays corresponding IFs of these three damage cases extracted using SST2. The dashed blue line represents the IF of an undamaged bridge, the dashed red line signifies a bridge with small damage, and the solid blue line indicates a bridge with large damage. From the figure, the undamaged bridge maintains a relatively stable and high frequency, suggesting a consistent dynamic response as vehicles pass over, with no significant changes in vibrational characteristics. In contrast, bridges with small damage shows a slight reduction in frequency, likely due to localized stiffness loss from the damage, affecting its dynamic behavior. Comparison of theoretical value, the MSE values for α=0, 0.3 and 0.6 are 0.0066, 0.0137 and 0.0185 respectively. The frequency of the significantly damaged bridge is notably reduced, indicating a more substantial impact from the damage, potentially leading to a considerable reduction in stiffness, and hence a

pronounced change in the dynamic response and vibrational modes as vehicles pass.

In the process of vehicles crossing the bridge, damage identification relies heavily on capturing changes in IFs. A high frequency stability is observed when vehicles pass over an undamaged bridge. When there is damage, the frequency decreases, with more severe damage resulting in a more pronounced drop.

**3.3.5.2 Effect of the parameter β**

As listed in Eq. (3-9), the parameter $\beta$ represents the relative range of the damage zone along the bridge, with a range between 0.0 and 1.0. A smaller $\beta$ value indicates that the damage is concentrated in a small section of the bridge, while a larger $\beta$ value suggests a more extensive damage area. By adjusting the $\beta$ value, it is possible to simulate the impact of different damage lengths on the overall stiffness of the bridge, thus evaluating the varying effects of localized and distributed damage on the bridge's dynamic response. Based on Eq. (3-9), set $\beta$ to 0, 0.1, and 0.25, while maintaining α at 0.3 and m at 2. The damaged location is one-third of the bridge. Other parameters are the same as Section 3.3.3.

Figure 3-18 shows the IFs for different $\beta$ values using SST2. From the figure, the bridge frequency is reduced with the $\beta$ value. The bridge frequency is decreased slightly for a small damage ($\beta$=0.1). A large amount of damage ($\beta$=0.25) causes a big frequency reduction. Comparison of theoretical value, the MSE values for $\beta$=0.0, 0.1 and 0.25 are 0.0066, 0.0112 and 0.0185 respectively. As for vehicle frequency, meanwhile, is much less impacted by the bridge damage, though a small frequency shift is still discernible as

a fading. The bridge damage affects the dynamic of the vehicle over the bridge. Therefore, the $\beta$ value under various damage scenarios shows up in the IFs of the bridge and the vehicle. The shifts in these IFs can be used to measure the damage of the bridge effectively when the frequency shifts are more extreme in cases of small or severe damage.

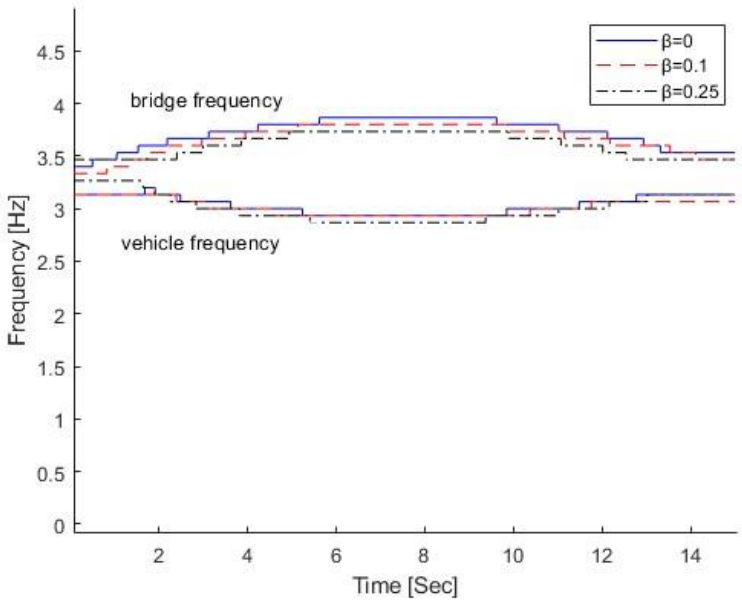


Figure 3-18 IFs for different $\beta$ values using SST2

### 3.3.5.3 Effect of damage locations

The theoretical foundation rests on the premise that damage reduces the local stiffness of the bridge, influencing its capacity to react dynamically. The reduction in stiffness due to damage is effectively modeled by the decrease in the effective moment of inertia ($I$, which alters the bridge's natural frequencies and mode shapes. This is why, depending on the location of the damage $(l_c)$, the time-frequency analysis will show different patterns.

To analyze the effect mathematically, one would calculate the bridge's mode shapes and frequencies both with and without damage using the given $\mathrm{EI(x)}$ expression. Comparing

these calculations would reveal the specific influence of damage on the bridge's vibration characteristics, which is then reflected in the time-frequency plots.

It is important to note that the parameters $\alpha, \beta$, and $m$ are crucial in determining the extent and distribution of the damage influence on the bridge's stiffness. The term $\cos^2\left(\frac{\pi}{2}\left(\frac{|x-l_c|}{\beta L/2}\right)^m\right)$ models the variation of damage severity across the length of the bridge, with maximum damage at $x = l_c$ and tapering off to $x = l_c \pm \beta L/2$.

In this numerical analysis, we concentrated on examining how similar degrees of damage at varying locations on a bridge impact its dynamic characteristics, specifically in the context of VBI. The study focused on three different damaged locations along the bridge: one-fourth, the midpoint, and three-fourth of the bridge's length eg $l_c = 0.5L, 0.25L, 0.125L$. The primary aim was to understand how the location of damage influences the characteristics of VBI, particularly in terms of the bridge's first-order frequency response.

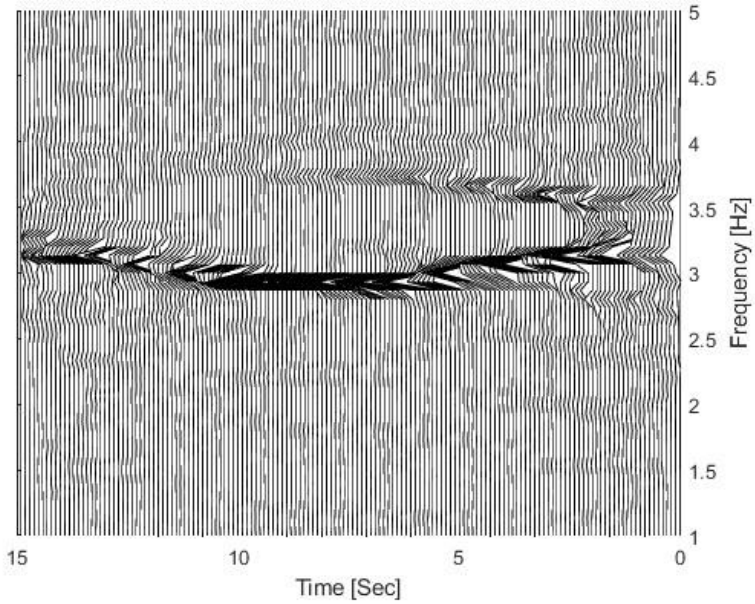


Figure 3-19 TFR for lc=0.5L

The dynamic responses of the bridge at these various damaged locations were analyzed using SST2 to obtain their corresponding TFRs. Figures 3-19, 3-20 and 3-21 show TFRs of dynamic responses for the bridge with different damage location. Here $\beta$ = 0.1, $\alpha$ =0.3 and m= 2. From these figures, there is a notable alteration in the frequency curve, despite the degree of damage being the same. There is a big bending upward or downward in the frequency curve when the damage location is at the mid-span of the bridge, and this shows there is a large frequency change when the vehicle is passing the bridge. For the damaged location at one-fourth span of the bridge, the frequency curve is much flat, and this shows there is a small frequency change when the vehicle is passing the bridge.

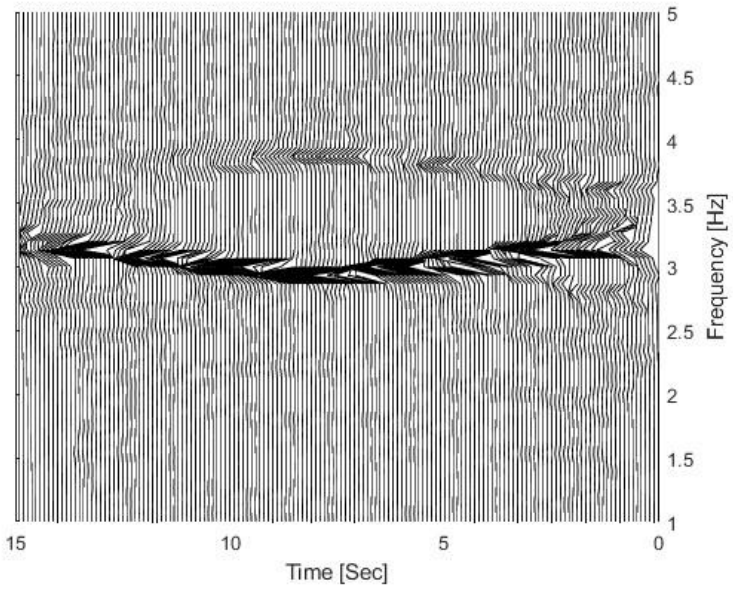


Figure 3-20 TFR for lc=0.25L

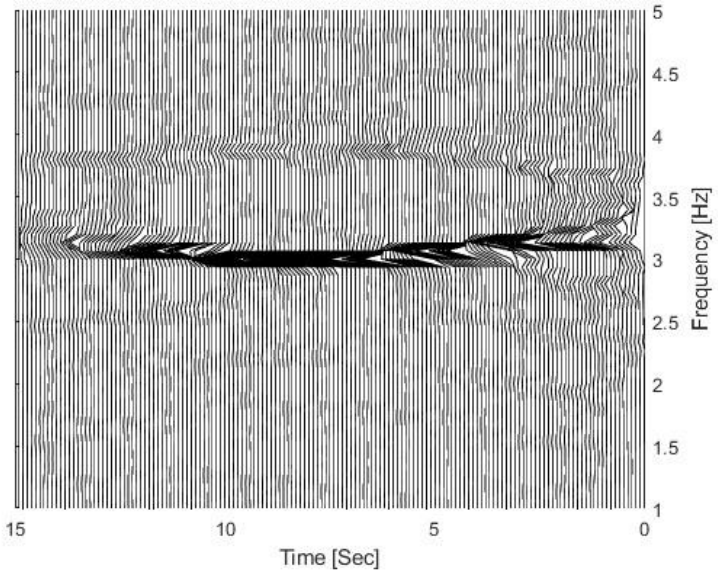


Figure 3-21 TFR for lc=0.125L

Figure 3-22 shows IFs for bridges with different damaged locations. From the figure, when damage occurs at the midpoint of the bridge, the IF significantly decreases. This typically indicates that damage at the midpoint has the greatest impact on the structural stiffness of the bridge, as the midpoint is the area of greatest stress, and damage here results in a substantial decrease in stiffness. Damage at the one-quarter point (1/4L) and one-eighth point (1/8L) also leads to a decrease in IF, but the impact is less significant compared to the midpoint. This may be because these positions, though close to support points, have load bearing and stress characteristics slightly different from the midpoint.

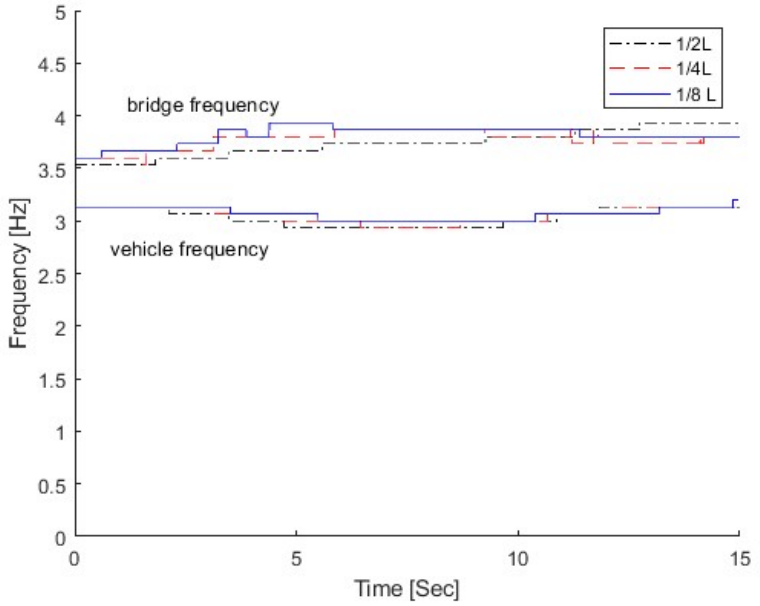


Figure 3-22 IFs for three different damage locations

Damage generally compromises the frequency stability of the bridge. Figure 3-22 indicates that post-damage frequency variations are more frequent and intense compared to the undamaged state, especially under dynamic loads such as moving vehicles. The damage location not only affects the absolute values of the frequencies but also influences the pattern of frequency response over time. The structure near the damaged areas might exhibit different dynamic responses under load, such as faster frequency decay or greater dispersion of frequencies. In summary, the location of the damage directly and significantly affects the time-varying features of the bridge, as reflected in changes in instantaneous frequencies. By analyzing these time-varying features, more accurately assess the health status and structural integrity of the bridge.

## 3.4. Experimental study

### 3.4.1 Experimental setup

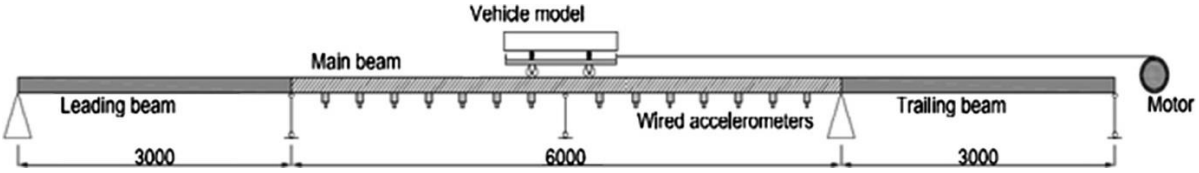


Figure 3-23 Vehicle-bridge interaction system

Figure 3-23 shows the finished VBI system that was built in the lab. There are three steel beams in our bridge model, with the central beam serving as the main beam, measuring 6 meters in length and having a cross-section of 100 mm × 15 mm. This main beam is a simply supported structure with two spans. Additionally, an anterior beam and a posterior beam, each 3 meters in length, are positioned in front of and behind the main beam to facilitate the vehicle's acceleration and deceleration. The first five bridge frequencies are 2.09Hz, 5.75Hz, 13.75Hz, 18.28Hz, 24.48Hz, respectively.

As shown in Figure 3-24, a two-axle vehicle model was designed. The wheels of this model are constructed from plastic rubber, making them very lightweight but remarkably robust. In this investigation, the masses of the front and rear axles, $m_1$ and $m_2$, are negligible and disregarded. The stiffness and damping coefficients of the tires, $K_t$ and $C_t$, are not considered. The vehicle model uses springs for its suspension system, and the damping $C_s$ is not included in this study. The mass of the vehicle body is 4.9 kg, and its rotational inertia is 0.06 kg·m². The stiffness of the vehicle suspension system is $k_{s1} = k_{s2}$ = 1.3e+5 N/m. These characteristics were established during modal testing of the vehicle. Adding 5kg mass to the main beam to simulate the damage. The mass is suspended at the midpoint of the initial span of the beam to replicate a modification of the bridge model, as illustrated in Figures 3-25 and 3-26

Figure 3-24 The vehicle and wireless accelerometers

Figure 3-25 The bridge model

Figure 3-26 Adding 5 mass to the main beam

Additionally, a wireless sensing system manufactured by Beanair Gmbh was used in the test. The vehicle's dynamic reaction was assessed using BeanDevice AX-3D wireless accelerometers, positioned on the front and rear axles, as seen in Figure 3-24. Laser sensors recorded the timestamps when the vehicle entered and exited the main beam, which were subsequently utilized to compute the vehicle's speed. The measurement sample frequency was 500 Hz.

### 3.4.2 Experiment results

### 3.4.2.1 Comparison of no damage and damage beams

Figures 3-27 and 3-28 presented illustrate the dynamic response and frequency analysis of a vehicle traveling over a bridge at a speed of approximately 0.62 m/s. Figure 3-27 provides a comparison between the experimental frequency response (solid blue lines), the instantaneous frequency fluctuates around 27 Hz and remains stable, indicating that the bridge structure has not been subjected to external disturbances or damage, and its dynamic characteristics are stable. After adding 5 kg mass to the beam to simulate damage (solid blue lines), the instantaneous frequency shows a decrease, particularly with the primary mode dropping from 27 to approximately 25 Hz. Adding the mass block causes a localized reduction in the stiffness of the bridge, leading to a significant decrease in the modal frequency, which is a typical characteristic of structural damage (or stiffness variation).

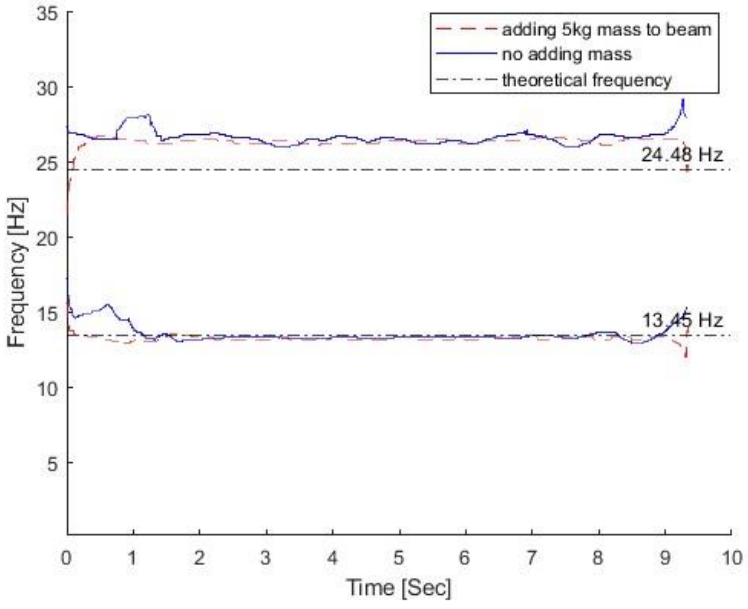


Figure 27 IFs of vehicle responses

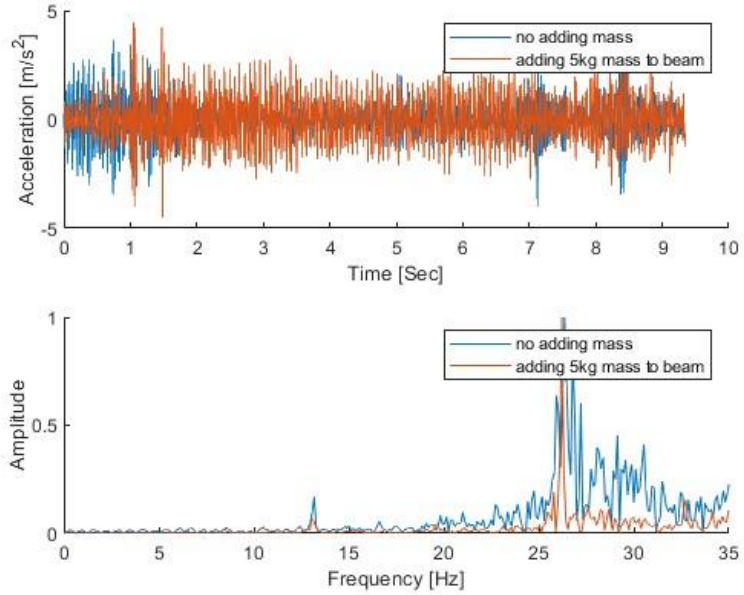


Figure 28 Original signal and FFT of vehicle responses

The addition of the mass block reduces the modal frequency from 27Hz to 25 Hz, indicating a localized stiffness reduction. This change can serve as an indirect indicator for bridge damage detection. By further combining instantaneous frequency and spectrum data, the extent and location of the bridge damage may be assessed.

### 3.4.2.2 Compare with results by other signal processing methods

Li et al (2020) proposed using Synchroextract transform (SET) to extract time-varying features. Figure 3-29 shows using SET to extract IFs of vehicle responses. The outcomes obtained using SET are juxtaposed with those derived from the suggested technique, as shown in Figure 3-27.

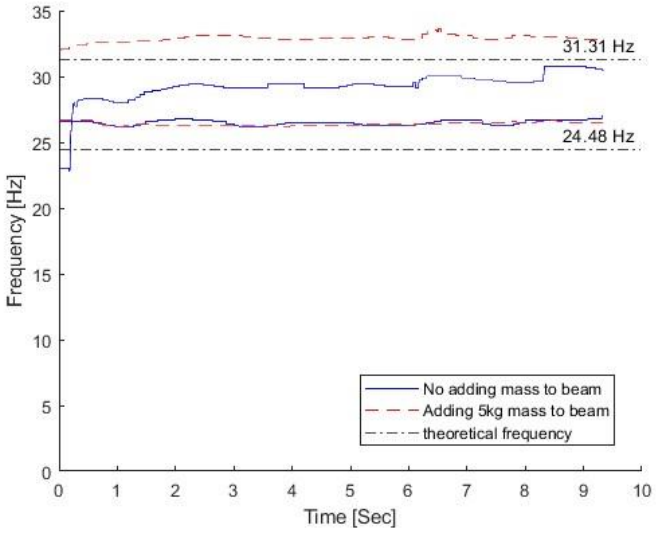


Figure 29 IFs of vehicle responses using SET

From Figures 3-27 and 3-29, there are some differences in IFs of vehicle responses using he SET and SST2 methods. Observations reveal several fluctuations in the frequencies identified using the SET approach, namely at high frequency (about 31.31 Hz) and mid frequency (around 24.48 Hz). The TFR of the SET method is relatively insufficient, and the experimental data exhibits diminished concordance with theoretical frequencies, particularly at elevated frequencies where the data is unstable. The SST2 method, in contrast, provides much enhanced time-frequency resolution through second-order reassignment, providing clearer and more stable frequency curves. The experimentally recorded frequencies closely approximate the theoretical frequencies in the low and mid-frequency regions (13.45 Hz, 24.48 Hz), showing little noise and variation. SST2 outperforms SET in IF extraction and offers superior frequency trend identification, making it the more effective approach for analyzing vehicle-bridge dynamic interactions.

**3.5 Summary**

A SST2 based method has been developed to extract time-varying characteristics from dynamic responses of the vehicle passing over the bridge. Numerical and experimental studies have been conducted to verify the performance of the proposed method. Some conclusions can be obtained as below,

Firstly, compared to the traditional SST, SST2 provides clearer and more accurate TFR when dealing with complex signals, especially those with rapidly changing frequency components. By analyzing the influence of elements including vehicle mass, velocity, damping characteristics, road surface profiles, measurement noise, and varying damage situations on the frequency fluctuations of VBI systems, SST2 has shown its strong potential in SHM.

Secondly, the results clearly demonstrate that SST2 can effectively capture the impact of damage on the vibrational characteristics of bridges when considering the dynamic responses of bridges under actual traffic loads and various states of damage. This is particularly important for bridge health monitoring and damage identification, aiding engineers in more accurately assessing the safety condition of bridges.

Lastly, the study validated the efficacy of the SST2 approach by numerical simulations and experimental analysis, providing a new analytical tool for the field of bridge engineering. This not only facilitates a deeper understanding of the dynamic characteristics of VBI systems but also provides valuable guidance for bridge design, monitoring, and maintenance.

SST2 exhibits constrained frequency resolution for strongly nonlinear signals and may

produce residual energy smearing in multicomponent vibrations. Its performance degrades under high noise conditions, and parameter selection remains challenging.

In summary, SST2 exhibits outstanding performance using the simplified VBI model and potential applications for bridge SHM using VBI monitoring data in practice. Future field study needs to be conducted for practical applications considering complex VBI systems using machine learning models.

# CHAPTER 4 Time-frequency characteristics of vehicle-bridge interaction system for structural damage detection using multi-synchrosqueezing transform based on bridge responses

## 4.1 Overview

A second-order sychrosqueezing transform (SST2) based method has been developed to extract time-varying characteristics from dynamic responses of the vehicle passing over the bridge in Chapter 3. To further enhance time-frequency resolution for the complex modulation characteristics of vehicle-bridge interaction systems, the multi-synchrosqueezing transform (MSST) is introduced to extract the time-varying characteristics from dynamic responses of the bridge under moving vehicles in this chapter.

The destruction of the bridge is a localized phenomenon. The localized, damage-responsive mechanism activates when a vehicle crosses the region. The VBI system is nonstationary and temporally variable. The localized damage can be readily discerned through the time-dependent bridge response to the traversing vehicle. SST, a reassignment technique for enhancing TFR, is an effective instrument for decomposing non-stationary signals into distinct components. Presenting a novel methodology employing MSST to extract time-varying features of VBI systems for the purpose of monitoring bridge structural integrity. A VBI model is developed to represent the bridge

ahead of the driving vehicle. The time-varying features of the VBI system are examined based on bridge specifications, vehicle velocity, and road roughness. Calculus and experimentation demonstrate that the presented method removes temporal variability from the VBI system, potentially serving as an indicator of bridge structural collapse.

The preliminary theory regarding to the time-varying dynamic VBI is first introduced. A new MSST based method is proposed to extract the time-varying features of the VBI system.

## 4.2 Theory

### 4.2.1 Vehicle-bridge interaction systems

#### 4.2.1.1 The VBI modeling

As shown in Figure 3-1, the VBI system is simplified to a simply supported bridge subjected to a vehicle moving at a constant speed v. The bridge is discretized using a finite element model, as illustrated in Figure 3-3. The vehicle is represented as a quarter-vehicle system with two degrees of freedom, representing the essential dynamic characteristics of vehicle-bridge interaction. This model includes key parameters such as the mass, stiffness, and damping coefficients of the vehicle, along with the mass, stiffness, and damping properties of the bridge. The parameters employed in this chapter are provided in Tables 3-1 and 3-2 (Li et al. 2020) same as Chapter 3.

### 4.2.2 Time-varying feature extraction using SST based method

#### 4.2.2.1 Synchrosqueezing transform (SST)

The STFT-based SST is used in this study. For a given response of the VBI system $s(t) \in L^2(\mathbb{R})$, It may pertain to the vehicle's response while traversing the bridge or the bridge's

response to a moving vehicle, as shown in Eqs. (3-1) and (3-2). The STFT of the response with a window function $g(t) \in L^2(\mathbb{R})$ is defined as

$$G(t,\omega) = \int_{-\infty}^{+\infty} g(\tau)s(\mathrm{t}+\tau)e^{-i\omega\tau}d\tau \tag{4-1}$$

where the window $g(t)$ compactly supports in $[-\Delta_t, \Delta_t]$.

For a non-stationary multicomponent signal $s(t)$ ,It can be represented as the superposition of the intrinsic mode functions (IMFs) as follows:

$$s(t) = \sum_{k=1}^{N} A_k(t)e^{i\varphi_k(t)} \tag{4-2}$$

where $A_k(t), \varphi_k(t)$ are the amplitude and phase of the kth IMF respectively. For a slow varying signal, there exists a small enough value ε, $|A'_k(t)| \le \varepsilon, |\varphi"_k(t)| \le \varepsilon \forall t$. Here, $A'_k(t)$ and $\varphi"_k(t)$ are the first derivative of the signal's amplitude function $A_k(t)$ and the second derivative of the phase function $\varphi_k(t)$, respectively. Under this assumption, each IMF can be approximated as a completely harmonic signal over a brief duration. In accordance with the Taylor expansion, the $k_{th}$ IMF can be expressed as,

$$x_k(t+\tau) = A_k(t+\tau)e^{i\varphi_k(t+\tau)} \approx A_k(t)e^{i(\varphi_k(t)+\varphi'_k(\mathrm{t})\tau)} \text{ for } \tau \approx 0 \tag{4-3}$$

Substituting Eq. (4-3) into Eq. (4-1), it can be written as follows,

$$\begin{aligned} G(t,\omega) &= \sum_{k=1}^{N} \int_{-\infty}^{+\infty} g(\tau)A_k(t)e^{i(\varphi_k(t)+\varphi_k'(t)\tau)}e^{-i\omega\tau}d\tau \\ &= \sum_{k=1}^{N} A_k(t)e^{i\varphi_k(t)} \int_{-\infty}^{+\infty} g(\tau)e^{-i\left(\omega-\varphi_k'(t)\right)\tau}d\tau \\ &= \sum_{k=1}^{N} A_k(t)e^{i\varphi_k(t)}\hat{g}\left(\omega-\varphi_k'(t)\right) = \sum_{k=1}^{N} G_k(t,\omega) \end{aligned} \tag{4-4}$$

where $\hat{g}(\omega)$ is Fourier transform of $g(t)$, $\hat{g}(\omega) \in [-\Delta\omega, \Delta\omega]$. Then the derivative with respect to time for $G(t,\omega)$ can be obtained as,

$$\begin{aligned}\partial_t G(t,\omega) &= \sum_{k=1}^{N} \partial_t \left(A_k(t) e^{i\varphi_k(t)} \hat{g}(\omega - \varphi'_k(t))\right) \\ &\approx \sum_{k=1}^{N} A_k(t) e^{i\varphi_k(t)} \hat{g}\left(\omega - \varphi'_k(t)\right) i\varphi'_k(t) \\ &= \sum_{k=1}^{N} G_k(t,\omega) i\varphi'_k(t)\end{aligned} \tag{4-5}$$

For which $G_k(t,\omega)\neq 0$, the instantaneous frequency (IF) $\hat{\omega}_k(t,\omega)$ can be obtained by

$$\hat{\omega}_k(t,\omega) = \varphi'_k(\mathrm{t}) = \frac{\partial_t G_k(t,\omega)}{i G_k(t,\omega)}. \tag{4-6}$$

Assuming ε being sufficiently small, let $\tilde{\varepsilon} = \varepsilon^{1/3}$, for $|G_k(t,\omega)| \geq \tilde{\varepsilon}$, it can be approximate as [5, 6],

$$\left|\hat{\omega}_k(t,\omega) - \varphi'_k(t)\right| \leq \tilde{\varepsilon} \tag{4-7}$$

Eq. (4-7) indicates that for a weakly time-varying signal, $\hat{\omega}_k(t,\omega)$ can be approximate as the IF $\varphi'_k(t)$ of the signal. The SST uses a frequency-reassignment operator to collect the time-frequency coefficient.

$$sst(t,\omega_k) = \int_{-\infty}^{+\infty} G(t,\omega)\delta(\omega_k - \hat{\omega}(t,\omega))d\omega \tag{4-8}$$

Using SST, the diffuse energy present in the STFT results can be localized within a compact region surrounding IF of each mode. This essentially enhances the TFR of the signal.

#### 4.2.2.2 Multi-synchrosqueezing Transform (MSST)

SST can provide a good TFA for signals if the signal is well separated with slow variations. When the signal variation is large, SST may not be able to provide an accurate and clear TFR (Daubechies, Lu et al. 2011). Although SST struggles with time-varying signals, a single SST operation can yield a clearer TFR than that by STFT. MSST is to execute another SST operation on the SST result for achieving an even sharper time

frequency representation as (Yu et al. 2018),

$$\begin{aligned} sst^{[2]}(t,\omega_0) &= \int_{-\infty}^{+\infty} sst^{[1]}(t,\omega)\delta(\omega_0-\hat{\omega}(t,\omega))d\omega \\ sst^{[3]}(t,\omega_0) &= \int_{-\infty}^{+\infty} sst^{[2]}(t,\omega)\delta(\omega_0-\hat{\omega}(t,\omega))d\omega \\ &\vdots \\ sst^{[N]}(t,\omega_0) &= \int_{-\infty}^{+\infty} sst^{[N-1]}(t,\omega)\delta(\omega_0-\hat{\omega}(t,\omega))d\omega \end{aligned} \tag{4-9}$$

where N is iteration number, and N > 1. By Eq. (4-10), SST can be executed multiple times to achieve the accurate time-frequency representation iteratively. As an example, N=2, the MSST can be expressed as

$$\begin{aligned} Ts^{[2]}(t,\omega_0) = & \int_{-\infty}^{+\infty} Ts^{[1]}(t,\xi)\delta(\omega_0-\hat{\omega}(t,\xi))d\xi \\ = & \int_{-\infty}^{+\infty}\int_{-\infty}^{+\infty} G(t,\omega)\delta(\xi-\hat{\omega}(t,\omega)) \\ & \times d\omega\delta(\omega_0-\hat{\omega}(t,\xi))d\xi \\ = & \int_{-\infty}^{+\infty} G(t,\omega)\int_{-\infty}^{+\infty}\delta(\xi-\hat{\omega}(t,\omega)) \\ & \times \delta(\omega_0-\hat{\omega}(t,\xi))d\xi d\omega \\ = & \int_{-\infty}^{+\infty} G(t,\omega)\delta(\omega_0-\hat{\omega}(t,\hat{\omega}(t,\omega)))d\omega \end{aligned} \tag{4-10}$$

The IF estimation $\hat{\omega}(t,\hat{\omega}(t,\omega))$ is obtained, and it is more appropriate for managing robust Frequency Modulated (FM) signals than $\hat{\omega}(t,\omega)$. For a general assumption, there exists ε, sufficiently small, such that |A'(t)|≤ε and |φ'''(t)|≤ε for all t. The signal can be seen as a linear chirp signal over a brief duration. The expressions are articulated as $A(t+\tau)=A(t)$ and $\varphi(t+\tau)= \varphi(t)+\varphi'(t)(\tau-t)+0.5\varphi''(t)(\tau-t)^2$, where terms of order O(A'(t)) and O(φ'''(t)) are disregarded. Consequently, the signal may be reformulated as

$$s(t+\tau)=A(t)e^{i\left(\varphi(t)+\varphi'(t)(\tau-t)+0.5\varphi''(t)(\tau-t)^2\right)} \tag{4-11}$$

According to Eq. (4-4), a window function is set as the Gaussian function $g(t)=e^{-0.5t^2}$.

The STFT of the signal is obtained as

$$\begin{aligned} G(t,\omega) = & \int_{-\infty}^{+\infty} e^{-0.5(\tau-t)^2} A(t) e^{i\left(\varphi(t)+\varphi'(t)(\tau-t)+0.5\varphi''(t)(\tau-t)^2\right)} \\ & \times e^{-i\omega(\tau-t)} d\tau \\ = & A(t) e^{i\varphi(t)} \int_{-\infty}^{+\infty} e^{-0.5\left(1-i\varphi''(t)\right)(\tau-t)^2} e^{-i\left(\omega-\varphi'(t)\right)(\tau-t)} \\ & \times d(\tau-t) \\ = & A(t) e^{i\varphi(t)} \frac{1}{\sqrt{1-i\varphi''(t)}} e^{-\frac{(\omega-\varphi'(t)^2)}{2\left(1-i\varphi''(t)\right)}} \end{aligned} \tag{4-12}$$

the two dimensional IF of the signal can be obtained as:

$$\begin{aligned} \hat{\omega}(t,\omega) = & \varphi'(t) + \frac{\varphi''(t)^2}{1+\varphi''(t)^2}(\omega-\varphi'(t)) \\ & -i\frac{\varphi''(t)}{1+\varphi''(t)^2}(\omega-\varphi'(t)). \end{aligned} \tag{4-13}$$

The IF is the real part of Eq. (4-13) as (Thakur and Wu, 2011),

$$\hat{\omega}(t,\omega) = \varphi'(t) + \frac{\varphi''(t)^2}{1+\varphi''(t)^2}(\omega-\varphi'(t)) \tag{4-14}$$

It can be observed that $\hat{\omega}(t,\omega)$ cannot provide an unbiased estimation of the true instantaneous frequency (IF). The error between $\hat{\omega}(t,\omega)$ and $\varphi'(t)$, i.e., $|\hat{\omega}(t,\omega) - \varphi'(t)|$, is dependent on two factors: the second-order derivative of the Instantaneous Phase and the distance between the frequency variable and the actual IF. In the case of strong frequency modulated signals, the term φ″(t) must not be disregarded, which leads to $|\hat{\omega}(t,\omega) - \varphi'(t)|$ becomes progressively larger as the gap between the frequency variable and the true IF increases. The original SST is incapable of producing a focused time-frequency representation for signals that exhibit significant time variability, the IF can be estimated by MSST (N=2) as,

$$\begin{aligned} \hat{\omega}(t,\hat{\omega}(t,\omega)) & = \varphi'(t) + \frac{\varphi''(t)^2}{1+\varphi''(t)^2}(\hat{\omega}(t,\omega)-\varphi'(t)) \\ & = \varphi'(t) + \left(\frac{\varphi''(t)^2}{1+\varphi''(t)^2}\right)^2(\omega-\varphi'(t)) \end{aligned} \tag{4-15}$$

Therefore, when N =3

$$Ts^{[N]}(t,\omega_0) = \int_{-\infty}^{+\infty} G(t,\omega)\delta\big(\omega_0 - \hat{\omega}^{[N]}(t,\omega)\big)d\omega \tag{4-16}$$

In addition, set a window function as Gaussian function the corresponding IF estimate of the MSST can also be calculated as

$$\hat{\omega}^{[N]}(t,\omega) = \varphi'(t) + \left(\frac{\varphi''(t)^2}{1+\varphi''(t)^2}\right)^N (\omega - \varphi'(t)) \tag{4-17}$$

#### 4.2.2.3 Time-dependent frequency extraction using ridge detection

Ridge detection is used to extract the higher resolution in TFR that can find the best frequency curve $\Omega(t)$. Brevdo et al. (2011) proposed a method to identify the optimal frequency curve, Ω(t), within TFR $S_x$, such that it maximizes the energy under a smoothness constraint enforced through a total variation penalization term. The detail function is shown as:

$$\hat{\Omega} = \arg\max_{\Omega} \int_{\mathbb{R}} |S_x(t,\Omega(t))|^2 \, \mathrm{d}t - \lambda \int_{\mathbb{R}} \left|\frac{\mathrm{d}\Omega}{\mathrm{d}t}(t)\right|^2 \, \mathrm{d}t \tag{4-18}$$

### 4.2.3 Validation of MSST

To show the performance of MSST for TFA, the following non-stationary signal is used as an example.

$$x(t) = \cos\big(2\pi * (0.1t^{2.6} + 3\sin(2t) + 10t)\big) + e^{-0.2t}\cos\,(2\pi * (40 + t^{1.3})t) \tag{4-19}$$

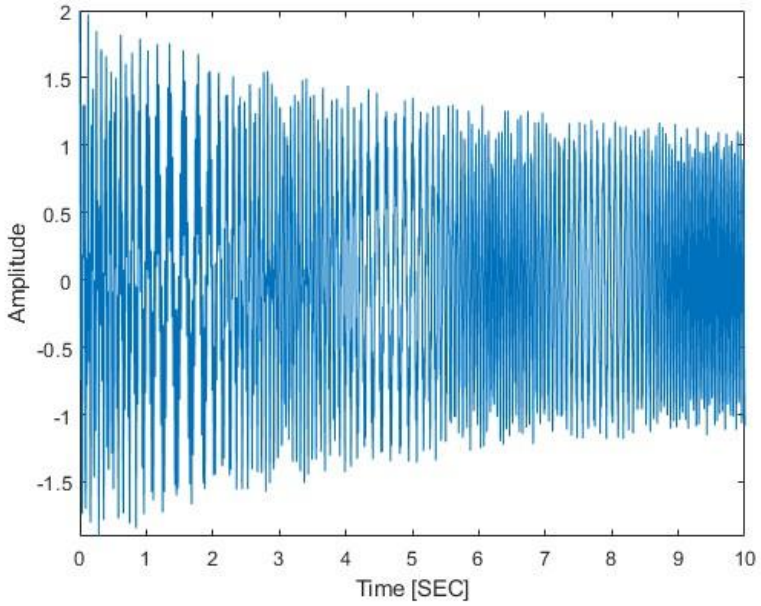


(a) The non-stationary signal

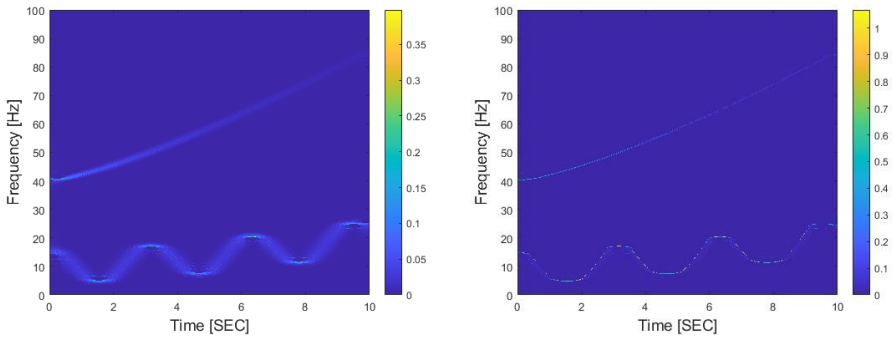


(b) TFR using SST (c) TFR using MSST

Figure 4-2 A non-stationary signal and its time-frequency representations using SST and MSST

As shown in Eq. (4-28), there are two components in the signal with the amplitudes and phases as $A_1(t) = 1$, $\varphi_1(t) = 0.1t^{2.6} + 3\sin(2t) + 10t$ and $A_2(t) = e^{-0.2t}$, $\varphi_2(t) = (40 + t^{1.3})t$ respectively. IFs of these two components are $\varphi'_1(t) = 2.6t^{1.6} + 6\cos(2t) + 10$ and $\varphi'_2(t) = 40 + 2.3t^{1.3}$ respectively. The non-stationary signal and its TFR are shown in Figure 4-1. Figure 4-1(a) shows the non-stationary signal and its

time-frequency representations (TFR) using SST and MSST are shown in Figure 4-2(b) and (c) respectively. The IFs of these two components are clearly shown in both Figures 4-2(b) and 4-2(c), and the results show that both SST and MSST can decompose the signal. Figure 4-2(c) provides quite sharp and clear representation of two components. The results show that MSST has a superior concentration of signal in the time-frequency representation. A high degree of signal concentration typically correlates with reduced time-frequency cross-terms, yielding a clearer and more precisely defined time-frequency characteristic representation. The enhanced concentration observed with MSST is attributed to more complex or optimized algorithmic mechanisms employed during processing, such as improved time-frequency resolution or refined techniques for the separation of frequency components. MSST is shown to more effectively suppress mode mixing and background noise, enhancing the signal's localization in the time-frequency domain, which is particularly crucial for the analysis of non-stationary and complex signals.

## 4.3 Numerical investigations on time-frequency characteristics extraction of VBI

### 4.3.1 Time-varying characteristics of the VBI system

The bridge is simplified as a simply supported beam. The length, mass density and flexural rigidity of bridge beam are L=30 m, ρ=6000 kg/m and EI=2.5e+10 Nm2 respectively. The damping is not considered. The bridge model is represented by 10 finite elements.

The investigation centers around the Vehicle-Bridge Interaction (VBI) system. This study

maintains the identical bridge properties for, but with the incorporation of bridge damping. The study assumes Rayleigh damping, formulated as $C_b = \alpha_1 M_b + \alpha_2 K_b$ where $\alpha_1$ is 0.243 and $\alpha_2$ is 0.0001. These coefficients are derived from meticulous consideration of the material properties and modal characteristics of the bridge, facilitating more accurate simulations. In the aforementioned equation, $M_b$, $C_b$, and $K_b$ denote the mass, damping, and stiffness matrices of the bridge, respectively.

The quarter-vehicle model with two degrees of freedom effectively captures fundamental aspects of VBI. The vehicle parameters are $m_v$=7000kg, $k_v$=2.82e+6 N/m, $c_v$=390 N/m/s. The natural frequency of the vehicle is 3.20 Hz. Furthermore, the vehicle/bridge mass ratio is noted to be 0.042. The bridge deck surface is presumed to be smooth. The vehicle-bridge response is derived by solving the coupled vehicle-bridge interaction equation using the Newmark-β method. A sampling rate of 500 Hz is selected in accordance with the Nyquist sampling theorem to precisely capture the system's dynamic responses. The computed acceleration is infused with 5% white noise according to the following equation.

$$\mathrm{acc}_m = \mathrm{acc}_{\mathrm{cal}} + E_p \times N_{\mathrm{noise}} \times \sigma(\mathrm{acc}_{\mathrm{cal}}) \tag{4-21}$$

where $\mathrm{acc}_{\mathrm{cal}}$ represents the computed acceleration response. $E_p$ indicates the proportion of noise being added, and $N_{\mathrm{noise}}$ is a vector that adheres to a conventional normal distribution, characterized by a mean of zero and a standard deviation of one. $\sigma(\mathrm{acc}_{\mathrm{cal}})$ is the standard deviation of the computed acceleration, determining the scale of the noise added.

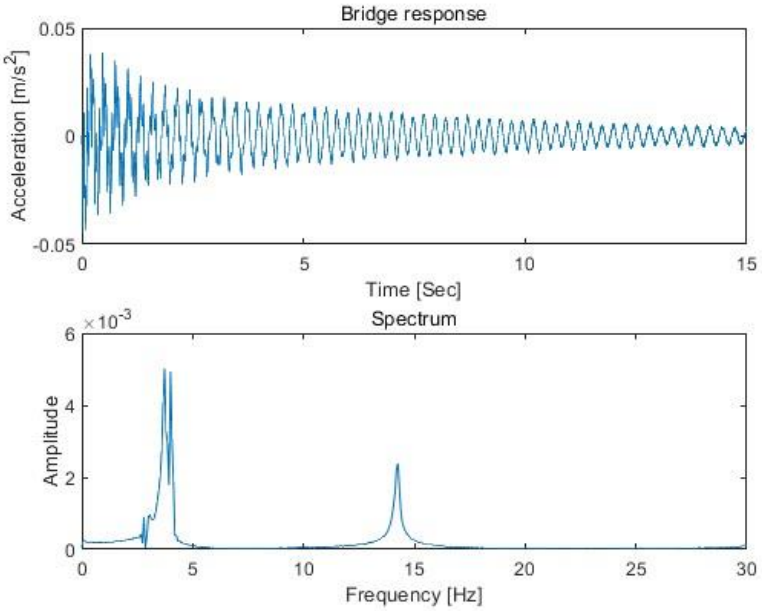


(a) The bridge response and its Fourier spectrum

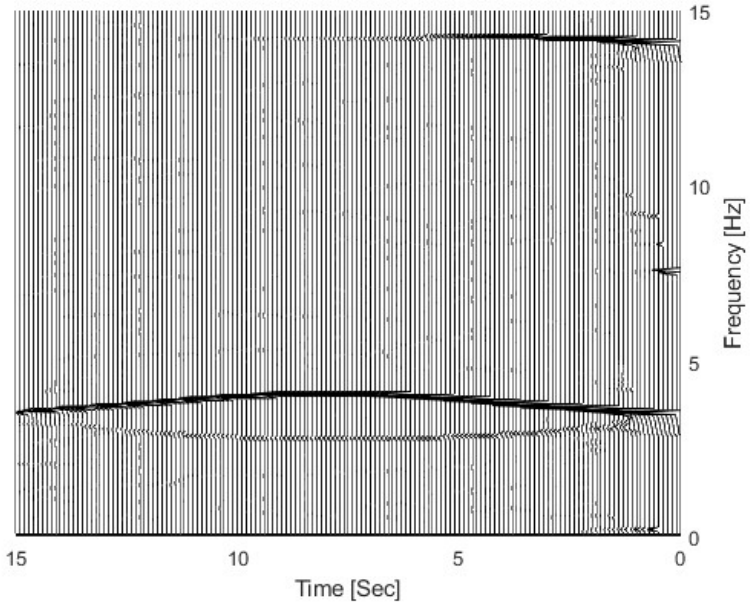


(b) TFR of bridge responses

Figure 4-3 The bridge response and its TFR

The bridge response measured at 3/10 span and corresponding spectrum when the vehicle advances at a steady speed of 2 m/s, is shown in Figure 4-3(a). There are two dominant peaks in the spectrum, which are located at 3.55 Hz and 14.10 Hz, which correspond to

the first and second natural frequencies of the beam bridge. The raw response data is further processed through the MSST with a window length of 2048.

Figure 4-3(b) shows the TFR of bridge and vehicle responses using the proposed MSST based method. From the figure, the energy of TFR by the proposed method is concentrated. The IF trajectories corresponding to the bridge response are around 3.55Hz and 14.10Hz respectively. Figure 33 shows the bridge frequency curve, positioned at a higher frequency around 3.5 Hz, demonstrates a parabolic shape, indicating a rise and fall in the natural vibration frequency of the bridge as it responds to the vehicle's load. On the other hand, the "vehicle frequency" curve, at a lower frequency around 3.1 Hz, exhibits a concave shape, with the frequency decreasing before reaching a nadir and then ascending, reflecting changes in the dynamic interaction between the vehicle and the bridge. These curves represent how the vibrational frequencies of the bridge and vehicle change over time, with the parabolic and concave shapes detailing their specific temporal evolution.

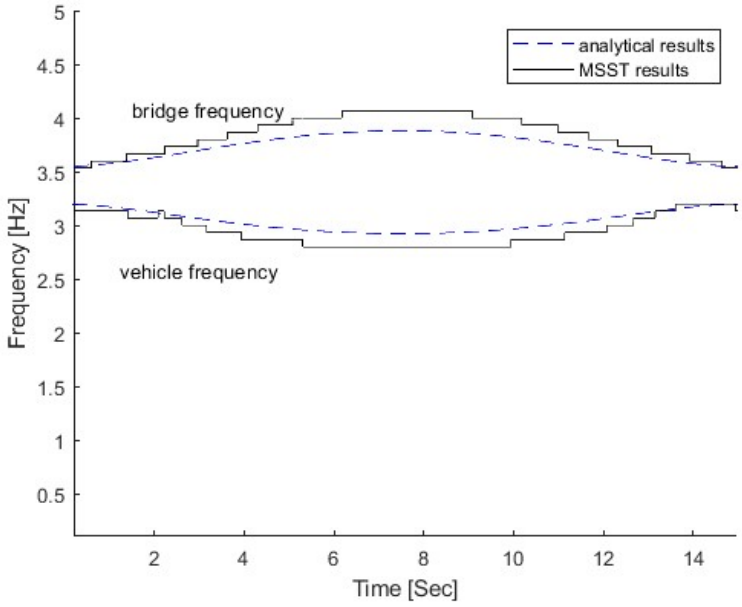

Figure 4-4 Instantaneous frequency of bridge response

Since the vehicle frequency of 3.2 Hz is lower than the bridge's first natural frequency of 3.5 Hz, Eqs. (3-7) and (3-8) are applied to compute the theoretical instantaneous frequencies (IFs). As depicted in Figure 4-4, the IF results obtained using MSST closely match the theoretical values. The curve above 3.5 Hz represents the bridge's IF, while the curve below 3.5 Hz corresponds to the vehicle's IF.

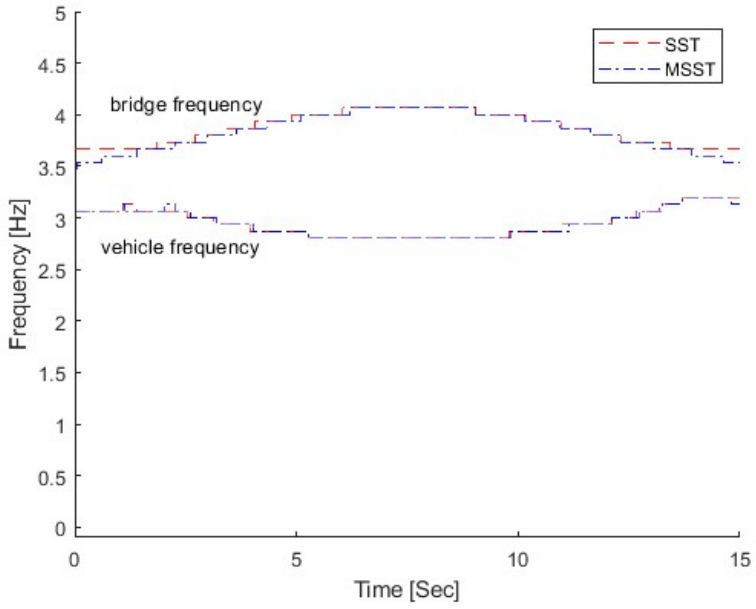


Figure 4-5 IF of the VBI response using MSST and SST

The performance of SST and MSST for the TFA of VBI dynamic responses is compared in this section. In Figure 4-5, the SST, represented by the red dashed line, displays slight fluctuations at the beginning and the end of the time series for the bridge frequency and more pronounced step-like changes for the vehicle frequency, indicating significant variations at specific times. In contrast, the MSST, depicted by the blue dash-dot line, shows a smoother transition throughout the time series for the bridge frequency and a

more continuous frequency change for the vehicle frequency, without the abrupt jumps observed in the SST method.

### 4.3.2 Parametric analysis

#### 4.3.2.1 Effect of different vehicle/bridge ratio

Figure 4-6 shows the IF of the VBI response with a 3000kg vehicle, and Figure 4-7 compares IFs with different vehicle weights, e.g. 500kg and 7000kg. Figure 4-8 shows the relationship between the bridge frequency ratio versus the vehicle/bridge mass and frequency ratios.

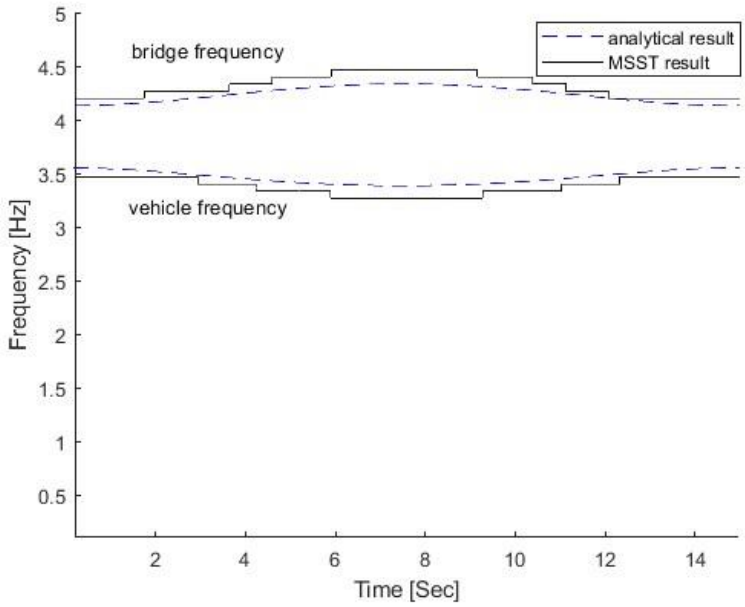


Figure 4-6 IF of VBI under 3000kg vehicle

These two figures demonstrate the impact of vehicle mass and analytical methods on the instantaneous frequencies of the bridge-vehicle coupling system. In Figure 4-6, the instantaneous frequencies extracted using MSST (black solid line) closely match the theoretical analytical results (blue dashed line). The bridge frequency fluctuates between

approximately 3.5 Hz and 4.5 Hz, while the vehicle frequency ranges between 2.8 Hz and 3.2 Hz. This close agreement indicates that MSST can accurately track instantaneous frequency variations under dynamic loads. Although slight deviations occur in regions with significant frequency fluctuations, likely due to noise or nonlinear effects in the actual signals, overall, the MSST results align well with the theoretical calculations, demonstrating its high accuracy and suitability for dynamic bridge-vehicle interaction analysis.

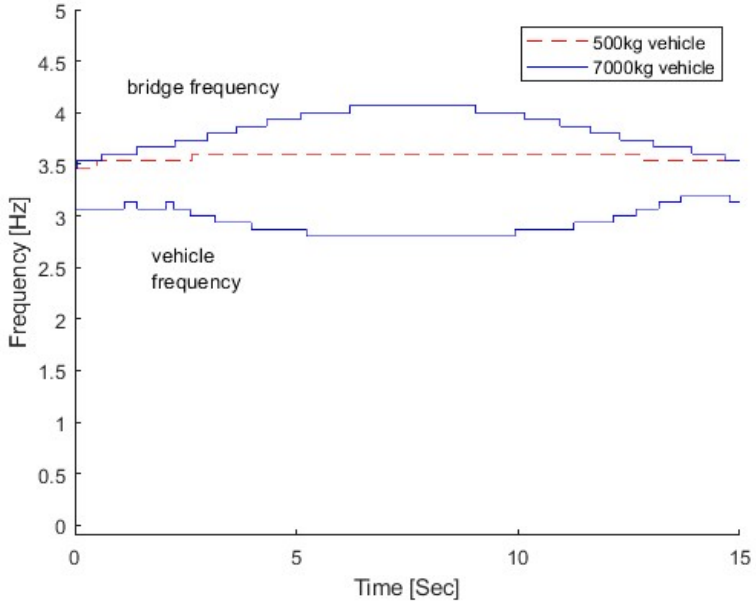


Figure 4-7 IF of VBI under 500kg and 7000kg vehicle

In Figure 4-7, when the vehicle mass is small (500 kg, represented by the red dashed line), the instantaneous frequency fluctuation of the bridge is minimal, and the frequency curve remains relatively stable around 3.5 Hz. This is because the dynamic coupling between the light vehicle and the bridge is weak, and the vehicle load has little influence on the bridge's stiffness and vibrational characteristics. However, when the vehicle mass

increases to 7000 kg (represented by the blue solid line), the bridge's instantaneous frequency fluctuation becomes significantly larger, with the frequency varying between approximately 3.5 Hz and 4.5 Hz. The frequency curve shows greater oscillations as the vehicle moves, reflecting the stronger dynamic response induced by the heavy vehicle's load, leading to more pronounced changes in stiffness and frequency.

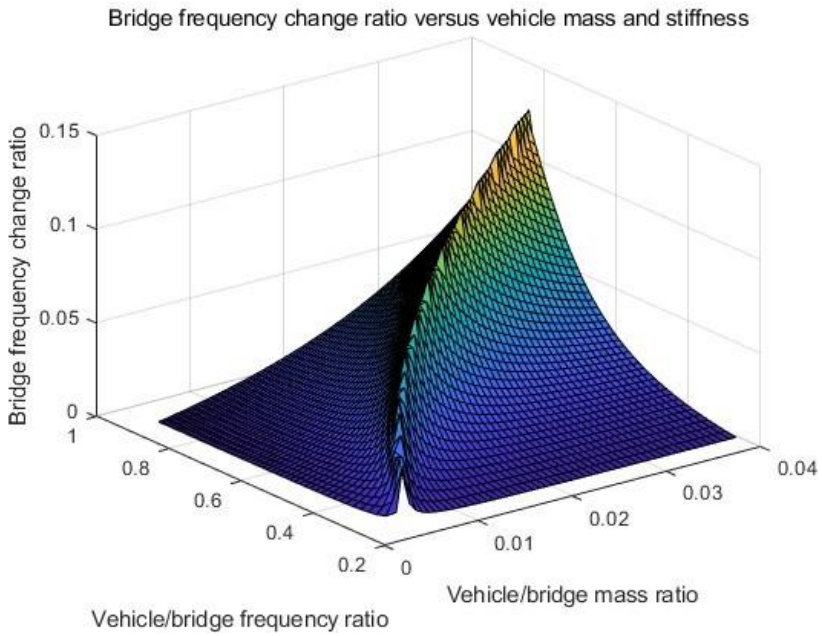


Figure 4-8 Bridge frequency change ratio versus vehicle mass and vehicle/bridge frequency ratio

Table 4-1 Bridge frequency ratio versus vehicle mass and stiffness

| Stiffness (N/m) | Mass of vehicle (kg) | Frequency of vehicle (Hz) | Mass ratio | Frequency ratio |
|---|---|---|---|---|
| 2.02e5 | 500 | 3.20 | 0.003 | 0.9 |
| 2.82e6 | 7000 | 3.20 | 0.039 | 0.9 |
| 2.02e6 | 3500 | 3.82 | 0.019 | 1.07 |

Figure 4-8 and Table 4-1 show the relationship between the bridge frequency change ratio and the mass ratio of the vehicle and the frequency ratio of the vehicle to the bridge. As

the mass of the vehicle increases and the frequency ratio between the vehicle and bridge rises, the ratio of frequency change in the bridge likewise escalates. A high vehicle/bridge frequency ratio indicates a more pronounced dynamic response of the bridge, accompanied by more frequency variation. When the vehicle mass is small (e.g., 500 kg, with a mass ratio of 0.003 and a frequency ratio of 0.9), the bridge's frequency variation is minimal, and its dynamic characteristics remain stable. However, when the vehicle mass increases to 7000 kg (with a mass ratio of 0.039 and the same frequency ratio of 0.9), the larger mass ratio leads to a significantly enhanced frequency variation of the bridge, despite the frequency ratio being unchanged. Additionally, when the vehicle mass is 3500 kg and the frequency ratio reaches 1.07, the bridge frequency change ratio increases to 1.07. This indicates that when the vehicle frequency approaches or exceeds the bridge's natural frequency, a stronger dynamic coupling occurs, causing significant fluctuations in the bridge's frequency. This demonstrates that under resonance or near-resonance conditions (with a frequency ratio close to 1), the dynamic response of the bridge system becomes more intense.

In summary light vehicles have a minimal impact on the dynamic features of the bridge, and the frequency variation of the bridge is relatively small. Heavy vehicles significantly impact the dynamic characteristics of the bridge, and the frequency variation of the bridge is more pronounced. As the vehicle/bridge frequency ratio increases, the frequency variation of the bridge becomes more apparent. This indicates that in resonance or near-resonance conditions (value is near 1), the dynamic response of the bridge system is more significant.

#### 4.3.2.2 Effect of road surface roughness on VBI system

According to (ISO and TC 1995), level B road surface roughness is selected.

As the road surface roughness changes from smooth to ISO B level, the time-frequency spectra (Figure 4-9) and the vehicle frequency component graphs reveal significant variations in the dynamic response of the VBI system. On a smooth bridge surface, the time-frequency spectrum displays a uniform distribution of frequency components, indicating a gentle and predictable bridge response to the vehicle. However, with the introduction of roughness, the spectrum becomes more complex, especially with energy concentration in the low-frequency area, reflecting an increased energy input into the system, particularly in the low-frequency range that corresponds to the lower-order vibration modes of the bridge.

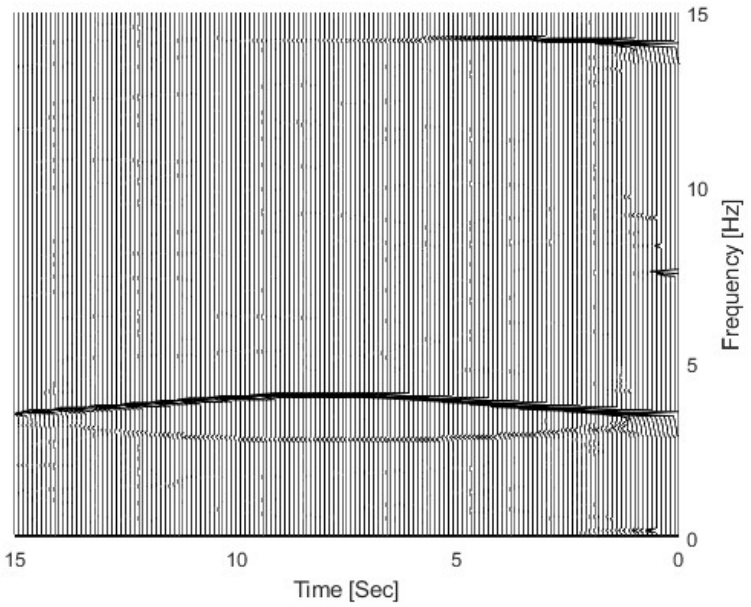


(a)TFR of smooth surface

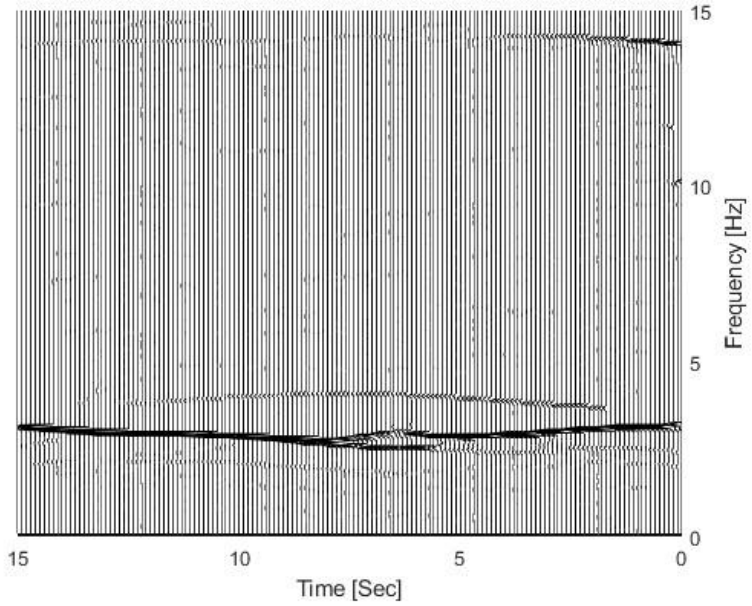


(b)TFR of ISO level B

Figure 4-9 TFR and IF based on MSST under different road surface roughness

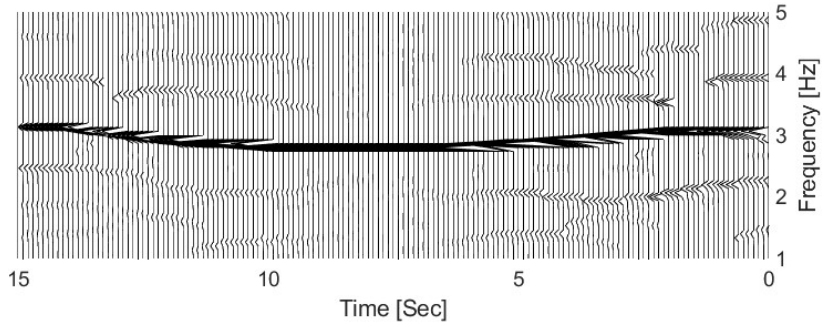


Figure 4-10 TFR and IF based on MSST under vehicle frequency component(smooth)

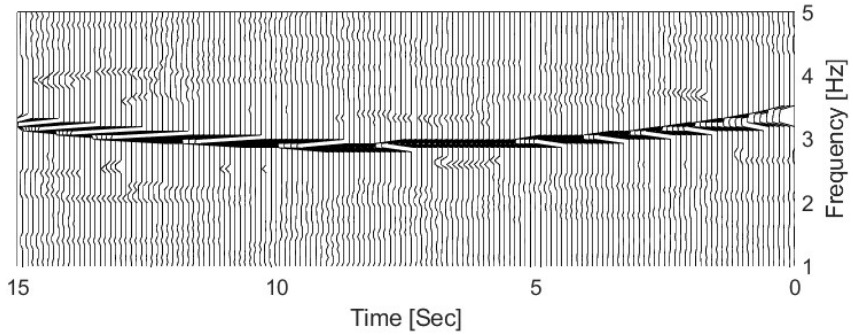


Figure 4-11 TFR and IF based on MSST under vehicle frequency component (ISO B)

The vehicle frequency component graphs (Figures 4-10 and 4-11) show a similar pattern of change, with a broader distribution of vehicle vibration frequencies on the rough bridge surface, especially with an extension into the low-frequency area. This suggests that

vehicles experience more random excitations when traveling over rough surfaces, which are reflected in a wider range of frequency responses.

A smooth bridge surface creates stable contact conditions that reduce vehicle vibrations across the bridge, resulting in a consistent frequency distribution and predictable dynamic reactions for the bridge and the vehicle. The vehicle experiences repeated shocks and vibrations while in motion as a result of surface irregularities that increase with bridge surface roughness. Because the bridge and vehicle's lower-order modes are readily excited at these frequencies, resulting in a focused energy distribution, irregular excitations increase the system's frequency response range with the most effect in the low-frequency region. A rough road surface affects the vibrations of the car and strengthens the dynamic forces acting on the bridge due to the weight of the vehicle, resulting in more complex dynamic responses.

#### 4.3.2.3 Effect of vehicle speed

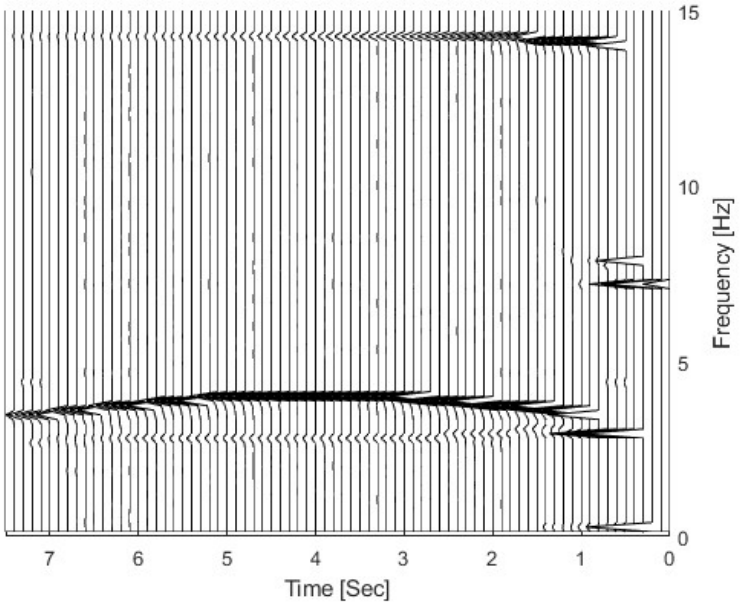


(a)TFR

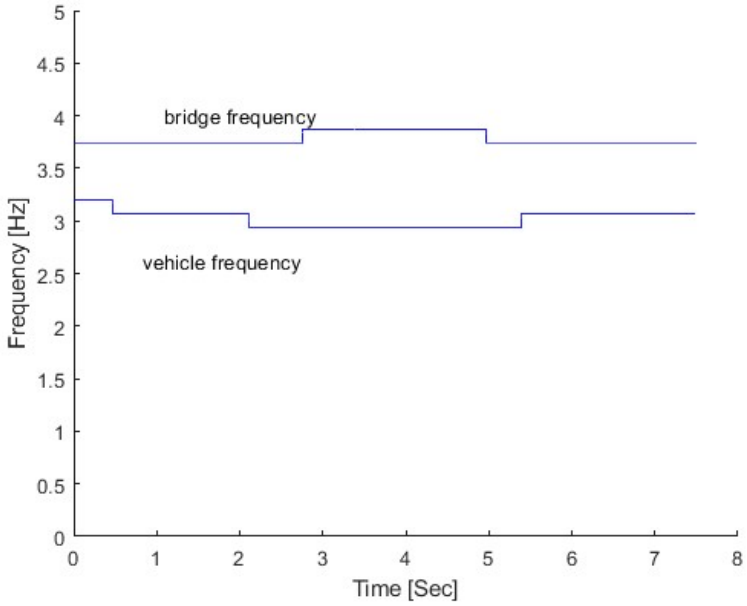


(b) IF

Figure 4-12 TFR and IF of the bridge response by MSST for Vehicle 2 under 4 m/s

At a velocity of 4 m/s, the TFR (Figure 4-12(a)) appears to exhibit a lower resolution with a smoother and more widespread distribution, despite some instances of concentrated frequencies. This suggests that vehicle-induced vibrations are distributed across a wider frequency range rather than being confined to specific frequencies. Correspondingly, the instantaneous frequency (Figure 4-12(b)) demonstrates a relatively smooth curve, which may be attributed to the smoothing effect of the lower resolution, rendering minor frequency variations less discernible.

Conversely, at a velocity of 2 m/s, the time-frequency spectrum (Figure 4-3) reflects a higher resolution, indicated by sharper and more well-defined frequency changes. At this reduced speed, the system's response tends to be more focused, with energy more concentrated at certain frequencies, implying that the vehicle's impact on the bridge structure is more localized and confined. The instantaneous frequency (Figure 4-(b), at

higher speeds, the changes in the time-frequency spectrum become more intense, with frequency lines rapidly changing and spreading. This indicates that the rapid movement of the vehicle triggers more structural responses, increasing the dynamic stress and vibrational disturbances the bridge may experience.

### 4.3.3 Nonstationary characteristic of VBI considering bridge damage

#### 4.3.3.1 Effect of different damage parameter $\alpha$

In this research, there are four different damage parameters to simulate damage with the open crack model. The parameters for small damage are set as follows: $\alpha$ is 0.3, $\beta$ is 0.1, lc equals half of the beam length (1/3L), and m is 2.0. For large damage, the parameters are adjusted to $\alpha$ being 0.6, $\beta$ at 0.1, m remaining 2.0, and lc set at half the beam length (1/3L). Figure 4-13 shows time-frequency representation of bridge under different damage. Figure 4-14 shows instantaneous frequency variations under different bridge damage conditions highlights how structural integrity impacts time-variant characteristics.

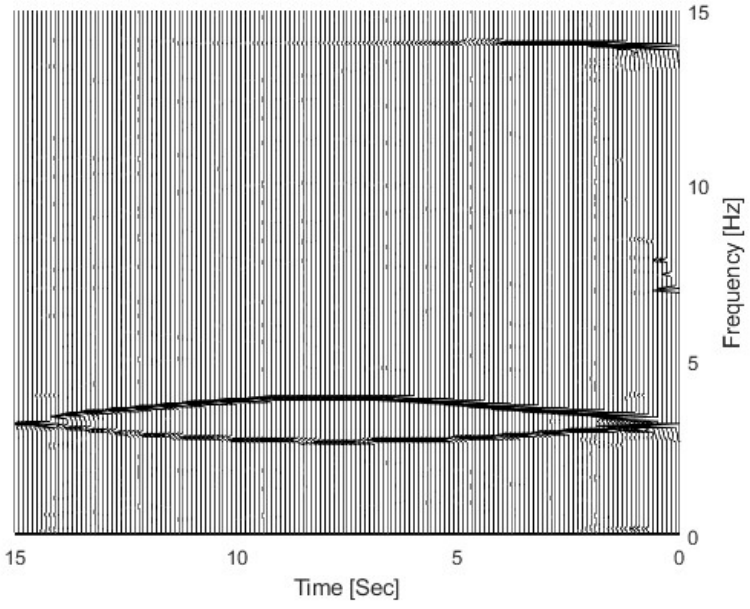

(a) small damage $(\alpha = 0.3)$

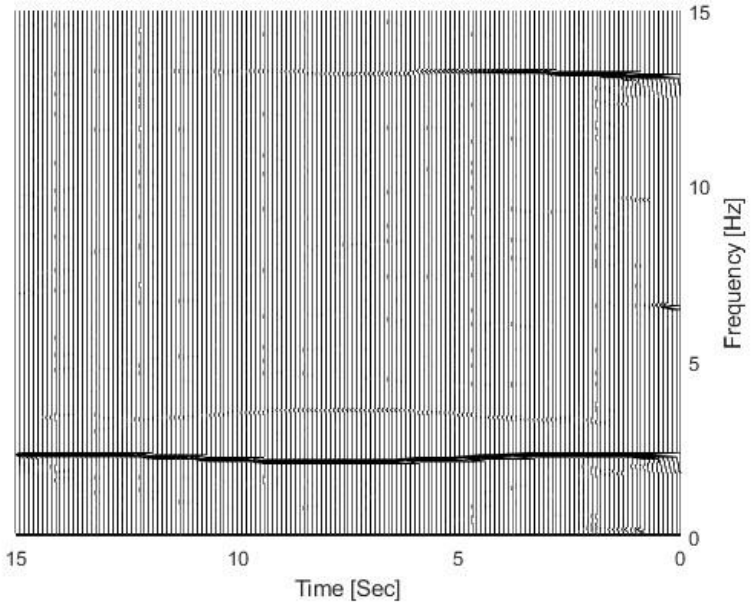


(b) large damage $(\alpha = 0.6)$

Figure 4-13 TFR of bridge (a) Small damage (b) Large damage

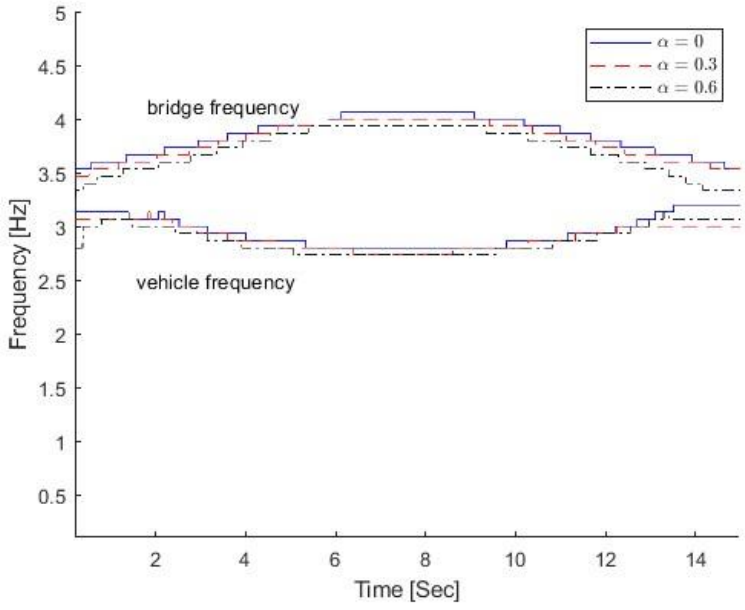


Figure 4-14 Instantaneous frequency of different $\alpha$

Different damage conditions caused substantial changes in the bridge's IF according to the figure 4-14. Comparison of theoretical value, the MSE value for α=0 is 0.0066, the MSE values for α=0.3 is 0.0137 and the value for α=0.6 is 0.0185. The MSE value could be a damage indicator. When the bridge is undamaged at α=0 the blue solid line demonstrates how its instantaneous frequency maintains stability within the 3.5 Hz to 4.5 Hz range which shows the bridge's stiffness remains intact and its dynamic response stable. The red dashed line in the slightly damaged condition (α=0.3) reveals a minimal frequency decline in the middle and latter segments towards 3.5 Hz showing minor localized stiffness degradation. When the bridge is in a severely damaged state with α=0.6 this condition results in a black dotted line showing major frequency decline and extreme fluctuations during middle to late phases which clearly demonstrates a major stiffness decrease and significant effects on the dynamic response. The vehicle maintains a consistent instantaneous frequency at approximately 3 Hz for all bridge damage states which shows that bridge damage does not directly alter the vehicle's dynamic characteristics. The dynamic interaction between the vehicle and bridge grows stronger as the bridge damage increases.

Shown as Figure 4-14, for the undamaged state, the frequency remains stable over time, suggesting consistent dynamic behavior. With minor damage, there's a slight decline in frequency, particularly mid-duration, indicating a marginal reduction in structural stiffness and a limited effect on the bridge's time-variant response. The large damage condition shows a significant drop and instability in frequency, especially in the latter half of the observed period, revealing increased unpredictability and a potential

progression of damage over time. Although the vehicle frequency remains relatively unaffected across all states, the bridge frequency changes indicate a varying dynamic interaction between the vehicle and bridge damaged structure, which is crucial for damage identification and SHM.

#### 4.3.3.2 Effect of different damage parameter $\beta$

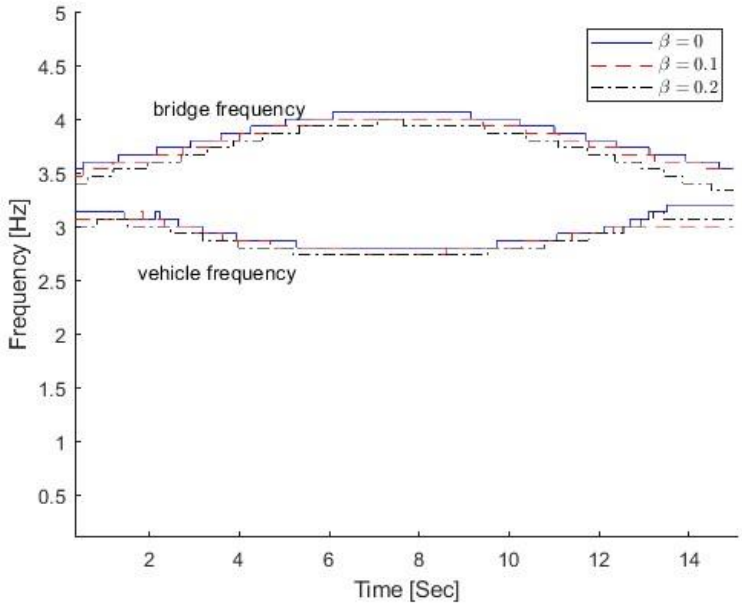


Figure 4-15 Instantaneous frequency of different $\beta$

The parameter $\beta$ represents the length of the damaged region. It is used to determine the extent of the damaged area along the beam. Through $\beta$, the length of the damaged region can be described relative to the total length of the beam. The study set $\beta = 0.1$ for small damage, $\beta = 0.2$ for large damage, other parameter is same, $\alpha$ is 0.3, lc equals half of the beam length (1/3L), and m is 2.0. Compared with the three cases, Figure 4-15 shows IF of different $\beta$ using MSST.

The variations in instantaneous frequency indicate the bridge's dynamic responsiveness

differs according to the type of damage present. Comparison of theoretical value, the MSE value for $\beta$=0 is 0.0073, the MSE value for $\beta$=0.1 is 0.0102 and the MSE value for $\beta$=0.25 is 0.0307. When undamaged ($\beta$ = 0 blue line), the frequencies of the bridge and vehicle remain constant, with the bridge frequency approximately 3.5 Hz and the vehicle frequency approximately 3 Hz, indicating uniform dynamic behavior devoid of peaks and troughs. With minimal damage ($\beta$ = 0.1 red dash line), the bridge frequency experiences a tiny drop and exhibits minor fluctuations in the mid-period (5-10 seconds), although the vehicle frequency remains largely steady with just negligible variations. This indicates that minor tangles result in negligible variations in the bridge's rigidity. With increased damage ( $\beta$ = 0.2 black dash line), the bridge's frequency exhibits greater instability, especially between 2–6 seconds and 10–14 seconds, whereas alterations in stiffness and dynamic characteristics are much diminished. The car frequency is largely unchanged during this period. Overall, bridge frequency is more adversely affected by damage, exhibiting greater fluctuations in relation to the amount of damage, which reflects its influence on the bridge's dynamic nature. The frequency of vehicles is largely unaffected by bridge damage.

#### 4.3.3.3 Effect of different damage locations

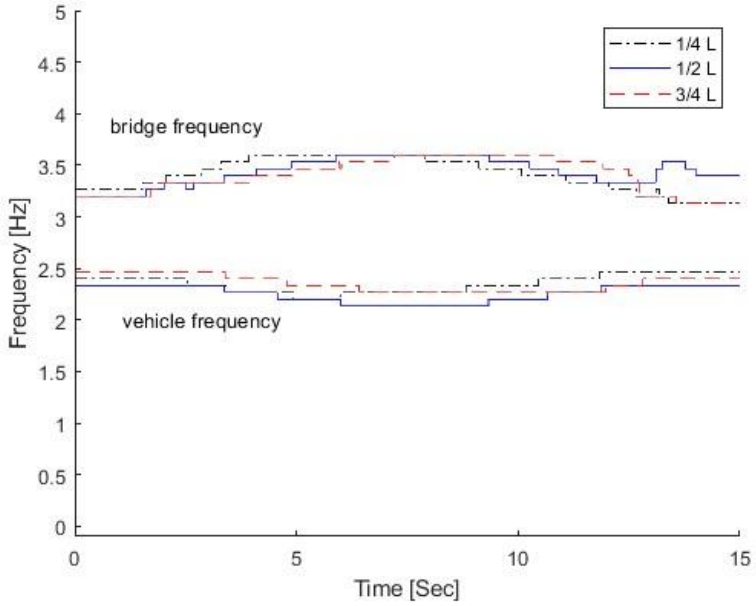


Figure 4-16 Instantaneous frequency of different damage location

Three distinct damaged areas along the bridge were the subject of the study: one-fourth, the middle, and three-fourths of its length (e.g., 0.5L,0.25L,0.125L). The primary aim was to comprehend how the location of damage affects VBI properties, especially with regard to the bridge's first-order frequency response.

Figure 4-16 shows the variations in instantaneous frequency across different damage locations on the bridge reflecting the impact of damage on the structure's dynamic characteristics. Damage at the 1/4 L position, which is closer to the bridge's support point, exhibits a slightly higher frequency response, suggesting that damage in proximity to the supports may have a relatively minor overall dynamic impact on the structure. The lower frequency observed at the mid-span position (1/2 L) indicates a more significant impact on the bridge's dynamic properties, especially considering this location typically corresponds to the point of maximum deflection and is thus more sensitive to changes in

overall stiffness. The 3/4 L damage location shows a rightward shift in time-variant features, implying that the effect of damage becomes more evident during the latter half of the load application. This is because the damage at this location, being farther from the supports, takes longer to manifest in the bridge's overall response. Taken together, these changes in IF introduce the extent of the damage based on the location.

## 4.4 Experimental study

### 4.4.1 Experimental setup

A VBI model has been developed in the lab, as illustrated in Figure 3-23. The bridge model is the same as Figure 3-25 in Chapter 3, and Figure 3-26 shows the vehicle model. Bridge parameter is same as experiment of Chapter 3. The bridge frequency is from first to fifth mode is 2.09Hz, 5.75Hz, 13.75Hz, 18.28Hz, 24.48Hz, respectively. The vehicle speed is 0.35m/s. Figure 3-26 shows adding 5kg mass block was added to the mid-span of the first span of the bridge model to simulate damage. Sensor and sensor location is same as experiment of Chapter 3.

### 4.4.2 Comparison of damage and no damage

Figure 4-17 shows original signal and FFT of bridge response, based on the bridge's reactivity, the results show that the IF is the primary mode of vibration for the first bridge. As shown in Figure 4-18, the IF with the mass is typically lower than that without the supplementary mass. The vehicle response indicates that IF increases with the added mass.

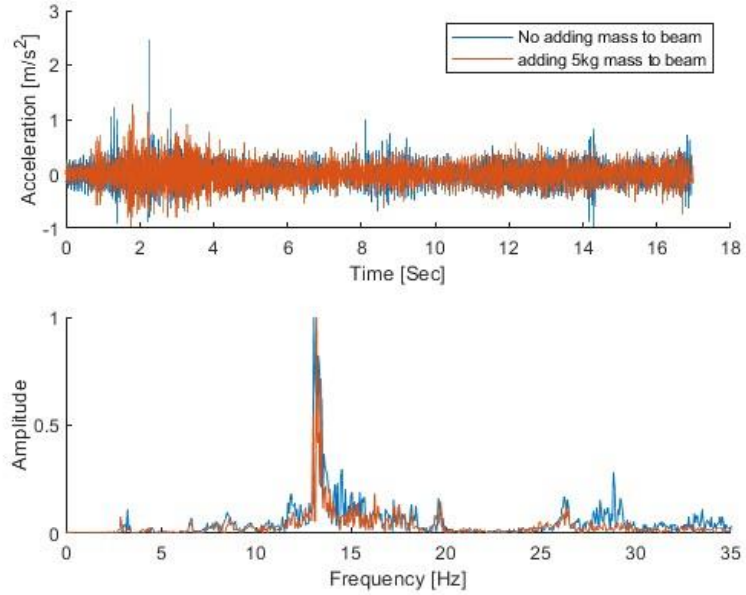


Figure 4-17 Original signal and FFT of bridge response

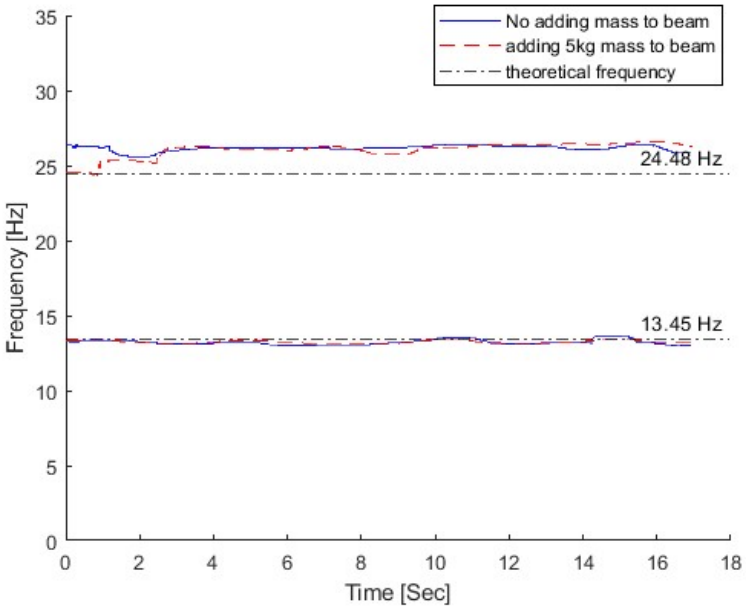


Figure 4-18 IF of bridge response

Figure 4-18 shows the frequency response of the beam over time in undamaged (blue line)

and simulated damage (red line, with 5 kg added mass) conditions, with theoretical frequencies (13.45 Hz and 24.48 Hz) marked. In the undamaged state, the frequency is close to theoretical value, while the frequency slightly decreases under the simulated damage condition. Figure 4-17 (upper part) shows the time-domain acceleration response of the beam, where the waveforms under both conditions are similar, but the acceleration under the damaged condition is slightly smaller. The lower part shows the frequency spectrum, where damage causes a slight shift in the main frequency and small changes in the amplitude.

The added mass simulates localized damage, which effectively triggers complex time-varying characteristics in the response of the VBI system. The localized damage reduces the stiffness of the beam, leading to a decrease in the system's natural frequency and making VBI system more sensitive. As the vehicle moves across the bridge, this sensitivity can induce nonlinear vibrations or localized resonance effects. The damage-induced dynamic characteristics manifest not only in the time-domain response (with reduced acceleration amplitude and slower vibration decay) but also as a shift in the main frequency and changes in the energy distribution in the frequency domain.

Furthermore, vehicle-bridge interaction exhibits typical time-varying characteristics, as the beam's dynamic response changes continuously with the moving vehicle. Damage-induced stiffness reduction enhances the bridge’s transient response, especially when the vehicle approaches or crosses the damaged region, potentially causing abrupt changes in acceleration and vibration amplitude. This time-varying effect increases the complexity

of the system's vibration and causes the bridge to exhibit non-constant frequency characteristics at different times. Thus, the added mass simulating localized damage not only alters the overall dynamic frequency but also amplifies the time-varying response characteristics triggered by vehicle excitation in the bridge's damaged region.

### 4.4.3 Compare with Sychroextracting transform (SET)

Li et al (2020) proposed use Sychroextracting transform (SET) to extract time varying feature, compare with SET under this experiment, Figure 4-19 shows using SET method to extract IF of bridge response.

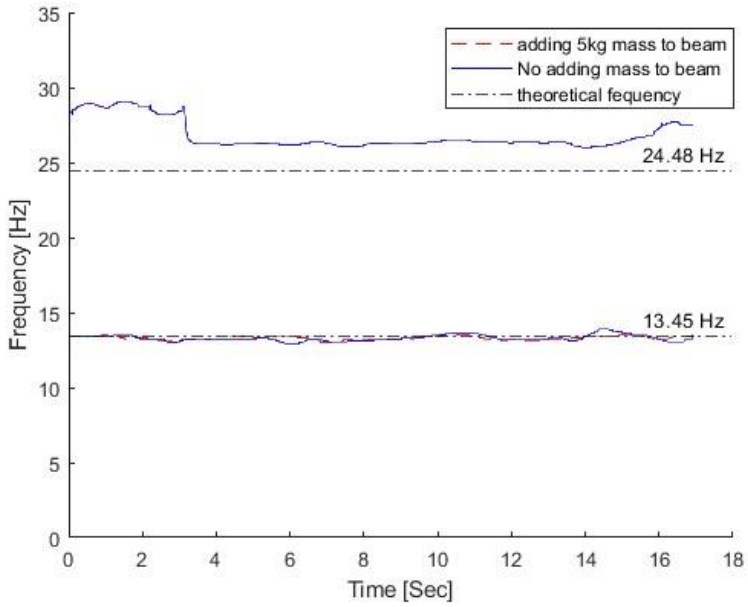


Figure 4-19 IF of bridge response using SET

The performance of the SET and MSST methods in frequency analysis shows significant differences. The SET method demonstrates the frequency variations of the beam with and without the addition of a 5 kg mass, but it exhibits considerable fluctuations and instability, particularly in the high-frequency range (e.g., above 25 Hz). Although the primary frequencies (approximately 13 Hz and 25 Hz) are observable, the distinction is less clear,

indicating that the SET method has lower time-frequency resolution, unclear trends, and higher noise levels. In contrast, the MSST method provides a much clearer and more stable frequency representation. The theoretical frequency lines (13.45 Hz and 24.48 Hz) added to the plot align closely with the experimental results, showcasing the high resolution and reliability of the MSST method. Even with the addition of the 5 kg mass, the frequency variations remain smooth, with significantly less fluctuation compared to the SET method. Overall, the MSST method outperforms the SET method in terms of stability, clarity, and consistency with theoretical results, making it more suitable for accurately identifying frequencies in the analysis of bridge-vehicle dynamic interactions.

### 4.5 Study with a cable-stay bridge

Figure 4-20 The cable stayed bridge

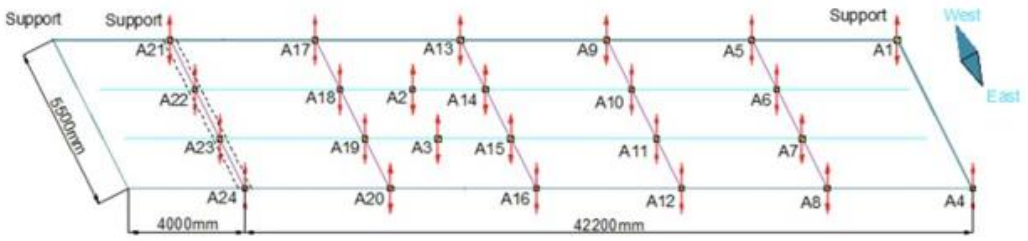


Figure 4-21 Sensor location

A cable-stayed bridge links the South and North campuses of Western Sydney University, The construction supports a single-lane roadway of 46 meters in length and 5 meters in width Figure 4-20 illustrates that the bridge deck has two continuous spans, with the structural mast serving as an interior support situated in proximity to the southern entrance of the bridge. The bridge deck is equipped with 24 accelerometers. Figures 4-21 illustrate the sensor positions. A data collection system always captures data from sensors at a sample frequency of 600 Hz. This research will analyze the vehicle-induced reactions of the bridge.

### 4.5.1. The situation on the bridge with varying traffic conditions

Measurements A11 are obtained under three distinct traffic conditions. This investigation compares the bridge's acceleration reactions with and without automobiles. Case 1 depicts a condition devoid of automobiles on the bridge, while Case 2 includes instances when a vehicle crosses the bridge. Figure 4-22 shows the acceleration responses and FFT spectrum. Figure 4-23 shows the IF of the two cases.

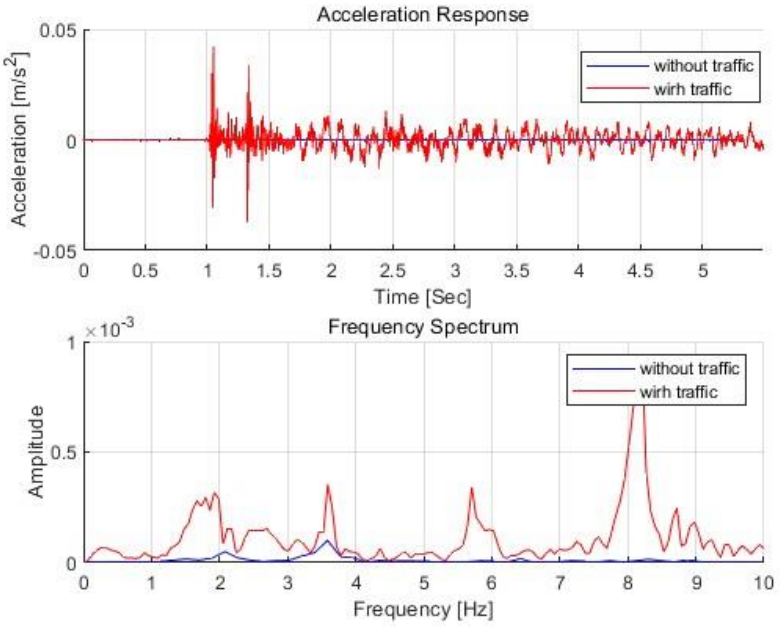


Figure 4-22 Acceleration responses and FFT spectrum of different traffic condition

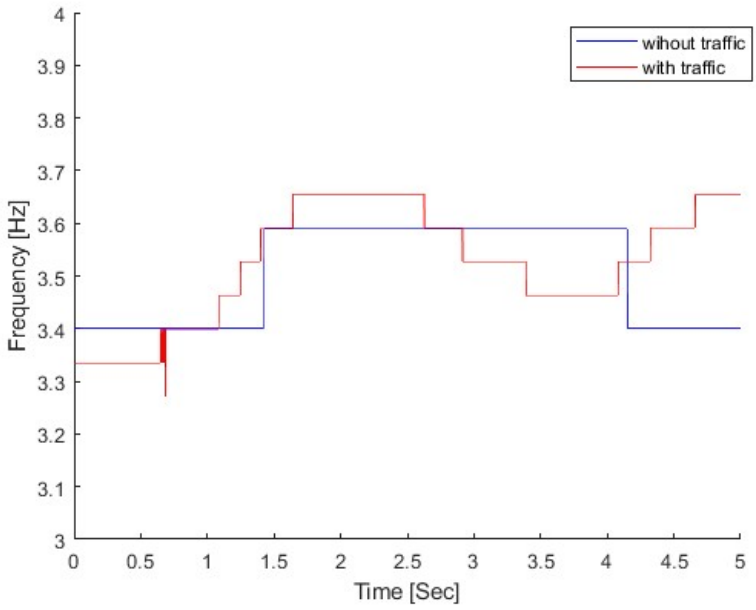


Figure 4-23 IF of different traffic conditions

Figures 4-22 shows the significant impact of traffic loads on the dynamic feature and frequency characteristics of the cable bridge. Under traffic conditions, the bridge exhibits

stronger acceleration responses, especially during the 1 to 2-second interval when the vibration amplitude significantly increases (red curve). Figure 4-23 shows that higher frequency components (notably around 8 Hz) are significantly amplified under traffic, indicating resonance induced by the passing vehicles. Meanwhile, the time-frequency curve reveals larger frequency fluctuations over time due to traffic loads, reflecting the dynamic characteristics of the bridge under operational conditions.

Comparing the acceleration and instantaneous frequency between the without traffic and with traffic cases, Figure 4-27 highlights that the second frequency of the bridge is more pronounced in the range of 3 to 4 Hz. When comparing the instantaneous frequency in this range, it can be observed that due to vehicle excitation, the bridge's mode shape becomes more prominent. In the absence of traffic, the frequency of the second mode shape shows minimal variation. However, under the condition of vehicular passage, the corresponding frequency trajectory of the bridge exhibits significant fluctuations.

As above, applying MSST to complex bridge geometries faces three key challenges: limited resolution for closely spaced modes in cable-stayed/suspension bridges, difficulty in handling non-stationary vibrations of irregular configurations (e.g., curved/variable-section girders), and high computational cost for large datasets. These limitations could be examined through shaking table tests, field measurements, and algorithm optimization to assess and improve the method's practical applicability.

### 4.6. Summary

A novel bridge health monitoring based on MSST is adopted for the analysis of the

nonstationary dynamics of VBI in this chapter. The study highlights the significance of bridge vibration responses during vehicle passage and explores the application of TFR in modern bridge engineering.

The MSST-based method proposed in this chapter is particularly adept at extracting time-varying features from VBI systems for bridge SHM. The MSST method demonstrates high concentration and clarity in time-frequency representation, effectively suppressing mode mixing and background noise, thereby more accurately extracting signal features. Furthermore, a series of numerical simulations and experimental studies validate the method's accuracy in detecting damage location and assessing the severity of damage quantitatively.

Experimental research further corroborates the effectiveness of this method, particularly in analyzing the behavior of bridges under various moving load conditions. Experimental findings show significant differences in strain, displacement, and acceleration responses of bridges under varying nature and magnitude of loads. These findings not only affirm the efficacy of the MSST method but also highlight the consistency between experimental observations and simulated data, enhancing the credibility of the computational approach as a reliable tool for structural analysis and bridge assessment studies.

While MSST provides enhanced resolution, its computational intensity hinders real-time applications. The method is sensitive to parameter tuning and may generate artificial components.

In summary, the MSST-based bridge health monitoring method proposed in this paper

enhances the accuracy and efficiency of bridge health monitoring and provides new tools for future bridge maintenance work. This method's practical value and potential for broad application signify a significant advancement in the field of vibration based SHM. Future experimental validation will assess its performance across different bridge types and operational scenarios, including varying traffic loads and environmental conditions.

# CHAPTER 5 Dual-source vehicle-bridge interaction analysis using dual-stream CNN and synchrosqueezing transform for structural health monitoring

## 5.1 Overview

In Chapters 3 and 4, two methods have been developed to extract time-varying characteristics of VBI systems using SST2 and MSST. Numerical and experimental results show that the change for the pattern of time-varying characteristics could be an indicator of the bridge damage. This chapter discusses bridge damage detection via dual stream CNN with the time-varying characteristics as the input.

Building upon the feature extraction results from the previous two chapters, Chapter 5 develops a dual-stream CNN architecture: the vehicle feature stream and the bridge feature stream are coupled via a weighted fusion layer. It employs dynamic response data from vehicles and bridges to generate high-resolution time-frequency spectrograms, which are processed through two distinct streams of the dual-stream CNN for feature extraction. Features derived from the retrieved data are subsequently amalgamated and organized within a Support Vector Machine (SVM) to identify and assess bridge deterioration. A vehicle-bridge linked dynamic model, simulated under various damage scenarios, considering road surface roughness, vehicle speed, and noise levels, shows robustness and accuracy even in extreme conditions. The approach, when integrated with time-frequency signals from vehicles and structures, captures dynamic interactions on an

extensive scale, facilitating the identification of intricate damage patterns. Establishing the potential of using a dual-stream CNN with SST for bridge health monitoring. Feature efforts will concentrate on optimizing the model architecture, enhancing multi-scale feature extraction and attention algorithms, and utilizing larger datasets to improve generalization for additional applications in structural health monitoring.

The rest of this chapter is framed as follows: VBI model is first discussed and then the SST-based time-frequency analysis approach and dual-stream CNN is presented. There are then numerical and experimental studies, and conclusion.

## 5.2 Theory

This section first gives an overview of the general design of the proposed approach, and then describes in detail some of the basic steps and underlying concepts like Vehicle-Bridge Interaction (VBI) modeling, SST, and dual-stream CNN structure.

Structured damage detection and classification method formulated here has 3 stages: VBI (Vehicle-Bridge Interaction) system modeling stage, feature extraction step, and damage classification step. Figure 3-1 VBI system modelling requires (1) creating vehicle-bridge coupled dynamic model and (2) modeling vehicle-bridge system at various damage scenarios with the Matlab to get acceleration response. The time-dependent details of the bridge and vehicle responses are computed in Section 2.2 using SST and Figure 5-2 shows how the damage classification algorithm is built on the dual-stream CNN.

### 5.2.1 Dual stream CNN

#### 5.2.1.1 Data normalization

When damage classification is done before, data from multiple sensors can be very amplitude differences, therefore the data needs to be normalized. Normalization – Normalization, that is, normalizing the data to maintain a constant range of values, in most cases using Min-Max normalization procedure to normalize the data ([0, 1] or [-1, 1] range). It keeps the number constant in training and enhances convergence time.

The formula is:

$$x' = \frac{x - \min(x)}{\max(x) - \min(x)} \tag{5-1}$$

where $x$ is the original data value. $x'$ is the normalized data value. $\min(x)$ is the minimum value of the data. $\max(x)$ is the maximum value of the data.

For image pixel values, the minimum is typically 0, and the maximum is 255. Therefore, the normalization formula simplifies to:

$$x' = \frac{x}{255} \tag{5-2}$$

#### 5.2.1.2 Model Architecture

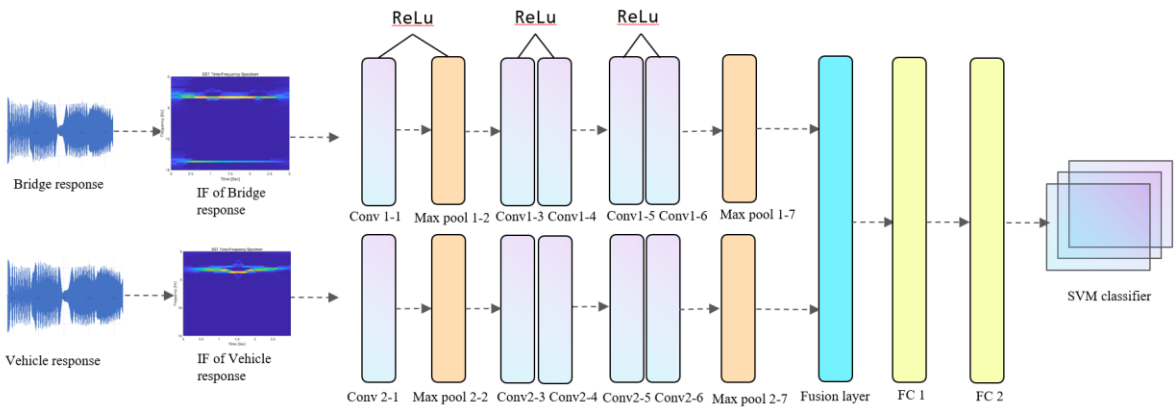

Figure 5-2 dual stream CNN model architecture

The model of the dual-stream CNN after preprocessing the data receives the TF spectrogram of the vehicle and TF spectrogram of the bridge using two parallel convolution streams. Figure 5-2 outlines two parallel convolution streams, each of which processes the real-time frequency from the vehicle and bridge respectively. Each stream gets the necessary features by using convolutional and pooling layers, both streams are combined by feature fusion, then grouped by fully connected layers and SVM classifier.

(1) Convolutional layer

Convolutional layer: This is the basis of CNNs, where local features are derived from input data. In a two-stream CNN, each stream is multiple convolutional layers (Purwono et al. 2022):

Convolution operation – it passes convolution kernels (filters) over the input data, then dot product to create feature maps. Step by step instructions are as follows: Let's say input data is a two-dimensional matrix $X$ of dimensions $H \times W$ where $H$ and $W$ are height and width respectively. Second the convolutional kernel K is kk in dimensions, and k should be an odd number (3, 5, 7). At the last stage, the result of the convolutional process $Y$ is obtained like this:

$$Y(i,j) = (X * K)(i,j) = \sum_{m=0}^{k-1} \sum_{n=0}^{k-1} X(i+m, j+n) \cdot K(m,n) \quad (5\text{-}3)$$

where, * denotes the convolution operation, and $X(i+m, j+n)$ and $K(m,n)$ represent elements of the input data and convolutional kernel, respectively.

Activation Function:

Once the convolution is complete, a nonlinear activation function usually gets used to add nonlinearity so that the model can take on additional features. Especial ReLU (Rectified Linear Unit):

$$\text{Re } LU(x) = \max(0, x) \tag{5-4}$$

ReLU turns negative values into 0 and positive values into 1 (Wang et al. 2020). Thus, we get nonlinearity.

(2) Pooling layer

Pooling layer is mostly used to shrink feature map spatial dimension (height and width) with respect to some important features. This is done to reduce the network parameter and calculation footprint and reduces overfitting (Zafar et al. 2022).

Max pooling (Hussain and Hesheng 2019): picks the maximum amount of any given pool window. This process reduces the input spatial size but retains the prominent elements. Formula is shown:

$$Y(i,j) = \max_{m=0,\ldots,k-1} \max_{n=0,\ldots,k-1} X(i \cdot s + m, j \cdot s + n) \tag{5-5}$$

where $Y(i,j)$ is the value output to position $(i,j)$, $X$ is the input feature map, $k$ is the window size for pooling, s is stride (step size for sliding the window) max chooses maximum value of window.

(3) FC layer and dropout

The fully connected layer collects the features extracted by various convolution kernels of the layers above and performs the final classification. A single vector is created by merging the input characteristics in a certain order. All feature values $x^{m-1}$ get weight $W^m$ and a bias $b^m$. Such feature values are filtered via an activation function $f(\cdot)$ to get the features more linearly separable to facilitate classification. Function of fully connected layer is as follows (Zhou et al. 2022):

$$f(a^m) = f(W^m x^{m-1} + b^m) \tag{5-6}$$

The dropout layer is applied to give the model generalization power and robustness (Xiao et al. 2021). During training, some neurons are removed from the calculation on a random basis by some ratio. Dropout layer output is the final extracted feature which is sent to classification layer for final classification.

(4) SVM

After FC layer feature map classification layer. Support Vector Machines (SVMs) employ the polynomial kernel function to deal with non-linear data. It efficiently and simply separates the initially indivisible data by transforming it into a higher-dimensional space and then drawing a straight line between the two sets of data (Mao et al. 2016).

$$K(x_i, x_j) - (\gamma \cdot x_i^T x_j + r)^d \tag{5-7}$$

where $\gamma$ is a scaling parameter, controlling the influence of the polynomial. The default value is 1, $r$ is a constant term in the kernel function, usually referred to as the bias. The default value is 0, $d$ is the degree of the polynomial.

When Lagrange multipliers are added, the optimization problem is now converted to a double problem. The dual problem's objective function is the following in SVM using a polynomial kernel function:

$$\max_{\alpha} \sum_{i-1}^{n} \alpha_i - \frac{1}{2} \sum_{i-1}^{n} \sum_{j-1}^{n} \alpha_i \alpha_j y_i y_j \left(\gamma \cdot x_i^T x_j + r\right)^d \tag{5-8}$$

where $\alpha_i$ are the Lagrange multipliers, $y_i$ are the labels of the samples, taking values $\pm 1$, $x_i, x_j$ are the input samples.

The constraints are:

$$\begin{array}{l} \sum_{i-1}^{n} \alpha_i y_i - 0 \\ 0 \leq \alpha_i \leq C, \forall i \end{array} \tag{5-9}$$

By solving the above dual problem, the Lagrange multipliers $\alpha_i$ can be obtained, and then the weight vector $w$ and bias $b$ can be computed.

Calculation of Weight and Bias. Once $\alpha_i$ are solved, the weight vector $w$ and bias $b$ can be computed as:

$$\begin{array}{l} w - \sum_{i-1}^{n} \alpha_i y_i x_i \\ b - y_k - \sum_{i-1}^{n} \alpha_i y_i K(x_i, x_k) \end{array} \tag{5-10}$$

The decision function of SVM is:

$$f(x) - \text{sign}\left(\sum_{i-1}^{n} \alpha_i y_i K(x_i, x) + b\right) \tag{5-11}$$

For the polynomial kernel function, the equation becomes:

$$f(x) - \text{sign}\left(\sum_{i-1}^{n} \alpha_i y_i (\gamma \cdot x_i^T x + r)^d + b\right) \tag{5-12}$$

#### 5.2.1.3 Fusion of Vehicle-Bridge Coupled Features

In vehicle-bridge couplings, the dynamic response under VBI can tell us about the health

of the bridge. As a vehicle goes over the bridge, the friction between the vehicle and the bridge results in complicated acceleration effects. Through the SST, time-varying properties can be computed from the acceleration responses – the IF features of the system under a range of damage states.

In this study, two input streams of the dual stream CNN are divided between the IF data of the car and bridge. Each stream is first filtered to local features from the IF spectrum, then the features are merged with a feature fusion algorithm. The fusions features are then assigned to an SVM classifier which returns the damage state of the system.

This dual-stream CNN design allows for an accurate representation of the VBI coupling system dynamic interactions, and thus the classification of damage. The processing of the vehicle and bridge response is carried out separately, so the model can see a lot of patterns of damage and dealing with different kinds of damage.

### 5.2.2 Parameter configuration

The dual-stream CNN architecture being proposed extracts the SST features from the car and bridge and extracts time-varying properties useful for structural health detection and damage identification. Each stream in the network has six convolutional layers and two fully connected layers (with dropout and pooling layers to avoid overfitting). Both streams' results are merged into a classification task by an SVM classifier which classifies extracted features according to damage type.

Model Architecture Overview

The architecture of the dual-stream CNN is carefully designed to capture the VBI. The key configurations are as follows:

Learning Rate: Initial learning rate of 0.001 to trade convergence time with stability. Learning rate might be too fast, which will create unpredictable training and poor performance, learning rate is too low, and that may slow convergence. For model optimization, a dynamic learning rate-adjustment is applied. If validation loss remains unchanged, the learning rate gets decreased by 0.01. This approach permits the model to converge without overfitting.

Batch Size: The batch size is 16. This size is selected so that it fits memory and have enough gradient update frequency. The larger the batch size, the slower the convergence (fewer updates per epoch) and the smaller the batch size, the noisier the gradient updates.

Dropout and Regularization: Dropout layers are included after each fully connected layer with a dropout rate of 0.2 for training part, 0.3 for test part.

SVM: Damage classification using SVM is done after feature extraction phase. The SVM use polynomial kernel to process nonlinear data and effectively partition damage classes in feature space.

It develops a dual-stream CNN model for damage detection and assessment of bridge, using SST features from the vehicle and bridge, SVM classification, and regression model to quantify the damage amount. The work is trained and tested on a dataset generated from finite element simulation with acceleration response data of bridges and cars under

different damage scenarios.

Table 5-1 Algorithm of dual stream CNN

| Algorithm |
| --- |
| Note: Input stream (X1, X2) and labels Y, X1 is first input stream, X2 is labels.<br>and X2 is the second stream. Be the feature generation (convolutional layer) G1 and G2.<br>each stream and C be the classifier network (all connected layers). The Adam optimization algorithm<br>learn is 0.01, Mini batch is 16, Epochs are 30.<br>For e = 1 to No. of epochs (i.e., 30):<br>To each batch of the data set:<br>1. Output X1 to G1 (Stream 1) to get feature maps.<br>2. Output X2 to G2 (Stream 2) to get feature maps.<br>3. Combine the feature maps G1 and G2.<br>4. Output the fusion of feature maps to the classifier C.<br>5. Calculate loss of categorical cross-entropy equation.<br>6. Back propagated Gradients G1, G2 and C.<br>7. Adam Optimizer: replace G1, G2 and C weights.<br>END |

### 5.2.3 Noise simulation

To simulate measurement conditions with a SNR of 26,5%, the computed acceleration is supplemented by white noise. as equation:

$$acc_m = acc_{cal} + E_p \cdot N_{\text{oise}} \cdot \sigma(acc_{cal}) \tag{5-13}$$

where $acc_{cal}$ denotes the computed acceleration response, $E_p$ denotes the noise level,

$N_{\text{oise}}$ is a vector adhering to a conventional normal distribution with a mean of zero and a variance of one, $\sigma(acc_{cal})$ represents the standard deviation of the computed acceleration.

### 5.2.4 Algorithm workflow

The workflow of the dual-stream CNN model for VBI coupled damage identification consists of several stages: data preprocessing, feature extraction, model training, and damage classification. The flow of the algorithm is illustrated in the text-based flowchart provided in Figure 5-3.

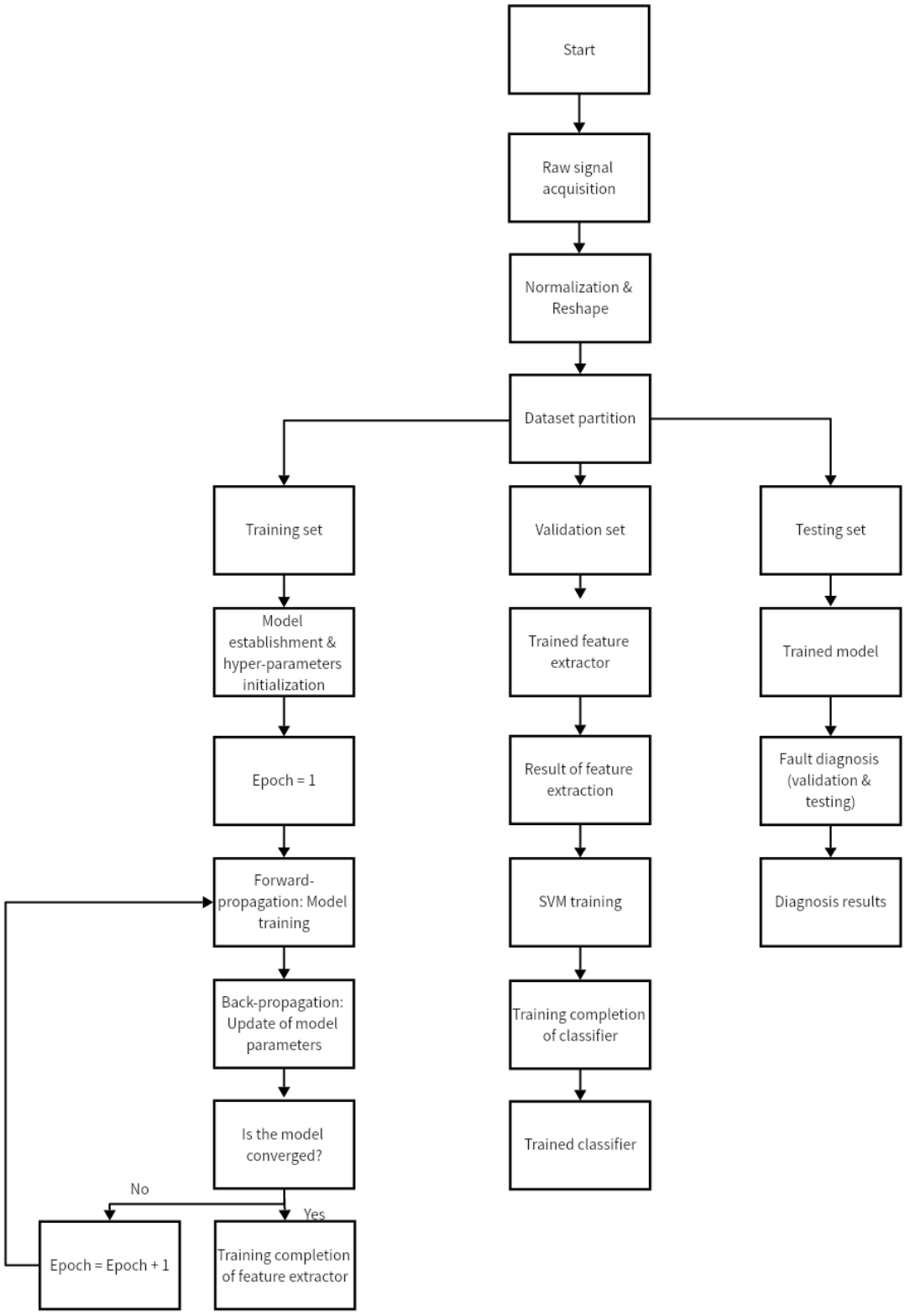


Figure 5-3 Schematic flowchart of the proposed model.

The training set, validation set, and testing set are partitioned as described. The model is

trained on the training set to adjust parameters, and validation is used to tune hyperparameters, such as the learning rate and dropout rates. During this phase, different values for the parameters are selected, and to guarantee improved generalization to unknown data, the model is tested on the validation set. After the optimal model is obtained, the testing set is used to make predictions, which evaluates the final performance of the model. No parameter updates occur during this stage.

The entire model is trained as a pipeline of three stages: feature extraction from both the vehicle and the bridge, feature fusion, and classification using an SVM classifier.

In the first part of the pipeline, the feature extraction stage uses a dual-stream convolutional architecture to separately process the vehicle and bridge acceleration signals. Each stream consists of multiple convolutional and pooling layers designed to capture essential time-varying features. Afterward, the extracted features from both streams are concatenated and fed into the classification stage.

The second stage combines the extracted features through feature fusion. These fused features are then passed through fully connected layers.

In the final stage, classification is performed using a SVM classifier. The SVM uses a polynomial kernel to distinguish between various damage states of the bridge structure based on the fused features extracted from the vehicle-bridge system. The classifier outputs the predicted damage class, which corresponds to specific damage scenarios or health conditions of the bridge.

**5.3. Case study**

### 5.3.1 Bridge and vehicle parameters

This study employs a simplified quarter-vehicle model to analyze this dynamic interaction. Despite its simplicity, the model is essential, encompassing key parameters such as wheel stiffness, damping coefficients, vehicle mass, and bridge mass, which directly influence the vehicle's response to the bridge's dynamic behavior. The model also considers the bridge's length, a significant factor in determining its dynamic response under vehicular loads. By focusing on the bridge's mass and length, the study aims to understand how different vehicles interact with various bridge spans and how these interactions impact the overall response of the bridge. The vehicle and bridge parameters are listed on Tables 3-2 and 3-3.

Wahab et al.'s model (Wahab et al. 1999) is used to simulate damage scenarios. As shown Eq.3-9. The parameter β, representing the length of the damaged zone, is established as 0.25, while n is designated as 2. The parameter α, indicating the extent of damage, varies from 0 to 1 in increments of 0.005 to model different levels of damage severity. is utilized to provide eleven damage classifications.

The dataset utilized in this study is sourced from finite element simulation. The bridge in question is a reinforced concrete construction measuring 30 meters in length. The velocity of the vehicle is 10 meters per second. Accelerometers are positioned at three-tenths of the span, and data is recorded at a frequency of 200 Hz. Five percent white noise is incorporated into the signals to replicate realistic situations. The dataset comprises 1200 samples, each depicting a unique condition of the bridge, categorized into 10 separate

damage levels, from no damage to severe damage. The frequency range of these time-varying features is designated between 0 and 15 Hz, encompassing bridge frequencies of 3.90 Hz and 13.55 Hz, as well as a vehicle frequency of 3.20 Hz.

Table 5-2 Categorizes Road surface roughness

| Level | Range of Srr(ω0) e-6 m2/(cycle/s) | Mean of Srr(ω0) e-6 m2/(cycle/s) |
|---|---|---|
| Very good (A) | 2–8 | 5 |
| Good (B) | 8–32 | 20 |
| Normal (C) | 32–128 | 80 |
| Bad (D) | 128–512 | 320 |
| Very bad (E) | 512–2048 | 1280 |

The ISO 8608 standard categorizes road surface roughness into five classifications, as detailed in Table 5-2 (Talaei et al. 2023), according to the amplitude range of the power spectral density function at the standard frequency Srr(ω0).

### 5.3.2 Data preprocessing

In order to guarantee that the data is accurate and consistent, several preprocessing steps are undertaken:

Each acceleration response sample is normalized to have a mean of 0 and a standard deviation of 1. This standardization process helps in reducing the variability due to different scales of measurement and ensures that the data is centered around zero, which facilitates the training of the neural network by speeding up convergence and improving numerical stability.

The SST is applied to the normalized acceleration data to extract high-resolution time-frequency features. SST is particularly effective in revealing the detailed time-frequency structure of the signals, which is crucial for accurately detecting and assessing damage. The resulting SST representations are two-dimensional time-frequency maps that serve as inputs to the dual-stream CNN. These maps capture the intricate patterns associated with different damage levels, providing rich information for the subsequent classification and regression tasks.

To enhance robustness and prevent overfitting, this involves generating additional training samples by applying slight variations to the original data, such as random noise addition, time shifting, or scaling. Data augmentation helps in creating a more diverse training set, which improves the model's generalization capability.

The dataset is divided into training, validation, and test subsets. Generally, 70% of the data is allocated for training, 15% for validation, and 15% for testing. The training set is utilized to develop the model, the validation set to optimize hyperparameters and mitigate overfitting, and the dataset to evaluate the model's performance on fresh data.

By following these preprocessing steps, the quality and consistency of the dataset are maintained, ensuring that the model receives clean and well-prepared inputs. This preprocessing pipeline is critical for achieving high performance in both classification and regression tasks, as it maximizes the information extracted from the raw acceleration signals.

### 5.3.3 Training and feature extraction with dual-stream CNN

Different damage scenarios are simulated by different damage parameters $\alpha$ from 0 to 0.6, that is divided 10 categories. SST is used to extract time-varying features from vehicle and bridge responses. Figure 5-4 shows TFRs of vehicle responses with different bridge damage. Figure 5-5 shows TFR of bridge responses with different bridge damage. Roughness level C is considered, and SNR is 26dB.

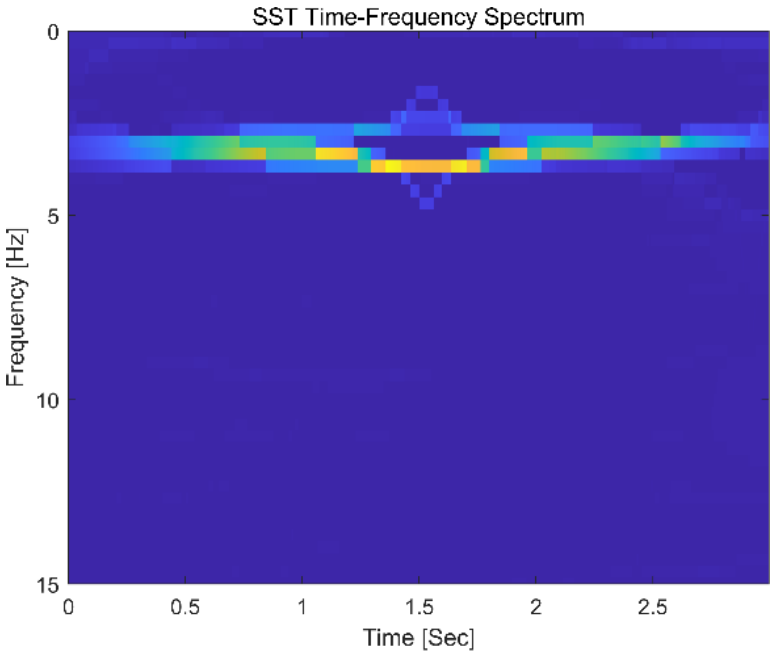


(a) no damage $\alpha = 0$)

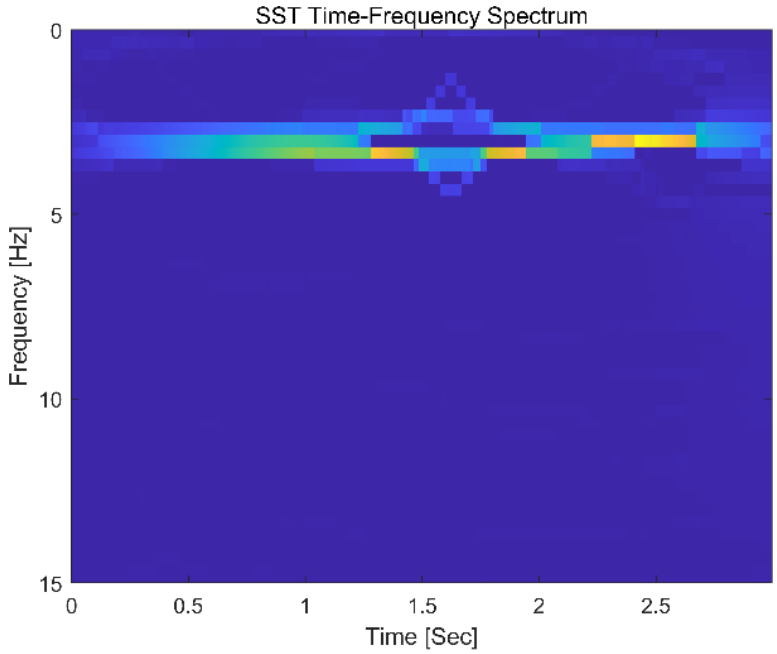


(b) Level 5 damage ($\alpha = 0.3$)

Figure 5-4 TFRs of vehicle responses with different bridge damage

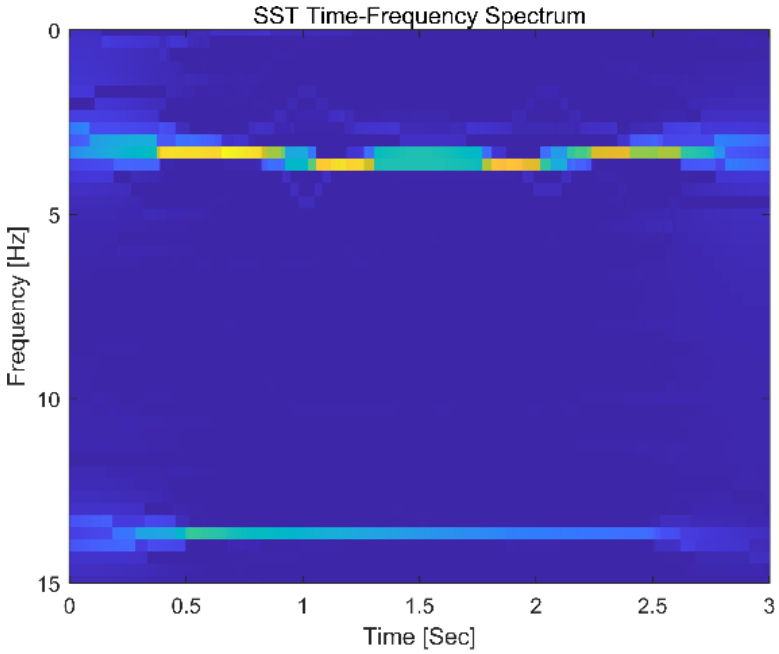


(a) no damage ($\alpha = 0$)

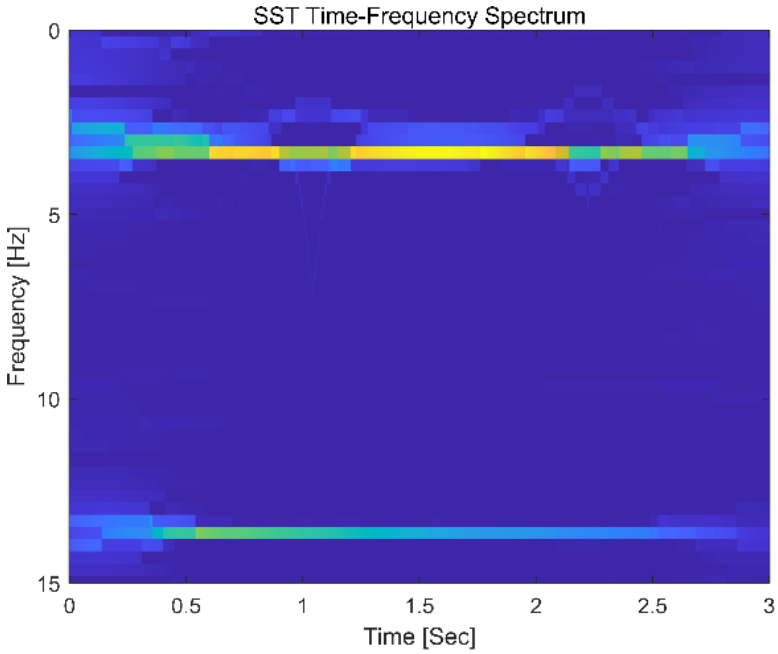


(b) Level 5 damage ($\alpha = 0.3$)

Figure 5-5 TFRs of bridge responses with different damage

### 5.3.4 Parameter Settings and Method Comparison

The comparison of different parameter settings and methods is summarized on Table 5-5. Figure 5-6 shows different CNN model performance, in the fusion layer, the outputs of the two streams are combined through an additional operation. The fused output is used for classification tasks. The classification task uses a fully connected layer with 128 units, activated by ReLU, followed by a dropout layer, and the output is fed into an SVM classifier for categorizing into 10 damage types. 200 samples are used. Figure 5-6 shows training accuracy and loss of each model, and the confusion matrix can be found in Figure 5-8. AUC curve is shown as Figure 5-7.

Table 5-3 Performance Comparison of CNN model

| Parameter/Method | Classification Accuracy (%) | Precision (%) | Recall (%) | F1 Score (%) | AUC | MCC |
|---|---|---|---|---|---|---|

| Model Comparison | | | | | | |
|---|---|---|---|---|---|---|
| Single Stream CNN (Vehicle SST Only) | 72.78 | 82.96 | 72.78 | 65.67 | 0.9835 | 0.7062 |
| Single Stream CNN (Bridge SST Only) | 77.78 | 91.39 | 77.78 | 80.46 | 0.9859 | 0.7665 |
| Dual Stream CNN (Vehicle and Bridge SST) | 91.67 | 91.81 | 91.67 | 91.94 | 0.9749 | 0.9030 |

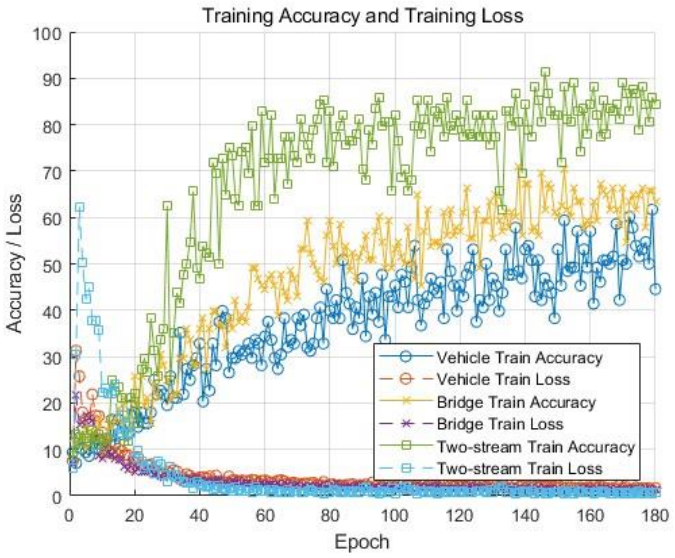


Figure 5-6 Training accuracy and loss of each model

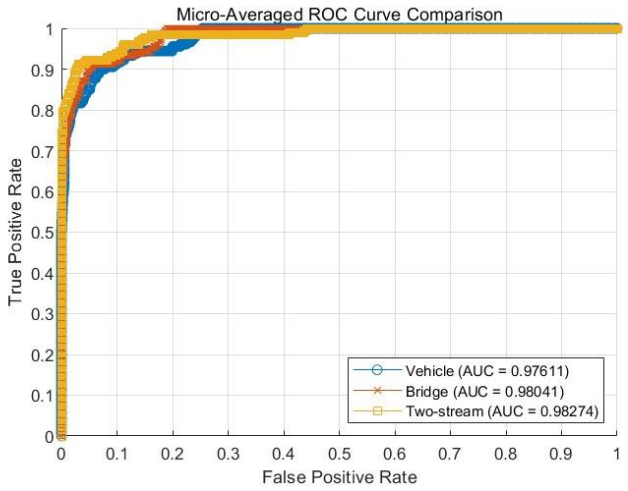


Figure 5-7 AUC curve of each model

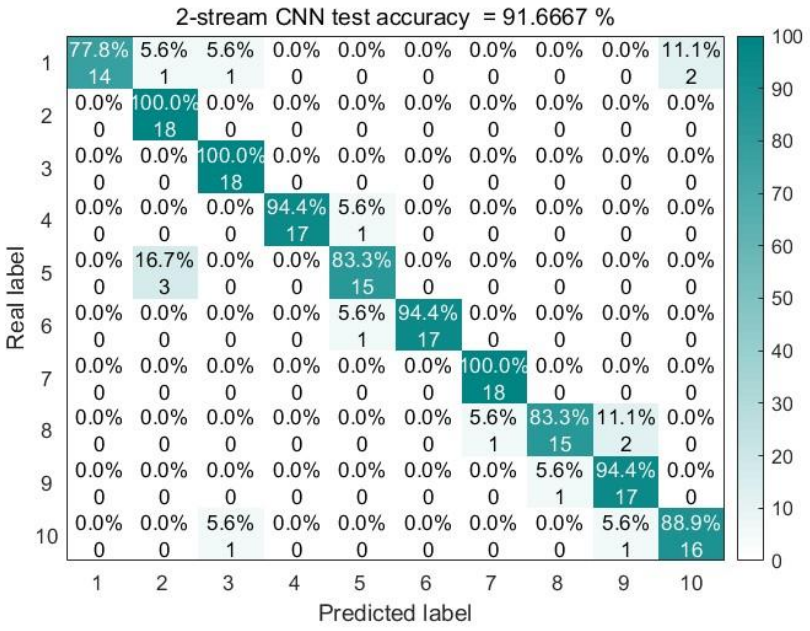


Figure 5-8 Confusion matrix of dual stream CNN

### 5.3.5 Discussion

In performance analysis, a learning rate of 0.001 provided the best results, indicating that a higher learning rate leads to unstable training, while a lower rate may result in slow convergence. A batch size of 32 was found to be optimal, as smaller or larger batch sizes affected the training performance. The combination of vehicle and bridge SST features significantly improved the model's accuracy and damage prediction precision, suggesting that the joint features provide more information for accurately identifying and measuring damage.

In error analysis, it was found that misclassified samples often had high noise or weak signals. Improving signal processing and noise filtering techniques could reduce these errors. For regression errors, samples with large prediction errors typically involved complex damage patterns or multiple damage effects. More detailed feature extraction

and multimodal fusion could further improve regression accuracy.

Regarding practical application potential, this method can perform SHM on real-world bridges in real-time by integrating data from vehicle-mounted sensors and bridge sensors, allowing real-time monitoring of bridge health status. Additionally, this method can be extended to other types of SHM, such as buildings and aircraft, providing a general approach for damage identification and measurement.

Future work directions include optimizing the model structure further, incorporating more feature fusion methods such as multi-scale feature extraction and attention mechanisms. To make the model more generalizable, we need add more bridge and vehicle types to the dataset.

In conclusion, the dual-stream convolutional neural network combined with SVM classification introduced in this chapter performs well in bridge damage identification and measurement tasks and shows broad practical application potential.

### 5.3.6 Comparison of different classification layer comparison

In a dual-stream neural network for vehicle-bridge communication, the selection of the classification layer will significantly influence the ultimate performance of the model. This research compares the performance of softmax layers, SVM classifiers, and other methods to evaluate which layers perform better. The vehicle response and bridge response datasets were utilized in tests to assess their impact on classification quality and robustness.

Table 5-4 Performance Comparison of Classification Layers

| Model | Classification Accuracy (%) | Precision (%) | Recall (%) | F1 Score (%) | AUC | MCC |
|---|---|---|---|---|---|---|
| Dual stream CNN Softmax | 83.33 | 84.53 | 83.33 | 83.76 | 0.9835 | 0.8271 |
| Dual stream CNN SVM | 91.67 | 91.81 | 90.67 | 91.94 | 0.9749 | 0.9030 |

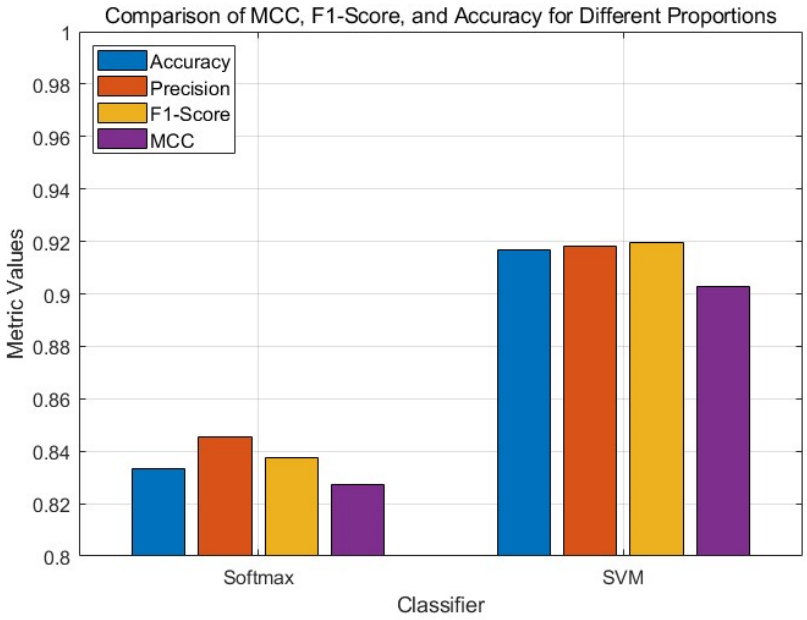


Figure 5-9 Performance Comparison of Classifier

According to Table 5-4 SVM has better performance than Softmax classifier, in the dual-stream CNN with vehicle bridge, the SVM classifier outperforms Softmax mostly due to its ability to accommodate intricate feature distributions and a substantial quantity of sparse features effectively. Performance comparison of CNN fusion layers is shown Figure 5-9. SVM aim to optimize the separation between decision boundaries of classes, making them more effective in scenarios of class imbalance or feature reduction. Furthermore, SVM emphasizes support vectors that are proximate to the decision border, rendering them less susceptible to noise and irrelevant samples. Conversely, Softmax

characterizes the feature distribution on a global level, perhaps underutilizing intricate characteristics. Furthermore, SVM employing kernel functions can enhance its modeling efficacy for non-linear distributions and demonstrate superior performance in two-stream feature fusion challenges.

### 5.3.7 Comparison of different fusion layer

In dual-stream neural network of vehicle bridge, the fusion layer combines the aspects of vehicle response stream and bridge response stream to produce more accurate input representations in classification task. To test the different fusion layers' performance, weighted fusion layers (vehicle stream: bridge stream is 2:8), concatenation fusion layers and addition fusion layers were chosen for comparison, and experiments were run on vehicle response and bridge response data sets. Table 5-5 shows the results.

Table 5-5 Performance Comparison of CNN Fusion Layers

| Model | Classification Accuracy (%) | Precision (%) | Recall (%) | F1 Score (%) | AUC | MCC |
|---|---|---|---|---|---|---|
| Concatenation fusion layers | 90.00 | 90.85 | 90.00 | 90.21 | 0.9809 | 0.8899 |
| Addition fusion layers | 91.67 | 91.81 | 90.67 | 91.94 | 0.9749 | 0.9030 |
| Weighted fusion layers | 92.78 | 93.27 | 92.78 | 92.90 | 0.9788 | 0.9205 |

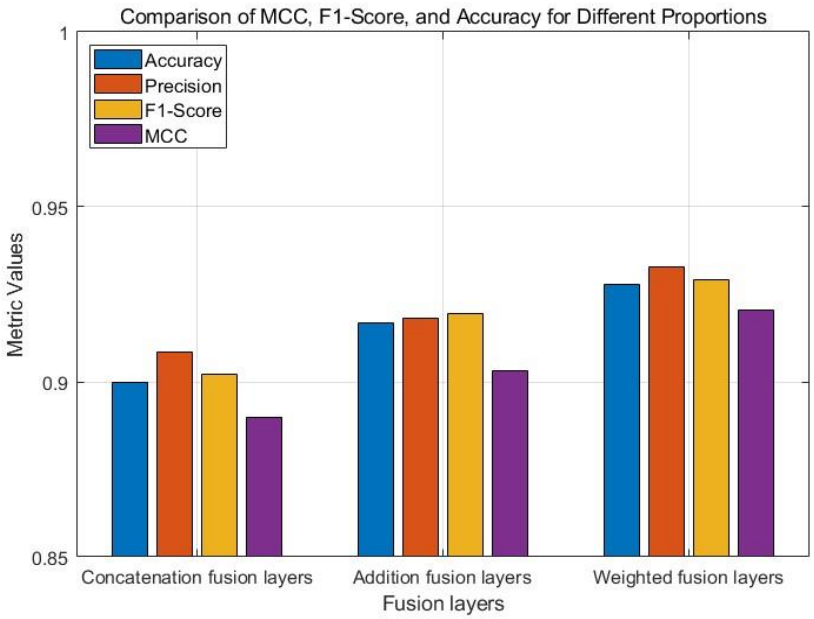


Figure 5-10 Performance Comparison of CNN Fusion Layers

The experimental results are shown as Figure 5-10. The weighted fusion layer surpasses both the concatenation and addition fusion layers across all assessment metrics—classification accuracy, precision, recall, F1 score, AUC, and MCC. Weighted fusion achieves the highest classification accuracy of 92.78%, with a precision and MCC of 0.9205, indicating its efficacy in successfully integrating and averaging data from both streams. The addition fusion layer surpasses concatenation fusion but remains inferior to weighted fusion. These results demonstrate that assigning appropriate weights to each stream during feature integration significantly enhances the model's classification capability. The weighted fusion layer is the optimal choice for the vehicle-bridge two-stream CNN model.

### 5.3.8 Impact of different weight ratios

The selection of weight ratios for the weighted fusion layer significantly impacts model

performance. The relative importance of each stream in the overall categorization is controlled by the weight combinations. The weighted fusion layer for vehicle-bridge interaction yielded optimal performance when the bridge response stream was assigned greater weight than the vehicle response stream. This is due to the fact that bridge response typically offers a more strong and dependable feature set for classification, whereas vehicle response serves as a supplementary filter. Experimentation with various ratios (e.g., 5:5, 2:8, 1:9) demonstrated that an increased contribution from the bridge stream correlates with enhanced classification accuracy, precision, and memory. Therefore, it is crucial to select weight ratios judiciously to ensure a balanced contribution and optimal categorization. Table 5-6 shows the performance comparison of data proportion.

Table 5-6 Performance Comparison of Data Proportion

| Vehicle/Bridge data ratio | Classification Accuracy (%) | Precision (%) | Recall (%) | F1 Score (%) | AUC | MCC |
|---|---|---|---|---|---|---|
| 5:5 | 89.44 | 89.82 | 89.44 | 89.54 | 0.9774 | 0.8833 |
| 2:8 | 92.78 | 93.27 | 92.78 | 92.90 | 0.9788 | 0.9205 |
| 1:9 | 90.00 | 90.87 | 90.00 | 90.22 | 0.9796 | 0.8910 |

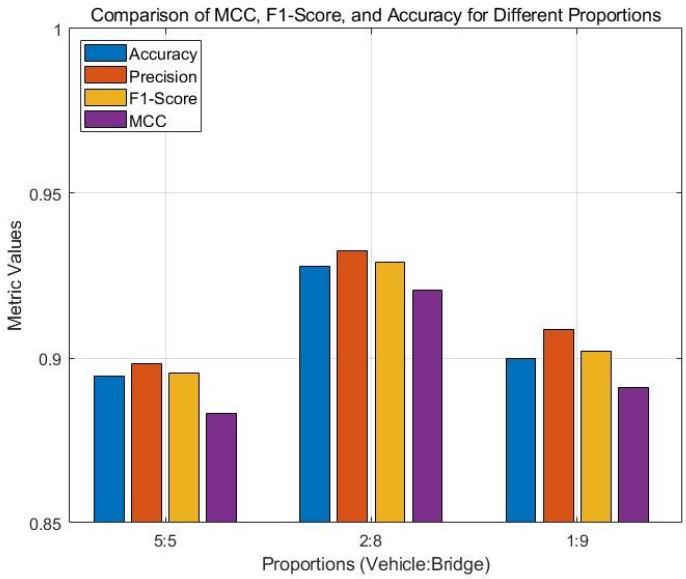


Figure 5-11 Performance Comparison of Data Proportion

The experiments demonstrate that a 2:8 weight ratio between vehicle and bridge data offers the best balance for the classification task, delivering the highest accuracy, precision, recall, F1-score, and MCC shown as Figure 5-11. This suggests that emphasizing bridge data slightly more than vehicle data allows the network to leverage the stronger signal in bridge response features while still benefiting from vehicle response data.

### 5.3.9. Impact of Vehicle Speed on the Performance of the Dual-Stream CNN for Classification

To comprehensively evaluate the model's performance under vehicle speeds, this research looks at how the categorization process is affected by various vehicle speeds. Vehicle speed directly affects the dynamic response generated when the vehicle passes over the bridge, thereby influencing the bridge's acceleration response data. Selected different vehicle speeds (6 m/s, 10m/s, and 14 m/s) for the experiments to analyze how

changes in vehicle speed impact the model's classification performance.

#### 5.3.9.1 Experimental Setup

Acceleration response data for VBI system were regenerated under the conditions of vehicle speeds at 6 m/s, 10m/s, and 14 m/s, road surface roughness is level A and SNR is 26dB. All other parameters in the dataset remained unchanged for each speed condition, and the same finite element simulation method was used to generate the data. To ensure fairness and comparability of the results, the number of samples and the distribution of damage levels in the dataset were consistent across different speeds.

#### 5.3.9.2Parameter/Method Comparison and Results Analysis

The model indicates that speed significantly influences the categorization efficacy of vehicle-bridge interaction models. As shown in Table 5-7 and Figure 5-12, the model demonstrates the highest accuracy at 93.33%, an F1 score of 93.67%, and an MCC of 0.9285 at a reduced speed of 6 m/s, exhibiting steady dynamics and effective feature extraction. At the speed 10 m/s, this method demonstrates commendable performance with minimal deterioration. However, at faster speeds (14 m/s), there is a notable decline in accuracy (86.67%) and F1 score (86.75%) due to noise and variability. The model performs well at slow and slower rates; nevertheless, at high speeds, significant preprocessing or careful adjustments are necessary to maintain classification quality and consistency.

Table 5-7 Performance Comparison of Different Speed

| Speed (m/s) | Classification Accuracy (%) | Precision (%) | Recall (%) | F1 Score (%) | AUC | MCC |
|---|---|---|---|---|---|---|
| 6 | 93.33 | 94.67 | 93.33 | 93.67 | 0.9733 | 0.9285 |
| 10 | 92.78 | 93.27 | 92.78 | 92.90 | 0.9788 | 0.9205 |
| 14 | 86.67 | 86.99 | 86.67 | 86.75 | 0.9618 | 0.8524 |

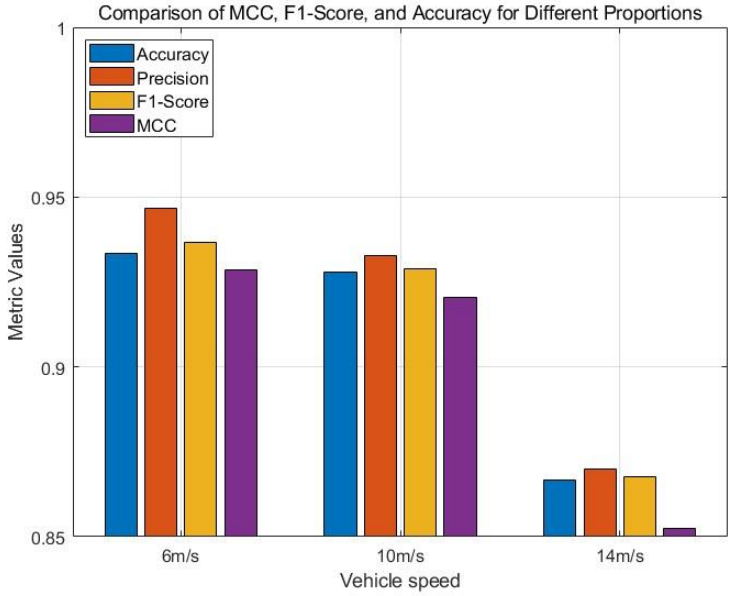


Figure 5-12 Performance Comparison of Different Speed

### 5.3.10. Impact of road roughness on the performance of the dual-stream CNN for Classification

To comprehensively evaluate the model's performance under different road roughness conditions, this study examines the impact of road roughness on the classification task. Road roughness is a critical factor because it directly affects the dynamic response generated when the vehicle passes over the bridge, thereby influencing the bridge's acceleration response data. We selected different road roughness levels (A-level, B-level, C-level) for the experiments to analyze how changes in road roughness impact the model's classification performance.

#### 5.3.10.1 Experimental Setup

Acceleration response data for the bridge and vehicle were regenerated under different road roughness conditions. Speed is 10m/s and SNR is 26dB. All other parameters in the dataset remained unchanged for each roughness condition, and the same finite element simulation method was used to generate the data. To ensure fairness and comparability of the results, the number of samples and the distribution of damage levels in the dataset were consistent across different roughness levels.

#### 5.3.10.2 Impact of Road Roughness on Model Performance

Table 5-8 Performance Comparison of Different Road Roughness

| Road Roughness | Classification Accuracy (%) | Precision (%) | Recall (%) | F1 Score (%) | AUC | MCC |
|---|---|---|---|---|---|---|
| A-Level | 92.78 | 93.27 | 92.78 | 92.90 | 0.9788 | 0.9205 |
| C-level | 93.33 | 94.02 | 93.33 | 93.51 | 0.9762 | 0.9269 |
| E-level | 92.22 | 93.24 | 92.22 | 92.48 | 0.9776 | 0.9151 |

Trained and tested the dual-stream convolutional neural network (CNN) model under different road roughness conditions. The results are shown in Table 5-8.

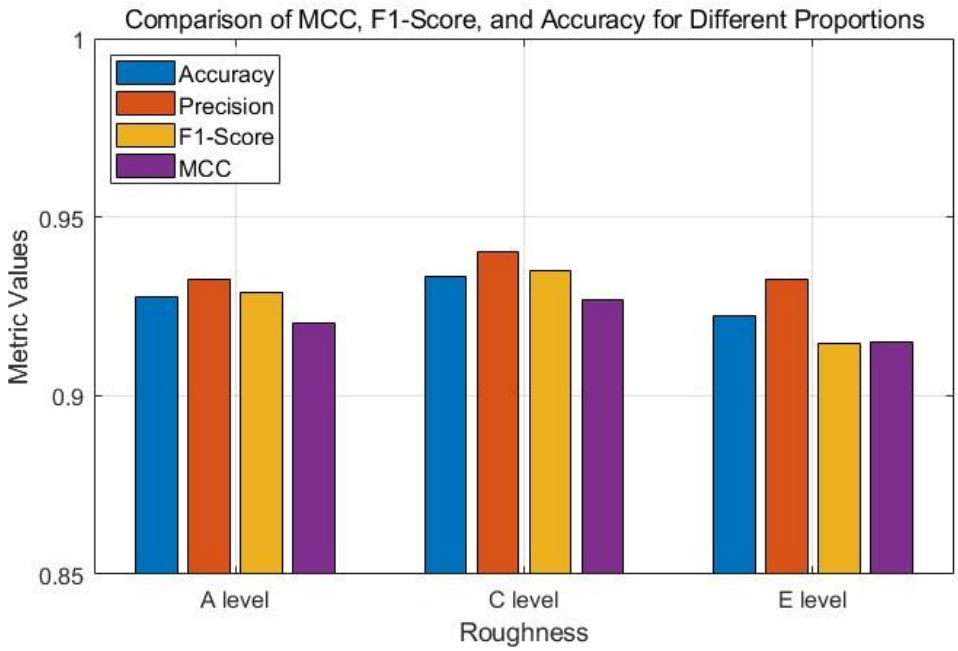

Figure 5-13 Performance Comparison of Different Road Roughness

Table 5-8 and Figure 5-13 shows road roughness influences the classification of the vehicle-bridge interaction model in several respects (as detailed below). The model demonstrates robust performance with A-level road roughness, with a classification accuracy of 92.78%, an F1 score of 92.90%, and a Matthews correlation coefficient of 0.9205. As road roughness escalates to C-level, the classification accuracy reaches 93.33%, the F1 score attains 93.51%, and the MCC climbs to 0.9269, indicating that moderate road roughness may enhance feature extraction and classification. However, if the road roughness exceeds the E-level, the classification performance diminishes somewhat to 92.22%, the F1 score declines to 92.48%, and the MCC reduces to 0.9151, likely due to excessive roughness introducing additional noise into the model, hence affecting feature extraction efficacy. The model has commendable performance across all roughness ranges; however, excessive roughness adversely affects classification accuracy.

This model demonstrates exceptional adaptability across the full spectrum of road

roughness conditions, with particularly remarkable performance stability. Even under the most challenging Class E rough road conditions, the model maintains a high accuracy of 92.22% (F1-score: 92.48%, MCC: 0.9151)—only about 1 percentage point lower than its optimal performance, a result that significantly outperforms comparable models. Notably, under moderate Class C roughness, the model's performance not only remains unaffected but improves, achieving peak accuracy of 93.33%. This clearly demonstrates the model's intelligent adaptability to variations in road roughness.

The experimental data unequivocally show that the model not only effectively resists interference caused by road roughness but can even enhance its performance within specific roughness ranges. This unique "roughness-performance" response characteristic makes it an ideal choice for practical engineering applications dealing with complex road conditions. Although extreme roughness introduces approximately 1% performance fluctuation, key metrics consistently remain at a high level above 92%. Such superior robustness ensures reliable monitoring results in various real-world road environments. Future research can build upon this advantageous feature to further expand the model's potential in more demanding road conditions.

### 5.3.11. Impact of Different Noise Levels on the Performance of the Dual-Stream Convolutional Neural Network for Classification

To comprehensively assess the efficiency of the model in the context of different noise conditions, this study examines the impact of varying noise levels on the classification task. Noise is a critical factor because it directly affects the quality of the data captured

from the bridge's acceleration response, thereby influencing precise categorization capabilities of the model structural health states. Selected different noise levels (5%, 10%, 15%) for the experiments, in order to examine the effect of noise variations on the classification accuracy of the model.

#### 5.3.11.1 Experimental Setup

Acceleration response data for the bridge and vehicle were regenerated under different noise conditions. For each noise condition, all other dataset settings stayed the same, and the data was generated using the same finite element simulation approach. To ensure fairness and comparability of the results, the number of samples and the distribution of damage levels in the dataset were consistent across different noise levels.

#### 5.3.11.2 Impact of Noise Levels on Model Performance

The dual-stream CNN model was trained and tested under different noise conditions. The results are as follows:

Table 5-9 Performance Comparison of Different Noise

| Parameter/Method | SNR | Classification Accuracy (%) | Precision (%) | Recall (%) | F1 Score (%) | AUC | MCC |
|---|---|---|---|---|---|---|---|
| Combined Vehicle and Bridge SST | 40 | 95.56 | 96.00 | 95.56 | 95.67 | 0.9776 | 0.9517 |
| Combined Vehicle and Bridge SST | 26 | 92.78 | 93.27 | 92.78 | 92.90 | 0.9788 | 0.9205 |
| Combined Vehicle and Bridge SST | 16.5 | 86.67 | 89.68 | 86.67 | 87.31 | 0.9732 | 0.8529 |

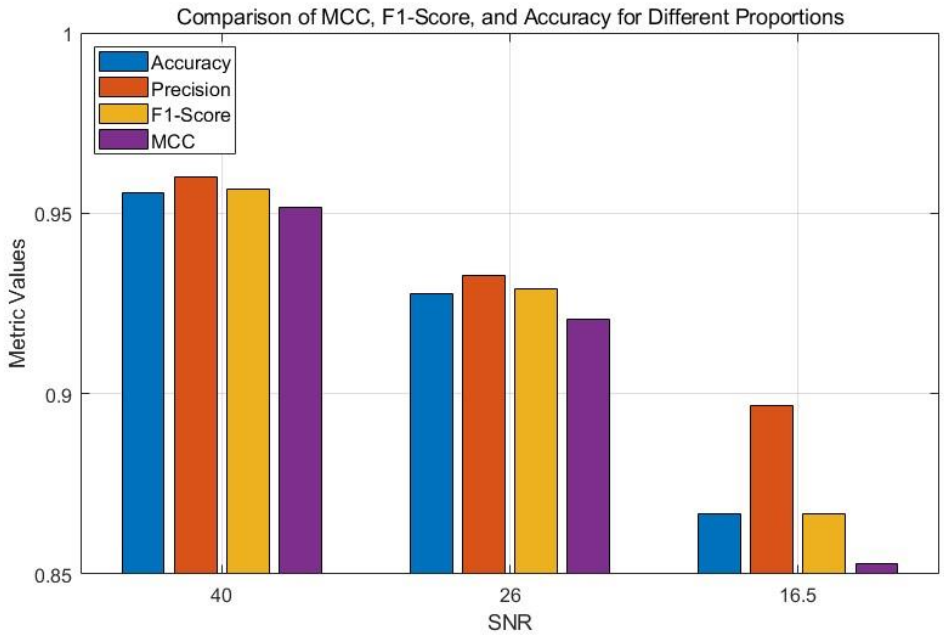


Figure 5-14 Performance Comparison of Different Noise

Table 5-9 and Figure 5-14 indicate that variations in SNR significantly influence the classification efficiency of the Combined Vehicle and Bridge SST model. The optimal outcomes with a high SNR of 40 include a classification accuracy of 95.56%, precision of 95.67%, recall of 95.67%, an AUC of 0.9776, and an MCC of 0.9517, reflecting the model's performance at the highest scores of 20 and 40, respectively. Despite a moderate SNR of 26, the model's performance remains commendable, with a classification accuracy of 92.78%, an F1 score of 92.90%, and a Matthews correlation coefficient of 0.9205, indicating robust performance notwithstanding moderate interference. As the SNR decreases to 16.5, the model's performance decreases, exhibiting a classification error of 86.67%, an F1 score of 87.31%, and a Matthews correlation coefficient (MCC) of 0.8529, thereby illustrating the detrimental impact of noise on feature extraction and classification. Conclusion: Signal-to-noise ratio significantly influences model performance, and enhancing the SNR or implementing noise suppression is crucial for

classification accuracy.

By analyzing the experimental results under different noise conditions, the model shows strong stability and resilience when exposed to different degrees of noise.

## 5.4 Experimental Cases

A VBI model has been constructed in the lab, as illustrated in Figure 3-23. The experimental parameter is the same as chapter 3's experiment.

The vehicle's speed over the main beam is around 0.61 m/s. The data for acceleration responses are taken at a midway of the first beam span, above the vehicle's front axle. Figures 3-24 and 3-25 show VBI model. Sensor and sensor location is same as experiment of Chapter 3.

Figure 3-26 shows adding 5kg mass block was added to the mid-span of the first span of the bridge model to simulate damage. Data augmentation was performed by adding 5% to 10% white noise. A total of 200 datasets for damaged conditions and 200 datasets for undamaged conditions were generated and categorized into two classes for analysis. The experiment utilized a 7:1.5:1.5 ratio for the division of training, testing, and validation data to ensure optimal feature learning and generalization. The model has significant generalization efficacy in classifying test data.

### 5.4.1 Experimental results

#### 5.4.1.1 Effect of different fusion layers

This study compares three fusion techniques (addition fusion layer, concatenation fusion

layer, and weighted fusion layer) within a dual-stream CNN for the classification of vehicle-bridge interaction (VBI) dynamic systems. Experimental findings indicate that the fusion layers significantly alter the model's classification capabilities.

Table 5-10 Performance Comparison of Different Fusion layer in experiment

| Vehicle/Bridge data ratio | Classification Accuracy (%) | Precision (%) | Recall (%) | F1 Score (%) | AUC | MCC |
|---|---|---|---|---|---|---|
| 5:5 | 93.33 | 93.55 | 93.33 | 93.40 | 0.9701 | 0.8845 |
| 2:8 | 96.67 | 97.10 | 96.67 | 96.77 | 0.9715 | 0.9354 |
| 1:9 | 95.00 | 95.26 | 95.00 | 95.24 | 0.9701 | 0.9045 |

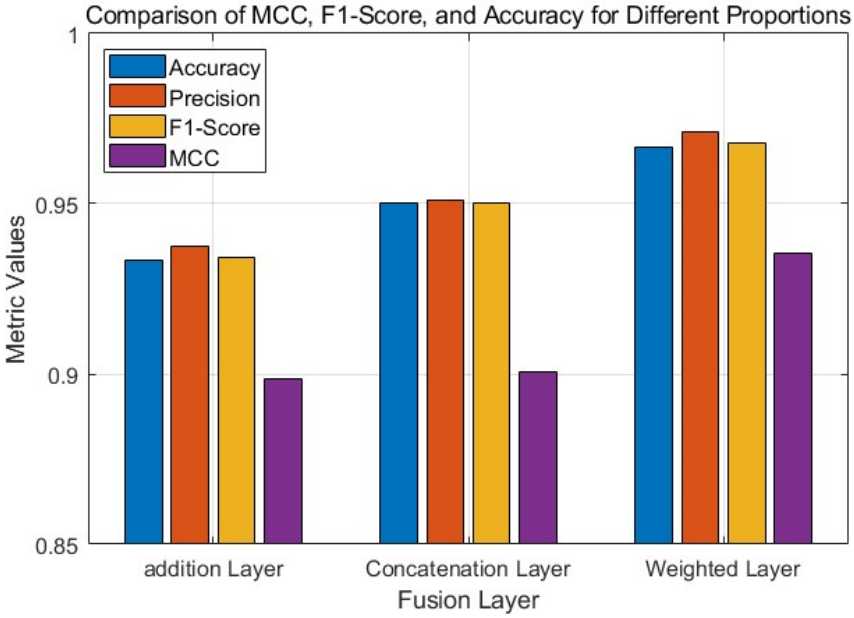


Figure 5-15 Performance Comparison of Different Fusion layer in experiment

As shown Table 5-10 and Figure 5-15, the addition fusion layer exhibited the poorest performance across all metrics, achieving a classification accuracy of 93.33%, precision of 93.75%, F1-score of 93.44%, and MCC of 0.8985. The addition approach is rather constrained in its ability to integrate feature data. Conversely, the concatenation fusion layer, which integrates features from different streams, enhanced the classification rate to 95.00%, the F1-score to 95.03%, and the MCC value to 0.9005, signifying superior

feature representation capabilities.

The weighted fusion layer outperformed the other two strategies, achieving a classification accuracy of 96.67%, precision of 97.10%, F1-score of 96.77%, and an MCC value of 0.9354. Incorporating weights to features from various streams accelerated feature integration, resulting in exceptional performance of the model on challenging VBI system classification tasks.

The weighted fusion layer is the optimal fusion technique for the dual-stream CNN model in this chapter, owing to its superior performance advantages. The results suggest that for the dynamic response features of VBI, weighted fusion can effectively capture feature information and expedite classification.

#### 5.4.1.2. Effect of different data ratios

Table 5-11 and Figure 5-16 examine the influence of the fusion ratio of vehicle data and bridge data on the classification efficacy of the dual-stream CNN, concentrating on model performance at three data ratios (5:5, 2:8, and 1:9). The experimental findings indicate that varying data ratios substantially influence classification performance, and appropriate weight distribution is crucial for enhancing the model's efficacy.

Table 5-11 Performance Comparison of Different proportion in experiment

| Vehicle/Bridge data ratio | Classification Accuracy (%) | Precision (%) | Recall (%) | F1 Score (%) | AUC | MCC |
|---|---|---|---|---|---|---|
| 5:5 | 93.33 | 93.55 | 93.33 | 93.40 | 0.9701 | 0.8845 |
| 2:8 | 96.67 | 97.10 | 96.67 | 96.77 | 0.9715 | 0.9354 |
| 1:9 | 95.00 | 95.26 | 95.00 | 95.24 | 0.9701 | 0.9045 |

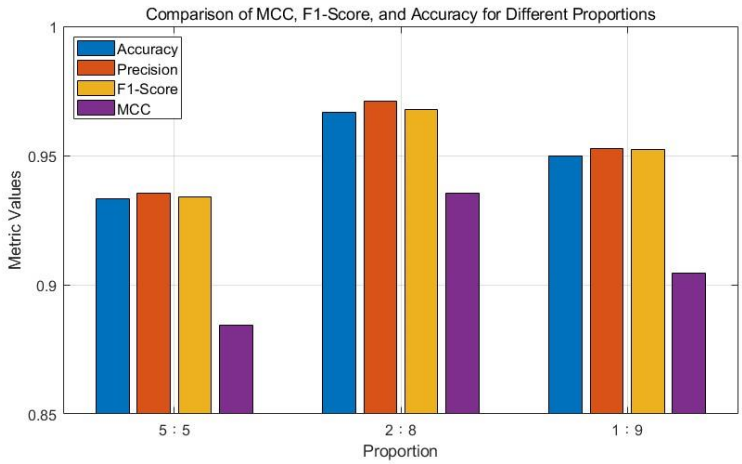


Figure 5-16 Performance Comparison of Different proportion in experiment

The fusion of vehicle and bridge data at a 5:5 ratio yielded a classification accuracy of 93.33%, an F1-score of 93.40%, and an MCC value of 0.8845, suggesting that the model's performance was generally balanced albeit suboptimal at this ratio. Conversely, when bridge data constituted a greater fraction (2:8), classification performance markedly enhanced, attaining an accuracy of 96.67%, an F1-score of 96.77%, and an MCC value of 0.9354. This illustrates the essential function of bridge data in the classification tasks of vehicle-bridge interaction systems. Nevertheless, when bridge data constituted the predominant element (1:9), although the classification accuracy (95.00%) and F1-score (95.24%) surpassed those of the 5:5 ratio, the overall performance experienced a minor decline, evidenced by a reduction in the MCC value to 0.9045. This indicates that vehicle data remains essential for feature fusion.

### 5.4.2 Discussion

This study selects three fusion strategies—addition, concatenation, and weighted fusion—based on the following key considerations: First, addition fusion is chosen for its computational efficiency and physical interpretability, making it particularly suitable for

combining linear features with clear physical meanings in vehicle-bridge systems. Second, concatenation fusion preserves the complete original feature space, effectively capturing complex nonlinear modal coupling characteristics in vehicle-bridge interactions—capabilities that strategies like multiplication fusion struggle to achieve. Finally, weighted fusion employs learnable weight parameters to adaptively adjust the contributions of vehicle and bridge features, a feature absents in fixed fusion strategies (e.g., average fusion).

Compared to more complex mechanisms like attention, these three strategies strike a better balance between computational efficiency and model performance, each addressing different levels of feature interaction needs in bridge health monitoring: addition fusion handles macroscopic vibration characteristics, concatenation fusion parses local damage features, and weighted fusion optimizes feature contribution allocation. Experiments demonstrate that other fusion methods (e.g., element-wise multiplication) either lead to feature information loss or introduce unnecessary computational complexity in this task, whereas the combination of these three strategies most effectively meets the multiscale analysis requirements for monitoring coupled vehicle-bridge systems.

This research demonstrates that fusion algorithms and data proportions significantly impact the classification performance of the dual-stream CNN model in VBI systems. Three fusion methods (addition, concatenation, weighted) were evaluated with three vehicle-to-bridge data ratios (5:5, 2:8, and 1:9). The subsequent section scrutinizes these results in detail.

The comparison of the three fusion layers indicated that the weighted fusion layer consistently surpassed both the addition and concatenation layers across all performance metrics, including classification accuracy, precision, F1-score, and MCC. The weighted layer achieved a classification accuracy of 96.67% and an MCC of 0.9354, significantly surpassing the addition layer (93.33%, 0.8985) and the concatenation layer (95.00%, 0.9005).

The weighted layer exhibited superior performance due to its allocation of distinct values to features within the vehicle and bridge streams. This layer enhances the coordination of supplementary information through feature weighting, enabling the model to consider the pertinent dynamic elements of the VBI system more effectively. The addition layer merely sums feature maps, while the concatenation layer merges feature maps without prioritization, resulting in a lack of granularity in the selection of informative features.

The inclusion of vehicle and bridge data significantly contributed to the effectiveness of classification. The optimal performance was achieved using a data ratio of 2:8 (vehicle: bridge), resulting in a classification accuracy of 96.67% and a Matthews correlation coefficient (MCC) of 0.9354. Bridge information is the paramount data for discerning the global dynamic structure of the VBI system since the bridge serves as the principal component in this interaction.

However, when the bridge data fraction was adjusted to 90% (1:9 ratio), the classification accuracy (95.00%) and MCC (0.9045) were somewhat inferior to those of the 2:8 ratio. A bias favoring bridge data may inhibit the incorporation of vehicle data, which also

encompasses significant local dynamic information. In contrast, a paired 5:5 had the poorest performance (93.33%, 0.8845), indicating that equal weighting fails to fully leverage the potential of bridge dynamics.

These findings endorse feature fusion and data weighting in the monitoring of VBI systems. The weighted fusion layer provides an open and efficient feature-integration mechanism, aligning with the physical interpretation of VBI interactions, where the bridge and vehicle are inherently distinct entities. The data proportion tests suggest that bridge data should be prioritized for feature extraction, while vehicle data must be sufficiently representative to ensure effective and balanced classification.

This chapter is informative concerning the efficacy of fusion layers and data ratios. Nevertheless, several drawbacks must be acknowledged:

1) The experiments maintained consistent data proportions. Future study is needed to explore dynamic weighting algorithms that adjust the significance assigned to vehicle and bridge data based on its relevance.
2) The wireless sensor network combines accelerometers, high-frequency strain gauges, and temperature/humidity sensors to form a multi-physical monitoring system (Noel et al 2017). The edge computing nodes employ FIR digital filtering and time-frequency analysis algorithms for preprocessing raw signals, while performing feature extraction (e.g., modal frequencies, strain time-history) to achieve millisecond-level latency in localized processing. This system enables collaborative analysis of vibration spectra, strain modal parameters, and environmental data, and it provides

the multidimensional support for bridge condition assessment.

3) The outcome is contingent upon specific VBI system configurations, including designated bridge and vehicle parameters. Further experimentation is required to validate the performance of the proposed method across various structural and dynamic settings.
4) Alternatively, alternative fusion methodologies, such as attention mechanisms or transformers, need to be explored to achieve the superior performance.

### 5.5. Summary

The paper outlines an innovative approach that integrates structural health monitoring using a dual-stream CNN and feature extraction using SST. The dual-stream CNN, utilizing TFR of VBI responses, demonstrates exceptional accuracy and resilience in many locations and operational conditions, including variable vehicle speeds, road surface irregularities, and noise in the environment. Important results include:

High Classification: Model performs with higher classification accuracy compared to single-stream CNNs by merging the vehicle and bridge data to find the dynamic interactions important for damage detection.

Flexibility: dual-stream CNN runs well in any environment — from road roughness to ambient noise — and shows the potential use for real-world applications.

Damage Detection Efficiency: With the assistance of SST, time-frequency features can be more accurately identified as structural damage even in complex scenarios.

While the approach shows promise, further optimization, such as incorporating advanced feature fusion techniques and expanding datasets to include diverse damage scenarios, can enhance model performance and generalizability. Future directions also include extending the framework to other structural systems and exploring multimodal data integration.

In conclusion, the dual-stream CNN model offers a powerful tool for non-intrusive and efficient bridge health monitoring, contributing to safer and more reliable infrastructure management.

# CHAPTER 6 Conclusions and recommendations

## 6.1 Conclusions

This study develops an innovative and data-driven approach to bridge SHM by leveraging the vehicle-bridge interaction (VBI) system through advanced signal processing techniques and machine learning-based classification. Addressing critical challenges in conventional SHM methods, this work introduces a wireless sensor network and time-frequency analysis methods, notably the MSST and the SST2, to efficiently extract nonstationary time-varying features of the bridge's dynamic response under vehicular loads.

The proposed framework demonstrates the following key contributions and findings:

1. Time-Frequency Analysis for Feature Extraction: The research establishes the effectiveness of advanced time-frequency analysis methods. By comparing SST, SST2, and MSST, it identifies MSST as a superior technique for extracting instantaneous frequencies and time-varying features from noisy and complex VBI signals, enhancing feature clarity, and improving downstream damage detection performance.
2. Vehicle-Bridge Coupled Feature Fusion: The fusion of time-varying features from both vehicle and bridge responses within a dual-stream CNN has proven to be an effective approach. This integration allows for robust damage classification, with significant improvements in detecting and localizing structural damage under various operating and environmental conditions.

3. Numerical Simulations and Experimental Validation: The numerical and experimental analyses validate the proposed method accurately detects bridge damage under different damage intensities, locations, and road surface conditions. The experiments also demonstrate that the system remains robust to varying levels of road roughness, noise, and vehicle speed.
4. Practical Implications for Bridge Networks: The research highlights the potential of the proposed system to deliver rapid, cost-effective, and scalable SHM for large bridge networks. By relying on a reduced number of sensors and employing wireless networks, the system minimizes the logistical challenges and costs associated with traditional monitoring methods.

**6.2 Recommendations**

A data-driven bridge SHM has been developed leveraging time-frequency features of VBI systems and machine learning. Numerical simulations and laboratory studies have been conducted to verify the performance of the proposed approach. The further study is needed for practical applications of the proposed approach. Some recommendations are as follows,

1) Numerical simulations and controlled laboratory conditions may not fully capture real-world complexities, such as the environmental temperature, multiple vehicles, and different type of bridges. Further field experimental study is needed to verify the performance of the proposed approach.
2) In practice, the high-quality data are difficult or impossible to obtain to train the

machine learning model, especially the data for different damage scenarios. The incomplete data problem needs to be further studied using domain adaptation-based frameworks.

3) A multi-source data integration can incorporate complementary data streams (e.g., environmental sensors, drone-based inspections, or traffic monitoring) to enhance diagnostic accuracy.
4) The beam bridge has been considered. Further study is needed to extend the proposed approach to different types of bridges.

With these advancements, the proposed SHM framework holds significant potential to deliver scalable, cost-effective damage detection—ultimately enhancing safety, durability, and maintenance efficiency in critical infrastructure.

**References:**


Abdeljaber, O., O. Avci, S. Kiranyaz, M. Gabbouj and D. J. Inman (2017). "Real-time vibration-based structural damage detection using one-dimensional convolutional neural networks." *Journal of Sound and Vibration* 388: 154-170.

Addison, P. S. (2018). "Introduction to redundancy rules: the continuous wavelet transform comes of age." *Philosophical Transactions of the Royal Society A: Mathematical, Physical and Engineering Sceinecs*, 376(2126): 20170258.

Agre, P. E. and D. Chapman (1987). "Pengi: An implementation of a theory of activity." *Proceedings of the sixth National conference on Artificial intelligence*, pp.268-272.

Armijo, A. and D. Zamora-Sánchez (2024). "Integration of Railway Bridge Structural Health Monitoring into the Internet of Things with a Digital Twin: A Case Study." *Sensors* 24(7): 2115.

A. B. Noel, A. Abdaoui, T. Elfouly, M. H. Ahmed, A. Badawy and M. S. Shehata(2017), "Structural Health Monitoring Using Wireless Sensor Networks: A Comprehensive Survey," in *IEEE Communications Surveys & Tutorials*, vol. 19, no. 3, pp. 1403-1423,

ASCE (2017). *2017 Infrastructure Report Card*. American Society of Civil Engineers.

Avci, O., O. Abdeljaber, S. Kiranyaz and D. Inman (2017). "Structural damage detection in real time: implementation of 1D convolutional neural networks for SHM applications." *Structural Health Monitoring & Damage Detection*, Volume 7: pp.49-54.

Behera, R., S. Meignen and T. Oberlin (2018). "Theoretical analysis of the second-order synchrosqueezing transform." *Applied and Computational Harmonic Analysis* 45(2): 379-404.

Braeewell, R. (1965). *The Fourier Transform and Its Application*. Mc Graw-Hill.

Brevdo, E., N. S. Fuckar, G. Thakur and H.-T. Wu (2011). "The synchrosqueezing algorithm: a robust analysis tool for signals with time-varying spectrum." *arXiv preprint arXiv:1105.0010*: 1-29.

Chen, S., F. Cerda, P. Rizzo, J. Bielak, J. H. Garrett and J. Kovačević (2014). "Semi-supervised multiresolution classification using adaptive graph filtering with application to indirect bridge structural health monitoring." *IEEE Transactions on*

*Signal Processing* 62(11): 2879-2893.

Chollet, F. (2017). *Deep Learning with Python*. Manning Publications.

Corbally, R. and A. Malekjafarian (2024) "Machine learning applications for drive-by bridge monitoring." *Proceedings of Civil Engineering Research in Ireland (CERI2024)*.

Daubechies, I., J. Lu and H.-T. Wu (2011). "Synchrosqueezed wavelet transforms: An empirical mode decomposition-like tool." *Applied and computational harmonic analysis* 30(2): 243-261.

de Rezende, S. W. F., J. d. R. V. de Moura, R. M. F. Neto, C. A. Gallo and V. Steffen (2020). "Convolutional neural network and impedance-based SHM applied to damage detection." *Engineering Research Express* 2(3): 035031.

Dey, A., S. Rajan, G. G. Xiao and J. Lu (2024). "Synchro-Squeezed Time-Frequency Representations for Radar-based Human Activity Recognition." Proceedings of International Symposium on Sensing and Instrumentation in 5G and IoT Era (ISSI), pp.1-6.

Durak, L. and O. Arikan (2003). "Short-time Fourier transform: two fundamental properties and an optimal implementation." *IEEE Transactions on Signal Processing* 51(5): 1231-1242.

Fan, W. and P. Qiao (2011). "Vibration-based damage identification methods: a review and comparative study." *Structural health monitoring* 10(1): 83-111.

Gao, M., X. Zhu and J. Li (2023). "Time-varying analysis of vehicle-bridge interaction system for bridge health monitoring using synchrosqueezing transform." *Proceedings of the 12th International Conference on Structural Health Monitoring of Intelligent Infrastructure*, pp.1-6.

Girshick, R., J. Donahue, T. Darrell and J. Malik (2015). "Region-based convolutional networks for accurate object detection and segmentation." *IEEE transactions on pattern analysis and machine intelligence* 38(1): 142-158.

Goebel, K. and W. Yan (2008). "Correcting sensor drift and intermittency faults with data fusion and automated learning." *IEEE systems journal* 2(2): 189-197.

Goodfellow, I. (2016). *Deep Learning*. MIT press.

Her, S.-C. and S.-C. Chung (2019). "Dynamic responses measured by optical fiber sensor for structural health monitoring." *Applied Sciences* 9(15): 2956.

Herrera, R. H., J. Han and M. van der Baan (2014). "Applications of the synchrosqueezing transform in seismic time-frequency analysis." *Geophysics* 79(3): V55-V64.

Huang, N. E. (2007). "An adaptive data analysis method for nonlinear and nonstationary time series: the empirical mode decomposition and Hilbert spectral analysis." *Wavelet analysis and applications*: 363-376.

Hussain, A. and W. Hesheng (2019). "Depth-wise pooling: A parameter-less solution for channel reduction of feature-map in convolutional neural network." *Proceedings of IEEE International Conference on Real-time Computing and Robotics (RCAR)*, pp.299-304.

ISO 8608 (1995). *Mechanical Vibration–Road Surface Profiles–Reporting of Measured Data*. International Standard.

Jian, X., Y. Xia and L. Sun (2022). "Indirect identification of bridge frequencies using a four-wheel vehicle: Theory and three-dimensional simulation." *Mechanical Systems and Signal Processing* 177: 109155.

Kim, B. and S. Cho (2018). "Automated vision-based detection of cracks on concrete surfaces using a deep learning technique." *Sensors* 18(10): 3452.

Kim, J., J. P. Lynch, J.-J. Lee and C.-G. Lee (2011). "Truck-based mobile wireless sensor networks for the experimental observation of vehicle–bridge interaction." *Smart Materials and Structures* 20(6): 065009.

Krizhevsky, A., I. Sutskever and G. E. Hinton (2017). "Imagenet classification with deep convolutional neural networks." *Coomunications of ACM*, 60(6): 84-90.

Law, S. and X. Zhu (2004). "Dynamic behavior of damaged concrete bridge structures under moving vehicular loads." *Engineering Structures* 26(9): 1279-1293.

LeCun, Y., Y. Bengio and G. Hinton (2015). "Deep learning." *Nature* 521(7553): 436-444.

Li, C., Y. Wan, P. Pan, B. Hu and J. Zhang (2024). "Improved windowed phase difference method for frequency estimation of distorted power signals." *Measurement and Control*: 00202940241237135.

Li, H., M. Soliman, D. M. Frangopol and H. Xia (2017). "Fatigue damage in railway steel

bridges: Approach based on a dynamic train-bridge coupled model." *Journal of Bridge Engineering* 22(11): 06017006.

Li, H., T. Wang and G. Wu (2021). "Dynamic response prediction of vehicle-bridge interaction system using feedforward neural network and deep long short-term memory network." *Structures*, 34: 2415-2431.

Li, J., X. Zhu, S. Chen and W. Ruan (2024). "Contact-point response reconstruction for indirect bridge monitoring via Bayesian expectation-maximization based augmented Kalman filter." *Engineering Structures* 309: 118066.

Li, J., X. Zhu, S.-s. Law and B. Samali (2020). "Time-varying characteristics of bridges under the passage of vehicles using synchroextracting transform." *Mechanical Systems and Signal Processing* 140: 106727.

Li, L., G. Liu, L. Zhang and Q. Li (2019). "Sensor fault detection with generalized likelihood ratio and correlation coefficient for bridge SHM." *Journal of Sound and Vibration* 442: 445-458.

Liang, X. (2019). "Image-based post-disaster inspection of reinforced concrete bridge systems using deep learning with Bayesian optimization." *Computer-Aided Civil and Infrastructure Engineering* 34(5): 415-430.

Lu, N., Y. Liu, J. Cui, X. Xiao, Y. Luo and M. Noori (2024). "A time–frequency-based data-driven approach for structural damage identification and its application to a cable-stayed bridge specimen." *Sensors* 24(24): 8007.

Luo, L., B. Li, Y. Yu, X. Xu, K. Soga and J. Yan (2016). "Time and frequency localized pulse shape for resolution enhancement in STFT - BOTDR." *Sensors* 2016(1): 3204130.

Magalhães, F., Á. Cunha and E. Caetano (2012). "Vibration based structural health monitoring of an arch bridge: From automated OMA to damage detection." *Mechanical Systems and Signal Processing* 28: 212-228.

Malekjafarian, A., P. J. McGetrick and E. J. OBrien (2015). "A review of indirect bridge monitoring using passing vehicles." *Shock and Vibration* 2015(1): 286139.

Mao, X., Z. Fu, O. Wu and W. Hu (2016). "Fast kernel SVM training via support vector identification." *Proceedings of the 23rd International Conference on Pattern*

*Recognition (ICPR)*, pp.1554-1559.

Mostafa, N., R. Loendersloot, D. Di Maio and T. Tinga (2020). "Application of wavelet synchro-squeezed transform (WSST) method to railway bridge health monitoring." *Proceedings of the 11th International Conference on Structural Dynamics, EURODYN*, pp.1388-1396.

Nagarajaiah, S. and B. Basu (2009). "Output only modal identification and structural damage detection using time frequency & wavelet techniques." *Earthquake Engineering and Engineering Vibration* 8(4): 583-605.

Nguyen, D. C., M. Salamak, A. Katunin, G. Poprawa and M. Gerges (2024). "Vibration-based SHM of railway steel arch bridge with orbit-shaped image and wavelet-integrated CNN classification." *Engineering Structures* 315: 118431.

Ni, Z., Y. Tong, Y. Song and R. Wang (2024). "Enhanced bearing fault diagnosis in NC machine tools using dual-stream CNN with vibration signal analysis." *Processes* 12(9): 1951.

N. Aloysius and M. Geetha, "A review on deep convolutional neural networks," *2017 International Conference on Communication and Signal Processing (ICCSP)*, Chennai, India, 2017, pp. 0588-0592

Noel, A. B., A. Abdaoui, T. Elfouly, M. H. Ahmed, A. Badawy and M. S. Shehata (2017). "Structural health monitoring using wireless sensor networks: A comprehensive survey." *IEEE Communications Surveys & Tutorials* 19(3): 1403-1423.

OBrien, E. J., A. Malekjafarian and A. González (2017). "Application of empirical mode decomposition to drive-by bridge damage detection." *European Journal of Mechanics-A/Solids* 61: 151-163.

Papernot, N., P. McDaniel, S. Jha, M. Fredrikson, Z. B. Celik and A. Swami (2016). "The limitations of deep learning in adversarial settings." *Proceedings of the IEEE European Symposium on Security and Privacy (EuroS&P)*, pp.372-387.

Pathirage, C. S. N., J. Li, L. Li, H. Hao, W. Liu and P. Ni (2018). "Structural damage identification based on autoencoder neural networks and deep learning." *Engineering Structures* 172: 13-28.

Plevris, V. and G. Papazafeiropoulos (2024). "AI in Structural Health Monitoring for

Infrastructure Maintenance and Safety." *Infrastructures* 9(12): 225.

Purwono, P., A. Ma'arif, W. Rahmaniar, H. I. K. Fathurrahman, A. Z. K. Frisky and Q. M. ul Haq (2022). "Understanding of convolutional neural network (cnn): A review." *International Journal of Robotics and Control Systems* 2(4): 739-748.

Polat, H., & Danaei Mehr, H. (2019). "Classification of pulmonary CT images by using hybrid 3D-deep convolutional neural network architecture." *Applied Sciences*, 9(5): 940

Qiao, H., S. Liu, Q. Xu, S. Liu and W. Yang (2021). "Two-Stream Convolutional Neural Network for Video Action Recognition." *KSII Transactions on Internet and Information Systems (TIIS)* 15(10): 3668-3684.

Sadowsky, J. (1996). "Investigation of signal characteristics using the continuous wavelet transform." *Johns Hopkins APL Technical Digest* 17(3): 258-269.

Sajedi, S. O. and X. Liang (2019). "A convolutional cost-sensitive crack localization algorithm for automated and reliable RC bridge inspection." *Risk-based Bridge Engineering,* CRC Press: pp.229-235.

Sandsten, M. (2016). *Time-Frequency Analysis of Time-Varying Signals and Non-stationary Processes*. Lund University.

Sazonov, E., K. Janoyan and R. Jha (2004). "Wireless intelligent sensor network for autonomous structural health monitoring." *Proceedings of SPIE*, Volume 5384: 540048.

Shang, W., K. Sohn, D. Almeida and H. Lee (2016). "Understanding and improving convolutional neural networks via concatenated rectified linear units." *Proceedings of the 33rd International Conference on Machine Learning*, Volume 48: pp.2217-2225.

Shokravi, H., H. Shokravi, N. Bakhary, M. Heidarrezaei, S. S. Rahimian Koloor and M. Petrů (2020). "Vehicle-assisted techniques for health monitoring of bridges." *Sensors* 20(12): 3460.

Shyam, R. (2021). "Convolutional Neural Network and its Architectures." *Journal of Computer Technology & Applications,* 12(4): 2021

Simonyan, K. (2014). "Very deep convolutional networks for large-scale image recognition." *arXiv preprint arXiv*:1409.1556.

Siringoringo, D. M. and Y. Fujino (2012). "Estimating bridge fundamental frequency from vibration response of instrumented passing vehicle: analytical and experimental study." *Advances in Structural Engineering* 15(3): 417-433.

Stanković, L., S. Stanković and M. Daković (2014). "From the STFT to the Wigner distribution." *IEEE Signal Processing Magazine* 31(3): 163-174.

Talaei, S., X. Zhu, J. Li, Y. Yu and T. H. T. Chan (2023). "Transfer learning based bridge damage detection: Leveraging time-frequency features." *Structures* 57: 105052.

Tan, C., N. Uddin, E. J. OBrien, P. J. McGetrick and C.-W. Kim (2019). "Extraction of bridge modal parameters using passing vehicle response." *Journal of Bridge Engineering* 24(9): 04019087.

Tan, C., H. Zhao, E. J. OBrien, N. Uddin and C.-W. Kim (2023). "Exploring Time-Varying Characteristics in Drive-By Bridge Frequency Extraction with the Second-Order Synchrosqueezing Transform." *Journal of Bridge Engineering* 28(4): 04023010.

Teng, S., G. Chen, G. Liu, J. Lv and F. Cui (2019). "Modal strain energy-based structural damage detection using convolutional neural networks." *Applied Sciences* 9(16): 3376.

Thakur, G., E. Brevdo, N. S. Fučkar and H.-T. Wu (2013). "The synchrosqueezing algorithm for time-varying spectral analysis: Robustness properties and new paleoclimate applications." *Signal Processing* 93(5): 1079-1094.

Thakur, G. and H.-T. Wu (2011). "Synchrosqueezing-based recovery of instantaneous frequency from nonuniform samples." *SIAM Journal on Mathematical Analysis* 43(5): 2078-2095.

Uijlings, J. R., K. E. Van De Sande, T. Gevers and A. W. Smeulders (2013). "Selective search for object recognition." *International Journal of Computer Vision* 104: 154-171.

Wahab, M. A., G. De Roeck and B. Peeters (1999). "Parameterization of damage in reinforced concrete structures using model updating." *Journal of Sound and Vibration* 228(4): 717-730.

Wang, L., Y. Qiao and X. Tang (2013). "Motionlets: Mid-level 3d parts for human motion recognition." *Proceedings of the IEEE Conference on Computer Vision and Pattern*

*Recognition*, pp.2674-2681.

Wang, X., H. Yu, J. Qi, X. Li, H. Zhang, X. Jia and N. Zhao (2024). "Research on application detection method of bolt vibration time-frequency analysis." *Proceedings of the 5th International Conference on Computer Engineering and Application (ICCEA)*, pp.1129-1133

Wang, Y., Y. Li, Y. Song and X. Rong (2020). "The influence of the activation function in a convolution neural network model of facial expression recognition." *Applied Sciences* 10(5): 1897.

Xiao, B.-Y., C.-C. Tseng and S.-L. Lee (2021). "Node classification using graph convolutional network with dropout regularization." *TENCON 2021-2021 IEEE Region 10 Conference (TENCON)*, pp.84-87.

Xiao, F., G. S. Chen, J. L. Hulsey and W. Zatar (2017). "Characterization of non-stationary properties of vehicle–bridge response for structural health monitoring." *Advances in Mechanical Engineering* 9(5): 1687814017699141.

Xin, Y., J. Li and H. Hao (2021). "Enhanced vibration decomposition method based on multisynchrosqueezing transform and analytical mode decomposition." *Structural Control and Health Monitoring* 28(6): e2730.

Xu, M., T. Li, P. Guan, X. Shen and Y. Fu (2024). "Bearing fault diagnosis based on dual-stream CNN using wavelet time-frequency FFT spectrum." *Proccedings of SPIE*, Volume 13180 3033775.

Yan, R. and R. X. Gao (2006). "Hilbert–Huang transform-based vibration signal analysis for machine health monitoring." *IEEE Transactions on Instrumentation and Measurement* 55(6): 2320-2329.

Yang, D. and C. M. Wang (2022). "Modal properties identification of damped bridge using improved vehicle scanning method." *Engineering Structures* 256: 114060.

Yang, Y., M. Cheng and K. Chang (2013). "Frequency variation in vehicle–bridge interaction systems." *International Journal of Structural Stability and Dynamics* 13(02): 1350019.

Yang, Y. and C. Lin (2005). "Vehicle – bridge interaction dynamics and potential applications." *Journal of Sound and Vibration* 284(1-2): 205-226.

Yang, Y., W. Tu, S. Huang, H. Lu, W. Wan and L. Gan (2021). "Dual-stream convolutional neural network with residual information enhancement for pansharpening." *IEEE Transactions on Geoscience and Remote Sensing* 60: 1-16.

Ye, H., Z. Wu, R.-W. Zhao, X. Wang, Y.-G. Jiang and X. Xue (2015). "Evaluating two-stream CNN for video classification." *Proceedings of the 5th ACM on International Conference on Multimedia Retrieval,* pp.435-442.

Yeum, C. M., J. Choi and S. J. Dyke (2019). "Automated region-of-interest localization and classification for vision-based visual assessment of civil infrastructure." *Structural Health Monitoring* 18(3): 675-689.

Yu, G., Z. Wang and P. Zhao (2018). "Multisynchrosqueezing transform." *IEEE Transactions on Industrial Electronics* 66(7): 5441-5455.

Zafar, A., M. Aamir, N. Mohd Nawi, A. Arshad, S. Riaz, A. Alruban, A. K. Dutta and S. Almotairi (2022). "A comparison of pooling methods for convolutional neural networks." *Applied Sciences* 12(17): 8643.

Zhai, W., K. Wang and C. Cai (2009). "Fundamentals of vehicle–track coupled dynamics." *Vehicle System Dynamics* 47(11): 1349-1376.

Zhang, X., Y. Lu, M. Cao, S. Li, D. Sumarac and Z. Wang (2024). "Instantaneous identification of tension in bridge cables using synchrosqueezing wave-packet transform of acceleration responses." *Structure and Infrastructure Engineering* 20(2): 199-214.

Zhou, W., H. Fan, J. Zhu, H. Wen and Y. Xie (2022). "Research on Generalized Hybrid Probability Convolutional Neural Network." *Applied Sciences* 12(21): 11301.

Zhou, Y., Y. Pei, S. Zhou, Y. Zhao, J. Hu and W. Yi (2021). "Novel methodology for identifying the weight of moving vehicles on bridges using structural response pattern extraction and deep learning algorithms." *Measurement* 168: 108384.

Zhu, X. and S. Law (2006). "Wavelet-based crack identification of bridge beam from operational deflection time history." *International Journal of Solids and Structures* 43(7-8): 2299-2317.

Zhu, X. and S.-S. Law (2015). "Structural health monitoring based on vehicle-bridge interaction: accomplishments and challenges." *Advances in Structural Engineering*

18(12): 1999-2015.

Zhu, X. and S.-S. Law (2016). "Recent developments in inverse problems of vehicle–bridge interaction dynamics." *Journal of Civil Structural Health Monitoring* 6(1): 107-128.